Syntheses and Structures of Stereoregular Hydrogenated Ring-Opened Poly(norbornene)s

A Doctoral Thesis

by

Yuki Nakama

Submitted to the Graduate School of Science, Osaka University

February 2024

Acknowledgement

The study presented in this thesis has been done at the laboratory of polymer assemblies in the department of macromolecular science under the direction of Professor Takahiro Sato.

First, I would like to show the utmost gratitude to Professor Sato for all the academic guidance on my doctoral program at Osaka University as a student with a full-time job in Zeon Corporation. I also wish to dedicate my gratitude to Professor Ken Terao for continuing to accept me as a doctoral candidate.

I would like to express my deepest appreciation to Professor Kohji Tashiro (Toyota Technological Institute) for providing me many essential supports on polymer crystal structure analysis and encouraging me warmly to accomplish my research any time.

I am indebted to R^3 Institute for Newly-Emerging Science Design and Professor Tadashi Itoh (Osaka University) for assisting me to enter Doctoral Special Course of Nanoscience and Nanoengineering for Working People in Industries. I also appreciate Professor Tatsuki Kitayama (Osaka University) from whom I learned how interesting the stereoregularity of polymer is in my master's degree.

I would like to thank my research colleagues in Zeon Corporation. I am thankful to Dr. Shigetaka Hayano for his guidance and support. My study was originated from his pioneering works on the syntheses of highly stereoregular cycloolefin polymers. Without his persistent help, this thesis would not have been possible. I would also like to thank Dr. Satoshi Natori for his support on the all-atom MD calculation in my work.

I would like to offer my special thanks to Dr. Muneki Ouchi (RIKEN) for his guidance for the ^{13}C NMR measurements, and to Dr. Yoshinori Matsumoto (Tosoh Analytical Technology Center) for his cooperation in SEC-MALS measurements. I have greatly benefited from Professor Toshikazu Miyoshi and Mr. Yuta Makita in The University of Akron by the collaboration and fruitful discussion in polymer dynamics. I also thank Quantum Beam Analyses Alliance for permission to access the research resources in Kyoto University.

I am also grateful to my bosses including Ex-bosses in Zeon Corporation, Mr. Takuji Kishimoto, Dr. Masami Koshiyama, Mr. Kenji Kuroyanagi, Dr. Yuki Ono and Ms. Mako Kurakata for their warm supports around my studying period.

Finally, I need to thank my family. I want to thank my mother and father for providing me long-time supports, also my parents in law for caring my family anytime. I am deeply grateful to my wife for her big patience and help, and three daughters for giving me much precious time and future.

February 2024

Yuki Nakama

Contents

Chapter I. General Introduction

Chapter II. Syntheses of Stereoregular Hydrogenated Ring-Opened Poly(norbornene)s

Chapter III. Crystal Structures of Stereoregular Hydrogenated Ring-Opened Poly(norbornene)s

Chapter I: General Introduction

I-1. Polyolefins

Polyolefins are industrially important synthetic polymers, synthesized from olefin monomers. According to the IUPAC Gold Book, *olefins* are "Acyclic and cyclic hydrocarbons having one or more carbon–carbon double bonds, apart from the formal ones in aromatic compounds. The class olefins subsumes alkenes and cycloalkenes and the corresponding polyenes."[1] Polyethylene and polypropylene are typical examples of polyolefins (Scheme I-1).

Scheme I-1. Chemical structures of polyethylene and polypropylene.

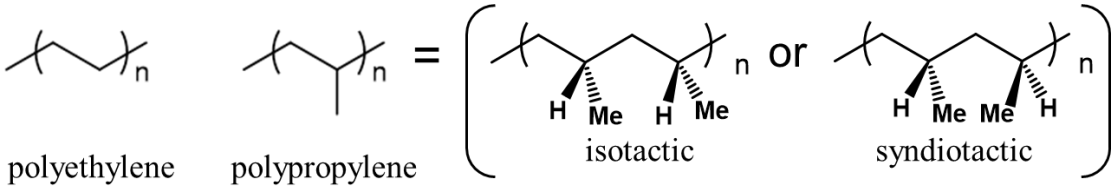

After Staudinger proposed the concept of macromolecules in 1920, polyethylene was synthesized as early as 1933 by Gibson and Fawcett at the British chemical company, ICI. It is well known that polyethylene was used as electrical insulators for air and shipborne radar in the Second World War. After the war, polyolefins have been at the center of the development of the polymer industry. Nowadays, polyethylene and polypropylene are used as wrapping films, bottles, toys, water and gas pipes, wire, cable

insulation, and so on. About half of global plastic production is polyethylene and polypropylene today.

I-2. Early Studies of Polyolefins

Because polyethylene has the simplest chemical structure among synthetic polymers, it was the standard polymer to establish polymer chemistry after Staudinger proposed the macromolecular concept.[2] As early as 1939, Bunn reported the crystalline structure of this simplest polyolefin, where the chain takes the zig-zag conformation in the orthorhombic lattice.[3] In 1953, Ziegler[4] discovered a new catalyst for the polymerization of ethylene at low temperatures. This catalyst produced high-density polyethylene, which is a harder material than low-density polyethylene produced by radical polymerization.

Just after the development of the Ziegler catalyst, Natta[5] succeeded in preparing stereoregular polypropylene (Scheme I-1) by use of the Ziegler-Natta catalyst in 1954. This catalyst made it possible to control the configuration of asymmetric carbon atoms not only in polypropylene but also in many other vinyl polymers.[6] The resulting polymer samples strongly promoted research in structural science and contributed to its development. Later, with the advent of metallocene catalysts in the 1980s, more precise structural and molecular weight control became possible. Since the 1990s, various catalysts called post-metallocenes have been developed and are still in use today. Polyolefins covering a wide range of physical properties have been developed one after another.

After the discovery of stereoregularity in polyolefins, it has begun to be understood that the stereoregularity (or tacticity) in the polymer chain plays a very important role in the formation of the crystal structure. Intensive studies of crystallography using X-ray diffraction technique were conducted. Natta and Corradini reported in the early 1960s the crystal structures of isotactic and syndiotactic polypropylenes.[7-10] The *isotactic* chain tends to have a 3/1 helix structure due to the repulsion between the substituents.[7,8] On the other hand, the syndiotactic one forms a 4/1 helix as the most stable state[9] and planar-zigzag conformation at the metastable state when it is drawn.[10] Their crystal structures as well as that of polyethylene are shown in Figure I-1.

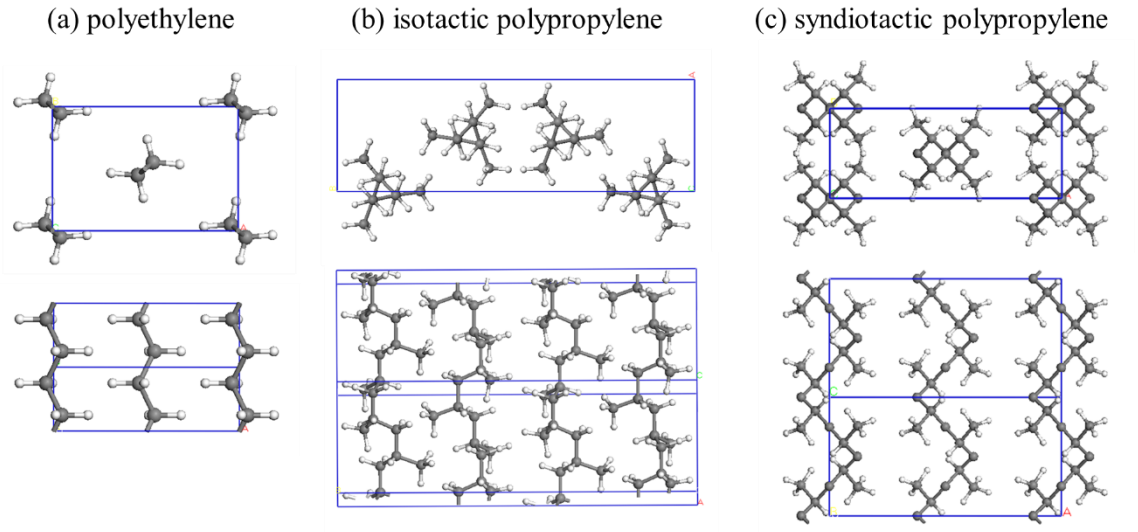

Figure I-1. Chain conformation and packing in the crystalline phase for (a) polyethylene, (b) isotactic polypropylene, and (c) syndiotactic polypropylene.

The relation between the conformational energy and the unperturbed dimension of the isolated polymer chain in dilute solutions is one of the most fundamental problems in polymer science. Due to their simple chemical structures, polyethylene and

polypropylene are the easiest polymers to calculate the conformational energy among polymers with symmetric and asymmetric structures, respectively. Although polyethylene and polypropylene are not suitable polymers for studying solution properties because of their high crystallinity, much effort was made to determine the unperturbed dimension in dilute solution.[11] The obtained experimental unperturbed dimensions of polyethylene and polypropylene were compared with the rotational isomeric state (RIS) model, in which the unperturbed dimension can be calculated from the conformational energy. The details were summarized in Flory's textbook in 1969.[11]

Polymer rheology is important to design the molding process and the mechanical properties of plastic materials. On the basis of the Doi-Edwards theory[12] and the experimental verification by Graessley,[13] the plateau modulus G_N^0 of polymer melts is attributed to the chain entanglement interactions. As the proposal by Lin-Noolandi[14-16], G_N^0 is related to the packing length p and the number n_t of entanglement strands in a cube with sides equal to the tube diameter by

$$G_N^\circ = \frac{RT}{n_t^2 N_A p^3} \tag{I-1}$$

where R, T, and N_A are the gas constant, the absolute temperature, and the Avogadro constant, respectively. Furthermore, p can be calculated from mean square end-to-end distance $\langle R^2 \rangle_0$ of the polymer chain in the unperturbed state by

$$p = \frac{\left(M / \rho N_A \right)}{\langle R^2 \rangle_0} \tag{I-2}$$

where M and ρ are the molar mass and melt density of the polymer. Fetters and his coworkers[17-19] extensively studied the relation between rheological properties and

unperturbed dimension for industrially important polyolefins. They obtained the linear relation between G_N^0 and p^{-3} illustrated in Figure I-2. The slope yields $n_t = 21.8$.[19] Their results demonstrate the close relation between polymer rheology and polymer chain conformation.

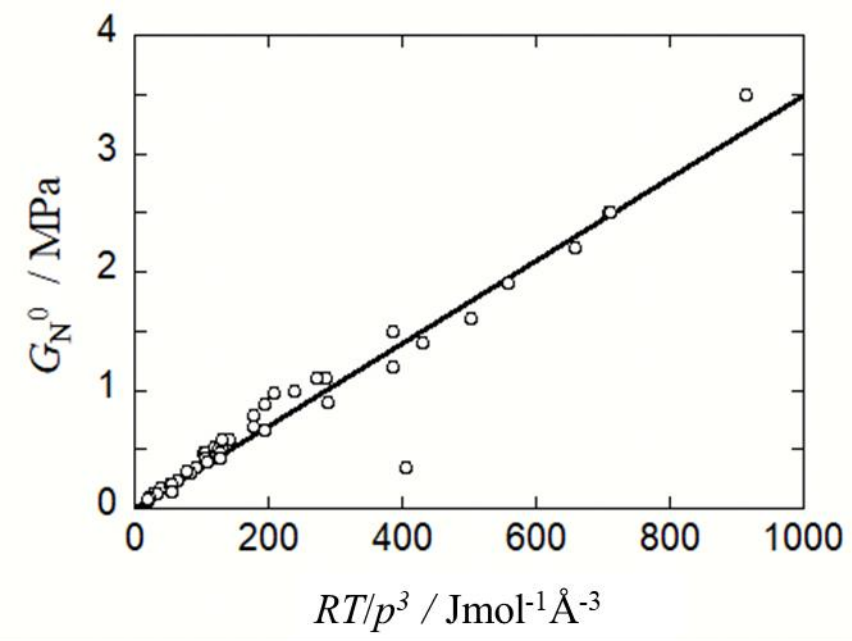

Figure I-2. Relation between the plateau modulus G_N^0 and packing length p for various polyolefins.

I-3. Poly(norbornene)s as Typical Examples of Cycloolefin Polymers

Norbornene is a bicyclic olefin, and polymerizes in two ways,[20] as shown in Scheme I-2. Through the addition polymerization, norbornene becomes a polymer retaining the bicyclic structure in the backbone. On the other hand, by ring-opening metathesis polymerization (ROMP), norbornene provides a polymer with double bonds and a cyclopentane ring structure in the backbone. After hydrogenation of the residual double bonds, the polymer becomes more thermally stable, more resistive against

oxidative degradation and applicable to various industrial materials.[21-23] In what follows, the hydrogenated ring-opened poly(norbornene) is abbreviated as H-poly(NB).

Scheme I-2. Two types of polymerization methods of norbornene.

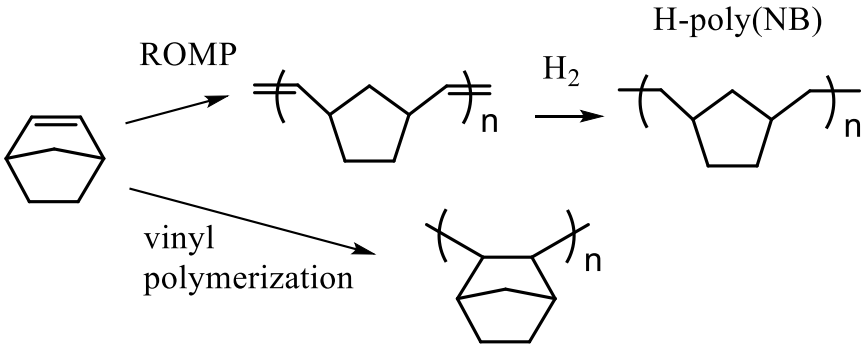

Hydrogenated ring-opened polymers obtained from norbornene and its derivatives (Scheme I-3) are referred to as 'cycloolefin polymers (COPs).' The representative COP resins, Zeonor® and Zeonex®, were developed by Zeon Corporation in the early 1980s and have been commercially produced since 1990. Because of their superior optical properties (high clarity, low birefringence), heat resistance, moisture resistance, chemical resistance, acid and alkali resistance, electric property (low dielectric constant), and good melt processability, they have been used for optical lenses and films, pharmaceutical packages, electrical insulators, and so on. [21-32]

Scheme I-3. Chemical structures of typical norbornene derivatives used to produce COP resins.

5-phenylnorbornene dicyclopentadiene (DCP) tricyclododecene (TCD)

On the other hand, poly(norbornene) formed by vinyl addition polymerization (Scheme I-2) has been reported to be stiffer than ordinary vinyl polymers without ring skeletal structures.[33-37] Compared with H-poly(NB), poly(norbornene) through addition polymerization is more brittle and difficult to use as a functional resin.

The possible microstructures of ring-opened poly(norbornene) [poly(NB)] and its hydrogenated product, H-poly(NB), are shown in Scheme I-4. The configuration of the cyclopentylene rings in H-poly(NB) is always *cis*, i.e., the hydrogens at the branching points face the same side of the cyclopentylene ring, because the monomer configuration is retained throughout the ROMP and following hydrogenation procedures. Stereoregularity is defined by the configuration relationship between the two asymmetric carbons that are distanced by five C-C bonds. When their configurations are the same [(*S*) and (*S*), or (*R*) and (*R*)], it is named the *meso* diad and the tacticity is isotactic. On the contrary, when their configurations are different [(*S*) and (*R*), or (*R*) and (*S*)] it is named the *racemo* diad and the tacticity should be syndiotactic. In other words, the tacticity for H-poly(NB) which has no substituents can be explained by the difference in the sequence of head-tail bonding. Hence, the isotactic and syndiotactic H-poly(NB) take the sequence of the configurations of asymmetric carbons [(*S*)-(*R*)]-[(*S*)-(*R*)]-[(*S*)-(*R*)]-[(*S*)-(*R*)]-…. and [(*S*)-(*R*)]-[(*R*)-(*S*)]-[(*S*)-(*R*)]- [(*R*)-(*S*)]-...., respectively.

Scheme I-4. Possible microstructures of ring-opened poly(NB) and H-poly(NB).

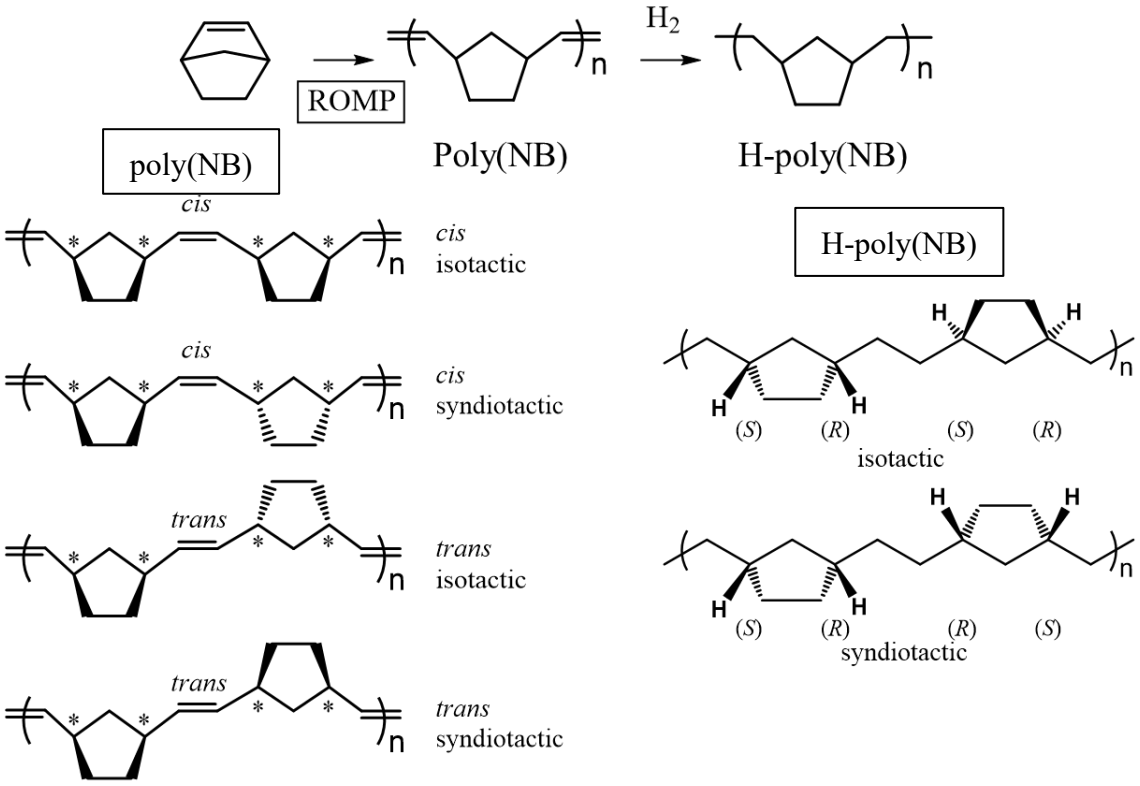

According to the IUPAC nomenclature,[38] the more precise name for stereoregular H-poly(NB) may be diisotactic and disyndiotactic instead of isotactic and syndiotactic, respectively. Some other poly(cycloolefin)s also have this type of stereoregularity: vinyl-addition polymerized poly(NB),[39] cationically polymerized poly(norbornadiene).[40] However, we will use the names isotactic and syndiotactic H-poly(NB)s because this type of nomenclature has long been accepted among researchers studying the polymers synthesized by the ROMP process.

I-4. Previous Studies on H-poly(NB)

The ring-opening metathesis polymerization (ROMP) of norbornene and its derivatives was first performed using the Ziegler type classical catalyst discovered in the 1960s. However, the design of ligands to make precise polymerization was so difficult that the tacticity of the main chain could not be controlled at all and the products were limited to atactic polymers.

In the 1980s, R. H. Grubbs developed a living ROMP system using metal alkylidene complexes.[41] This technology provided the basis for ROMP in a well-controlled manner. *Cis*/*trans*-selective ROMPs of various monomers had been successfully achieved.[42,43] On the other hand, the tacticity control of ROMP has been studied more recently. In the early 2000s, advances in the stereospecific ROMP have made it possible to polymerize norbornene derivatives with high stereoregularity by designing catalysts and ligands. Schrock and his co-workers shed light on a strategy of catalyst design for stereospecific ROMP[44] and *cis*-isospecific ROMPs of various norbornene derivatives were realized.[45-47] After that, *cis*-syndiospecific,[48,49] *trans*-isospecific[50] ROMPs of norbornene and its derivatives were achieved as well.

At the same time, Hayano *et al*. have reported that the Mo- and W-based binary catalysts promoted both highly *cis*-isoselective and *cis*-syndioselective ROMPs of dicyclopentadiene (DCP) which is one of the industrially important norbornene derivatives.[51-53] They have also discovered that the addition of stereoregularity induced crystallinity and improved heat resistance. However, studies on the stereoselective ROMP of NB as a simpler aliphatic cycloolefin have been insufficient. It is important to confirm how effective these catalysts are for NB.

The crystal structure of atactic H-poly(NB) or copolymers containing atactic H-poly(NB) block was studied already in the past.[54-58] It must be noted that the atactic H-poly(NB) can crystallize in spite of the random configuration. The polymer is thus regarded as one of the very unique atactic polymers including atactic poly(vinyl alcohol) and poly(acrylonitrile). Register et al.[54] investigated the thermal properties and crystal structure of atactic H-poly(NB) with a *meso* content of 44%. The melting temperature T_m was 143 °C. The monoclinic crystal structure was proposed by the analysis of X-ray diffraction data for the polymer species in the range of the *meso* content from 44% to 54%.[55] Furthermore, the monoclinic crystal structure for atactic H-Poly(NB) is transformed to the hexagonal phase above the transition temperature.[54,55] However, there are no reports on the crystal structure of stereoregular H-poly(NB)s.

The single chain conformation of H-poly(NB) and its analogue polymers has been little studied. Only recently, Hamidi and Ganewatta studied dilute solution properties of rosin-substituted atactic H-poly(NB) by size exclusion chromatography in tetrahydrofuran.[59] They analyzed the molecular weight dependences of the radius of gyration and intrinsic viscosity to estimate the chain rigidity of the polymer. There is no research on the single chain conformation of stereoregular H-poly(NB).

I-5. Purpose and Scope of This Work

As demonstrated above for polypropylene, stereoregularity plays an essential role in the structure and properties of polymers. Thus, it seems interesting to investigate the effects of stereoregularity on the crystal structure and single chain conformation of H-poly(NB). This is the motivation of this thesis work.

In this work, isospecific and syndioselective ring-opening metathesis polymerizations (ROMPs) of norbornene (NB) using Mo- and W-based catalyst precursors have been thoroughly investigated for the first time. *Cis*-isospecific ROMPs of NB were achieved with Mo-based catalyst, and *cis*-syndioselective ROMPs of NB proceeded in the presence of W-based catalysts. The results of this synthetic work are described in Chapter II.

The crystal domain controls the thermal properties such as melting temperature and the mechanical properties such as tensile strength where crystalline domains form physical cross-links. The knowledge in the crystal structure is fundamental to improve their physical and mechanical properties. Chapter III deals with the stereoregularity dependence of the crystal structure in solid state, and the crystal phase transition in isotactic and atactic H-poly(NB)s.

When the chemical structures of H-poly(NB) chain is seen from the architectural point of view (Scheme I-4), the internal rotation of C-C bonds along the cyclopentylene rings is strictly restricted. Only the bonds associated with the ethylene moieties connecting the rings can rotate against a low energy barrier. These characteristics allow us to expect that the conformation of H-poly(NB) may be rigid. To examine this expectation, I investigated the chain conformation of H-poly(NB)s with the different tacticity in dilute solution. Chapter IV is concerned with the characterization of the single chain conformation of isotactic, syndiotactic, and atactic H-poly(NB)s.

The main results and conclusions obtained in this work are summarized in the last Chapter V.

References

1. Olefins. 3.0.1 ed.; International Union of Pure and Applied Chemistry (IUPAC): 2019.
2. Flory, P. J. *Principles of Polymer Chemistry*. Cornell Univ. Press, Ithaca, New York (1953).
3. Bunn, C. W., The crystal structure of long-chain normal paraffin hydrocarbons. The “shape” of the <CH2 group. *Trans. Faraday Society* **1939,** *35* (0), 482-491.
4. Ziegler, K.; Holzkamp, E.; Breil, H.; Martin, H., Polymerisation von Äthylen und anderen Olefinen. *Angew. Chem.* **1955**, *67* (16), 426-426.
5. Natta, G.; Pino, P.; Corradini, P.; Danusso, F.; Mantica, E.; Mazzanti, G.; Moraglio, G., Crystalline High Polymers of α-Olefins. *J. Am. Chem. Soc.* **1955,** *77* (6), 1708-1710.
6. Natta, G., Une nouvelle classe de polymeres d'α-olefines ayant une régularité de structure exceptionnelle. *J. Polym. Sci.* **1955,** *16* (82), 143-154.),
7. Natta, G.; Corradini, P., Structure and properties of isotactic polypropylene. *Il Nuovo Cimento (1955-1965)* **1960,** *15* (1), 40-51.
8. Corradini, P., The discovery of isotactic polypropylene and its impact on pure and applied science. *J. Polym. Sci., Part A: Polym. Chem.* **2004,** *42* (3), 391-395.
9. Corradini, P.; Natta, G.; Ganis, P.; Temussi, P. A., Crystal structure of syndiotactic polypropylene. *J. Poly. Sci., Part C: Polym. Symp.* **1967,** *16* (5), 2477-2484.
10. Natta, G.; Peraldo, M.; Allegra, G., Crystalline modification of syndiotactic polypropylene having a zig-zag chain conformation. *Makromol. Chem.* **1964,** *75* (1), 215-216.
11. Flory, P. J. *Statistical Mechanics of Chain Molecules*; Wiley: New York, 1969.
12. Doi, M.; Edwards, S. The Theory of Polymer Dynamics; Oxford University Press: New York, 1988.
13. Graessley, W. W.; Edwards, S. F., Entanglement interactions in polymers and the chain contour concentration. *Polymer* **1981,** *22* (10), 1329-1334.
14. Lin, Y. H., Number of entanglement strands per cubed tube diameter, a fundamental aspect of topological universality in polymer viscoelasticity. *Macromolecules* **1987,** *20* (12), 3080-3083.
15. Kavassalis, T. A.; Noolandi, J., A new theory of entanglements and dynamics in dense polymer systems. *Macromolecules* **1988,** *21* (9), 2869-2879.

16. Kavassalis, T. A.; Noolandi, J., New view of entanglements in dense polymer systems. *Phys. Rev. Lett.* **1987,** *59* (23), 2674-2677.
17. Fetters, L. J.; Lohse, D. J.; Richter, D.; Witten, T. A.; Zirkel, A. Connection between Polymer Molecular Weight, Density, Chain Dimensions, and Melt Viscoelastic Properties. *Macromolecules* **1994**, *27*, 4639-4647.
18. Fetters, L. J.; Lohse, D. J.; Graessley, W. W. Chain Dimensions and Entanglement Spacings in Dense Macromolecular Systems. *J. Polym. Sci.: Part B: Polym. Phys.* **1999**, *37*, 1023-1033.
19. Fetters, L. J.; Lohse, D. J.; Garcia-Franco, C. A.; Brant, P.; Richter, D. Prediction of Melt State Poly(R-olefin) Rheological Properties: The Unsuspected Role of the Average Molecular Weight per Backbone Bond, *Macromolecules* **2002**, *35*, 10096-10101.
20. Shin, J. Y.; Park, J. Y.; Liu, C.; He, J.; Kim, S. C., Chemical structure and physical properties of cyclic olefin copolymers (IUPAC Technical Report). *Pure Appl. Chem.* **2005,** *77* (5), 801-814.
21. Kohara, T. Development of new cyclic olefin polymers for optical uses. *Macromol. Symp.* **1996**, *101*, 571−579.
22. Yamazaki, M., Industrialization and application development of cyclo-olefin polymer. *J. Mol. Catal. A: Chem.* **2004**, *213* (1), 81-87.
23. Mol, J. C., Industrial applications of olefin metathesis. *J. Mol. Catal. A: Chem.* **2004,** *213* (1), 39-45.
24. Inoue, T.; Takiguchi, O.; Osaki, K.; Kohara, T.; Natsuume, T., Dynamic Birefringence of Amorphous Polyolefins I. Measurements on Poly[l-ethyl-5-methyl-octahydro-4,7-methano-l*H*-indene-1^2,3-diyl]. *Polym. J.* **1994,** *26* (2), 133-139.
25. Inoue, T.; Okamoto, H.; Osaki, K.; Kohara, T.; Natsuume, T., Dynamic Birefringence of Amorphous Polyolefins II. Measurements on Polymers Containing Five-Membered Ring in Main Chain. *Polym. J.* **1995,** *27* (9), 943-950.
26. Bauer, T., OPTICAL MATERIALS | Plastics. In *Encyclopedia of Modern Optics*, Guenther, R. D., Ed. Elsevier: Oxford, **2005**; pp 480-488.
27. Nickel, A.; Edgecombe, B. D., 4.30 - Industrial Applications of ROMP. In *Polymer Science: A Comprehensive Reference*, Matyjaszewski, K.; Möller, M., Eds. Elsevier: Amsterdam, **2012**; pp 749-759.

28. Nunes, P. S.; Ohlsson, P. D.; Ordeig, O.; Kutter, J. P., Cyclic olefin polymers: emerging materials for lab-on-a-chip applications. *Microfluidics and Nanofluidics* **2010,** *9* (2), 145-161.
29. Inoue, K.; Yoda, K.; Murakami, T.; Kikukawa, M.;Komoto, S. Novel COP Optical Film with Durability for Flexible Displays, *SID Symposium Digest of Technical Papers*, **2017**, *48*, 631-633.
30. Harauchi, Y.; Houkawa T.; Adachi S.; Arai K.; Sawaguchi T.; Hayano S.; Uchiyama S. Recent developments of cyclo olefin polymers. *Kobunshi Ronbunshu*, **2018**, *75*, 477-485.
31. Maruno, T.; Watanabe, H.; Yoneda, S.; Uchihashi, T.; Adachi, S.; Arai, K.; Sawaguchi, T.; Uchiyama, S., Sweeping of Adsorbed Therapeutic Protein on Prefillable Syringes Promotes Micron Aggregate Generation. *J. Pharm. Sci.* **2018,** *107* (6), 1521-1529.
32. Yoneda, S.; Maruno, T.; Mori, A.; Hioki, A.; Nishiumi, H.; Okada, R.; Murakami, M.; Zekun, W.; Fukuhara, A.; Itagaki, N.; Harauchi, Y.; Adachi, S.; Okuyama, K.; Sawaguchi, T.; Torisu, T.; Uchiyama, S., Influence of Protein Adsorption on Aggregation in Prefilled Syringes. *J. Pharm. Sci.* **2021,** *110* (11), 3568-3579.
33. Haselwander, T. F. A.; Heitz, W.; Kru1gel, S. A.; Wendorff, J. H., Rigid Random Coils: Rotationally Confined Chain Molecules. *Macromolecules* **1997**, *30*, 5345-5351.
34. Ahmed, S.; Ludovice, P. J.; Kohl, P., Microstructure of 2,3 erythro di-isotactic polynorbornene from atomistic simulation. *Comput. Theor. Polym. Sci.* **2000**, *10*, 221-233.
35. Müller, K.; Kreiling, S.; Dehnicke, K.; Allgaier, J.; Richter, D.; Fetters, L. J.; Jung, Y.; Yoon, D. Y.; Greiner, A., Synthesis and Rheological Properties of Poly(5-n-hexylnorbornene). *Macromol. Chem. Phys.* **2006,** *207* (2), 193-200.
36. Chung, W. J.; Henderson, C. L.; Ludovice, P. J., RIS Model of the Helix-Kink Conformation of Erythro Diisotactic Polynorbornene. *Macromol. Theory Simul.* **2010**, *19* (7), 421-431.
37. Kai, H.; Izumi, A.; Hayakawa, S.; Niemiec, J. A.; Ebner, C.; Schofield, M.; Skilskyj, D.; Rhodes, L. F., Interchain ordering structure and main chain conformation analysis of thermal stability in vinyl-addition polynorbornene. *Polymer* **2022,** *257*.

38. *Compendium of Polymer Terminology and Nomenclature IUPAC Recommendations 2008*; Jones, R. G., Kahovec, J., Stepto, R., Wilks, E. S., Hess, M., Kitayama, T., Metanomski, W. V., Eds.; RSC Publishing: Cambridge, 2009.
39. Janiak, C.; Lassahn, P. G., Metal catalysts for the vinyl polymerization of norbornene. *J. Mol. Catal. A: Chem.* **2001,** *166* (2), 193-209.
40. De Rosa, C.; Malafronte, A.; Auriemma, F.; Scoti, M.; Di Girolamo, R.; D'Alterio, M. C.; Ricci, G.; Zanchin, G.; Leone, G. Synthesis, chain conformation and crystal structure of poly-(norbornadiene) having repeating 3,5-enchained nortricyclene units. *Polym. Chem.* **2019**, *10*, 4593−4603.
41. Grubbs, R. H.; Tumas, W., Polymer Synthesis and Organotransition Metal Chemistry. *Science* **1989,** *243* (4893), 907-915.
42. Grubbs, R. H. Handbook of Metathesis; Wiley-VCH: Weinheim, Germany, 2003.
43. Ivin, K. J.; Mol, J. C. Olefin Metathesis and Metathesis Polymerization; Academic Press: San Diego, CA, 1997.
44. Schrock, R. R. Handbook of Metathesis; Grubbs, R. H., Ed.; Wiley-VCH: Weinheim, Germany, 2003; Vol. 1, pp 8−32 and references therein.
45. Schrock, R. R.; Hoveyda, A. H. Molybdenum and Tungsten Imido Alkylidene Complexes as Efficient Olefin-Metathesis Catalysts. *Angew. Chem., Int. Ed.* **2003**, *42*, 4592-4633.
46. Schrock, R. R. Synthesis of stereoregular ROMP polymers using molybdenum and tungsten imido alkylidene initiators. *Dalton Trans.* **2011**, *40*, 7484-7495.
47. Zhu, L.; Flook, M. M.; Lee, S.-L.; Chan, L.-W.; Huang, S.-L.; Chiu, C.-W.; Chen, C.-H.; Schrock, R. R.; Luh, T.-Y. Cis, Isotactic Selective ROMP of Norbornenes Fused with *N*-Arylpyrrolidines. Double Stranded Polynorbornene-Based Ladderphanes with *Z*-Double Bonds. *Macromolecules* **2012**, *45*, 8166-8171.
48. Flook, M. M.; Ng, V. W. L.; Schrock, R. R. Synthesis of *cis,syndiotactic* ROMP Polymers Containing Alternating Enantiomers. *J. Am. Chem. Soc.* **2011**, *133*, 1784-1786.
49. Rosebrugh, L. E.; Marx, V. M.; Keitz, B. K.; Grubbs, R. H. Synthesis of Highly Cis, Syndiotactic Polymers via Ring-Opening Metathesis Polymerization Using Ruthenium Metathesis Catalysts. *J. Am. Chem. Soc.* **2013**, *135*, 10032-10035.
50. Flook, M. M.; Boener, J.; Kilyanek, S. M.; Gerber, L. C. H.; Schrock, R. R. Five-Coordinate Rearrangements of Metallacyclobutane Intermediates during Ring-Opening Metathesis Polymerization of 2,3-Dicarboalkoxynorbornenes by

Molybdenum and Tungsten Monoalkoxide Pyrrolide Initiators. *Organometallics* **2012**, *31*, 6231-6243.

51. Hayano, S.; Kurakata, H.; Tsunogae, Y.; Nakayama, Y.; Sato, Y.; Yasuda, H. Stereospecific Ring-Opening Metathesis Polymerization of Cycloolefins Using Novel Molybdenum and Tungsten Complexes Having Biphenolate Ligands. Development of Crystalline Hydrogenated Poly(endo-dicyclopentadiene) and Poly(norbornene). *Macromolecules* **2003,** *36* (20), 7422-7431.
52. Hayano, S.; Takeyama, Y.; Tsunogae, Y.; Igarashi, I. Hydrogenated Ring-Opened Poly(endo-dicyclopentadiene)s Made via Stereoselective ROMP Catalyzed by Tungsten Complexes: Crystalline Tactic Polymers and Amorphous Atactic Polymer. *Macromolecules* **2006,** *39* (14), 4663-4670.
53. Hayano, S.; Tsunogae, Y., Syndioselective Ring-Opening Metathesis Polymerization of endo-Dicyclopentadiene with Tungsten Complexes Having Imido Ligands: Development of Crystalline Syndiotactic Hydrogenated Poly(endo-dicyclopentadiene). *Macromolecules* **2006,** *39* (1), 30-38.
54. Lee, L.-B. W.; Register, R. A. Hydrogenated Ring-Opened Polynorbornene: A Highly Crystalline Atactic Polymer. *Macromolecules* **2005,** *38*, 1216-1222.
55. Bishop, J. P.; Register, R. A. The crystal–crystal transition in hydrogenated ring-opened polynorbornenes: Tacticity, crystal thickening, and alignment. *J. Polym. Sci., Part B: Polym. Phys.* **2011**, *49*, 68-79.
56. Lee, L.-B. W.; Register, R. A. Equilibrium Control of Crystal Thickness and melting Point through Block Copolymerization. *Macromolecules* **2004**, *37*, 7278-7284.
57. Li, S.; Myers, S. B.; Register, R. A. Solid-State Structure and Crystallization in Double-Crystalline Diblock Copolymers of Linear polyethylene and Hydrogenated Polynorbornene. *Macromolecules* **2011**, *44*, 8835-8844.
58. Showak, M. T.; Burns, A. B.; Stella, A. J.; Register, R. A. Counit Inclusion in hydrogenated polynorbornene Copolymer Crystals. *Macromolecules* **2013**, *46*, 9288-9295.
59. Hamidi, N.; Ganewatta, M. S. Influence of the rosin pendant groups on the solution properties of a high molecular weight hydrogenated polynorbornene. *Polymer* **2021**, *232*, 124167.

Chapter II: Syntheses of Stereoregular Hydrogenated Ring-Opened Poly(norbornene)s

II-1. Introduction

In general, the stereoselectivity of the enchainment reaction of metal-catalyzed polymerization would be influenced by a combination of catalyst structure and monomer structure. The propagation species derived from metal catalysts would possess their chirality centers both in their ligands and in their polymeryl group attached to the metal. Stereoregularity of the polymer chain can therefore be derived from the catalyst asymmetry (enantiomorphic site control/catalyst control) or the polymer asymmetry (chain end control/penultimate effect) or, most likely, a combination of the two. In the case of ROMP of norbornene, monomer coordination step may determine the stereoselectivity, and the formed stereostructure might be retained during the following steps such as cycloaddition and ring-opening (Scheme II-1).

Scheme II-1. Elementary reaction in the ROMP of norbornene.

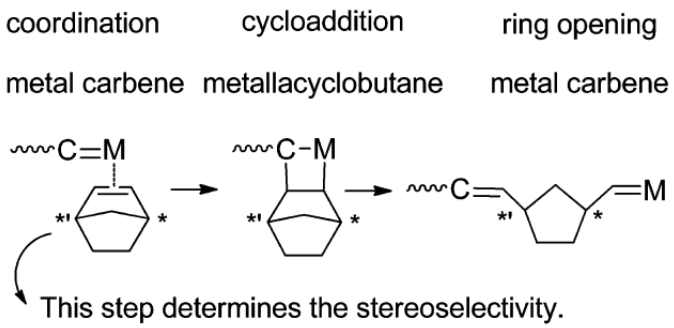

The absolute configurations of norbornene monomer's two bridgehead carbons, of which chiralities are opposite, would also be retained during the ROMP process. Therefore, the next enchainment of ROMP holds not only the asymmetry of the ligand but also the asymmetry of the one of the bridgehead carbons of the last inserted norbornene monomer. Namely, the alignment of the two bridgehead carbons of the penultimate repeating units directly correlates to the polymer asymmetry of the propagation species. Consequently, stereocontrol effect by polymeryl group would be influenced by steric structures of substituent on the repeating units.

The steric structure of the approaching monomer has a predominantly large effect on its insertion behavior to the propagation species. As reported, sterically demanding norbornenes might generally need higher energy to coordinate to the catalyst.[1] This means that the existence of the bulky substituent may result in the increase of the energy of coordination of the olefin moiety to the metal center. To summarize the above, the stereoselectivity of the ROMP process would possibly be affected by both the steric bulkiness and the functionality of the incoming monomer.

As introduced in Chapter I, Hayano *et al*.[2-9] have already reported that the Mo- and W-based binary catalysts promoted both highly *cis*-isoselective and *cis*-syndioselective ROMPs of dicyclopentadiene (DCP) which is one of the industrially important tricyclic cycloolefins. However, study of the stereoselective ROMP of simpler aliphatic cycloolefins seems to be insufficient. The addition of stereoregularity to the conventional H-poly(NB) may expand the possibilities for application as thermoplastic materials. For these reasons, this chapter focuses on the stereoselective ROMPs of NB as a sterically small nonpolar polycyclic olefin. Mo- and W-based catalyst precursors

examined for synthesizing tactic hydrogenated ring-opened polymers are illustrated in Scheme II-2. By applying these catalyst, isotactic and syndiotactic H-poly(NB) were synthesized and their stereoregularity was evaluated. The fundamental factors such as catalyst structure that would affect the stereocontrol of the ROMP of NB is also discussed in comparison with the polymerization results of dicyclopentadiene (DCP) and tetracyclododecene (TCD) (Scheme II-3) using the same catalysts, reported elsewhere.[10]

Scheme II-2. Tungsten- and molybdenum-based catalyst precursors employed in the present study[2-9]

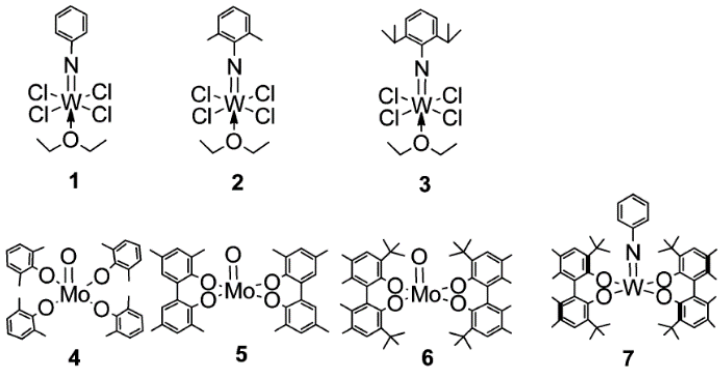

Scheme II-3. Chemical structures of dicyclopentadiene (DCP) and tetracyclododecene (TCD).

Dicyclopentadiene (DCP) Tetracyclododecene (TCD)

II-2. Experimental Section

II-2-1. General Remarks

All operations were carried out in a glovebox (nitrogen atmosphere, $O_2 < 1$ ppm and $H_2O < 1$ ppm) or under an argon atmosphere by using standard Schlenk techniques. WCl_6 (Soegawa Chemical), $MoOCl_4$ (Strem), $Et_2Al(OEt)$ (Kanto Chemical), and *n*-BuLi (Kanto Chemical) were used without further purification. $WOCl_4$ was synthesized from WCl_6 and hexamethyldisiloxane in methylene chloride.[5] $W(=NPh)Cl_4 \cdot Et_2O$ (**1**), W(=N-2,6-Me2-Ph)$Cl_4 \cdot Et_2O$ (**2**), and W(=N-2,6-*i*-Pr_2−Ph) $Cl_4 \cdot Et_2O$ (**3**) were synthesized from $WOCl_4$ and isocyanates in *n*-octane as previously reported.[8] MoO(2,6-Me_2-phenolate)$_4$ (**4**), MoO(3,3′,5,5′-Me_4-biphenolate)$_2$ (MoO(Me_4-biphenolate)$_2$) (**5**) and MoO(racemic-5,5′,6,6′-Me_4-3,3′-*t*-Bu_2-biphenolate)$_2$ (MoO(*rac*-biphenolate)$_2$) (**6**) were prepared from $MoOCl_4$ and phenolates in diethyl ether as previously reported.[2] W(=NPh)((*R*)-(+)-5,5′,6,6′-Me_4-3,3′-*t*-Bu_2-biphenolate)$_2$ (W(=NPh)((*R*)-(+)-biphenolate)$_2$) (**7**) were prepared from **1** and (*R*)-(+)-biphenolate-Li_2 in diethyl ether as previously reported.[8]

n-Octane, and diethyl ether were distilled over sodium metal under an argon atmosphere before use. Toluene and methylene chloride were distilled over calcium hydride. Cyclohexane and *p*-xylene were degassed and stored over molecular sieves. Hexamethyldisiloxane was distilled over molecular sieves under reduced pressure. Phenyl isocyanate (Tokyo Kasei) was distilled from calcium hydride just prior to use. Commercially available 2,6-Me_2-phenyl isocyanate (Tokyo Kasei), 2,6-*i*-Pr_2-phenyl isocyanate (Tokyo Kasei), 2,6-dimethylphenol (Wako Chemicals), 3,3′,5,5′-Me_4-1,1′-biphenyl-2,2′-diol (Me_4-biphenol) (Strem), racemic-5,5′,6,6′-Me_4-3,3′-*t*-Bu_2-1,1′-

biphenyl-2,2′-diol (*rac*-biphenol) (Strem), (*R*)-(+)-5,5′,6,6′- Me_4-3,3′-*t*- Bu_2-1,1′-biphenyl-2,2′-diol ((*R*)-(+)-biphenol) (Strem) and were used as received. Norbornene (Aldrich) was stored as cyclohexane solution over molecular sieves 3A. 1-Octene (Wako Chemicals) was distilled over calcium hydride. *p*-Tos-$NHNH_2$ (Aldrich) was used as received.

II-2-2. Catalyst Preparation

Polymerization catalyst solutions were prepared as follows unless otherwise stated. (i) For W imidos **1**−**3**, a toluene solution of W(=NPh)Cl_4·Et_2O (**1**) (0.0278g, 56.7 μ mol) (green solution) was mixed with three equivalents of Et_2Al(OEt) at room temperature, and the mixture was stirred. The catalyst mixture was aged at room temperature for an additional 15 min resulting in a light brown solution. (ii) For Mo and W phenolates **4**−**7**, the toluene solution of W(=NPh)((*R*)-(+)-Biphenolate)$_2$ (**7**) (0.0556g, 56.7 μ mol) (dark-red solution) was mixed with two equivalents of *n*-BuLi at −78 °C and allowed to warm up to room temperature, and the mixture was stirred for 15 min at room temperature. The reaction mixture turned into a light brown solution.

II-2-3. Polymerization

Polymerization was carried out in a prebaked ampule tube equipped with a rubber septum at 50 or 80 °C. A cyclohexane solution of NB (7.50g, 79.7 mmol) and 1-octene (0.450g, 3.98 mmol) was added to the catalyst mixture at the prescribed temperature. After stirring it for 3h, the polymerization was quenched with a small

amount of ethanol. The obtained polymer was reprecipitated from ethanol and dried in vacuo at 40 °C for 24 h. The polymer yield was determined by gravimetric measurement.

II-2-4. Hydrogenation

A *p*-xylene solution of poly(NB) and a *p*-xylene solution of 4-folds of *p*-Tos-$NHNH_2$ were mixed in a glass flask equipped with a three-way stopcock. The mixture was allowed to heat up to the reaction temperature while stirring. Chemical transfer hydrogenation was carried out at 125 °C for 5 h. After the hydrogenation reaction, the reaction mixture was cooled slowly to room temperature. In the course of the hydrogenation reaction, the recrystallization of crystalline H-poly(NB) might have proceeded from the dilute solution to form a fine powder of crystalline polymer.

II-2-5. Analyses of Complex and Polymer

^{1}H and ^{13}C NMR spectra were recorded on a Bruker Avance III 500 MHz spectrometer (500.13 MHz for ^{1}H, 125.77 MHz for ^{13}C) with Cryoprobe DCH 500/3 at 25−60 °C or on a Bruker Avance III HD 600 MHz spectrometer (150.91 MHz for ^{13}C) equipped with Cryoprobe DCH 600S3 at 125 °C. Chemical shifts were determined with reference to the tetramethylsilane (δ 0.00 ppm), tetrachloroethane (δ 5.97 ppm for ^{1}H, δ 73.8 ppm for ^{13}C) or chloroform (δ 7.24 ppm for ^{1}H, δ 77.2 ppm for ^{13}C). *Cis*/*trans* ratios of the poly(NB)s were calculated by the integration ratios of each peak of ^{1}H NMR spectra, and meso/racemo ratios were estimated by peak separation of each peak

of ^{13}C NMR spectra using Lorentzian function on JEOL Delta v5.0.2 NMR software.

The molecular weight distributions (MWD) of the polymers were estimated on a size exclusion chromatography (SEC) (Tosoh HLC-8220 GPC; eluent tetrahydrofuran). The relative number- and weight-average molecular weights (M_n and M_w, respectively) were acquired using a calibration curve obtained with polystyrene standards.

II-3. Results and Discussion

II-3-1. Isospecific and Syndioselective ROMPs of Norbornene with Various W- and Mo-Based Catalysts

Table II-1 summarizes the results of the optimized NB polymerizations by various molybdenum- and tungsten-based catalysts and the following hydrogenations of the obtained poly(NB)s. **1**−**3** were activated by 3-fold of $Et_2Al(OEt)$, while 2-fold of *n*-BuLi was used as cocatalyst for **4**−**7**. At first, all the NB polymerizations were performed without chain transfer agent. Similar to the case of the ROMP of DCP by them, the polymerization mixtures became very viscous gels, and the following hydrogenation of the obtained poly(NB)s leveled off. Therefore, I decided to add 1-octene as a chain transfer agent in all the polymerization systems, for the purpose of keeping the molecular weights in the moderate range to hydrogenate them with ease.

Table II-1. Polymerization of NB by various catalysts and sequential hydrogenation of the obtained ring-opened poly(NB)s (The samples derived from **1** and **6** will be used for structural studies in the later chapters)

catalyst precursors		poly(NB)s			H-poly(NB)s
		M_n M_w/M_n (GPC)	$M_{n(absolute)}$ (NMR)	*cis/trans*	meso/racemo [c] mm/mr·rm/rr [c]
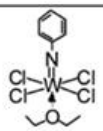	**1**[a]	21 700 2.2	17 800	85/15	10/90 11/17/100
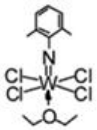	**2**[a]	13 500 1.7	10 800	89/11	8/92 6/12/100
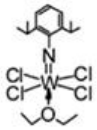	**3**[a]	5 800 1.8	4 100	67/33	30/70 31/39/100
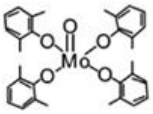	**4**[b]	50 900 2.4	23 100	30/70	50/50 61/100/51
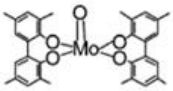	**5**[a]	8 200 2.1	5 600	80/20	78/22 100/24/17
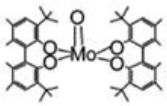	**6**[b]	34 300 5.2	23 400	100/0	100/0 100/0/0
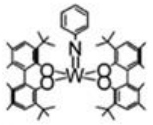	**7**[b]	6 400 1.6	5 200	90/10	89/11 100/12/10

(*a*) Polymerized in cyclohexane at 50 °C for 3h; [NB] = 20 wt % (2.12 M), [1-octene] = 106 mM, [W complex] = 2.12 mM, [W complex]:[$Et_2Al(OEt)$] = 1:3, all polymer yields were 100%. Hydrogenated in *p*-xylene at 125 °C for 5h; [*p*-Tos-$NHNH_2$]/[NB unit] = 4/1 in mol ratio, [poly(NB)] = 5 wt %, hydrogenation ratios for all polymers were 100%. (*b*) Polymerized in cyclohexane at 80 °C for 3h; [NB] = 20 wt % (2.12 M), [1-octene] = 53 mM, [Mo or W complex] = 2.12 mM, [W complex]:[n-BuLi] = 1:2, all polymer yields were 100%. Hydrogenated in *p*-xylene at 125 °C for 5 h; [*p*-Tos-$NHNH_2$]/[NB unit] = 4/1 in mol ratio, [poly(NB)] = 2.5 wt %, hydrogenation ratios for all polymers were 100%. (*c*) Tacticities were estimated based on ^{13}C NMR measurements in $C_2D_2Cl_4$ at 125 °C using Bruker Avance III HD 600 MHz spectrometer equipped with CRYO probe DCH 600S3.

The **1**−**7** induced the ROMP of NB smoothly to provide ring-opened poly(NB)s in quantitative yields under the presence of 1-octene. All the obtained poly(NB)s were highly soluble in ordinary organic solvents at room temperature. Therefore, the molecular weights of the poly(NB)s were characterized by the combination of ^{1}H NMR and SEC at 25 and 40 °C, respectively. It was found that the molecular weights of all the poly(NB)s were kept in the moderate range. Number average molecular weights M_n of the poly(NB)s acquired by SEC using polystyrene calibration were somewhat higher than absolute M_n measured by ^{1}H NMR.

II-3-2. Microstructures of the Synthesized Polymers

Next, microstructures of the obtained polymers were investigated. Ratios of *cis* junction of the double bonds of the main chain could be determined based on the splitting of vinyl proton by ^{1}H NMR measurements of poly(NB) (in $CDCl_3$ at 25 °C). On the other hand, it has already reported by Hamilton *et al*. that the tacticity of the poly(NB) could be determined only by ^{13}C NMR measurements of hydrogenated poly(NB)s [H-poly(NB)].[11] Therefore, the hydrogenation of the poly(NB)s was conducted in order to investigate tacticities of their hydrogenated products. The saturation of the polymer backbone proceeded fully by chemical transfer hydrogenation using *p*-Tos-$NHNH_2$. ^{13}C NMR spectra of the syndiotactic and the atactic-H-poly(NB)s were recorded in $CDCl_3$ at 60 °C, and those of all the H-poly(NB)s were recorded in $C_2D_2Cl_4$ at 125 °C. The selected ^{13}C NMR charts of methylene carbons C5,6 measured in $CDCl_3$ at 60 °C were described in Figure II-1(a), and those of methine carbons C1,4 and methylene carbon C7 in $C_2D_2Cl_4$ at 125 °C were described in Figure II-1 (b).

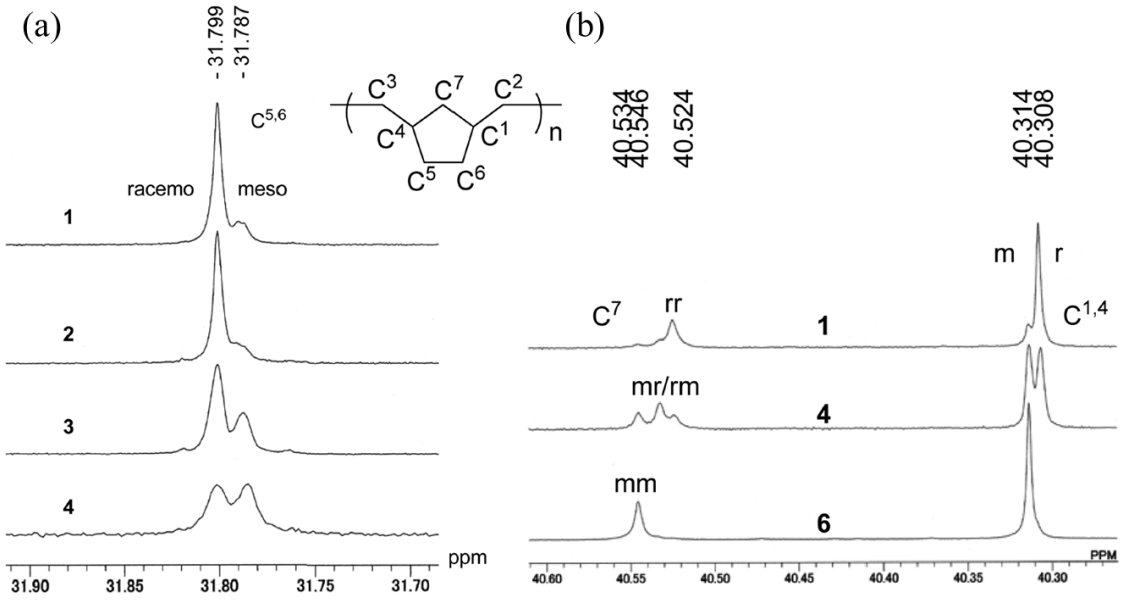

Figure II-1. Selected ^{13}C NMR spectra of (a) methylene carbons C5,6 (recorded in $CDCl_3$ at 60 °C, [H-poly(NB)] = 0.5 wt %.) and of (b) methylene carbon C7 and methine carbons C1,4 (recorded in $C_2D_2Cl_4$ at 125 °C, [H-poly(NB)] = 0.5 wt %) of H-poly(NB)s shown in Table II-1

As seen in Table II-1, it is noteworthy that W(=NPh)Cl_4·Et_2O (**1**) promoted *cis*-syndioselective ROMP of NB. The splitting of methylene carbons in Figure II-1a clearly suggested the formation of syndiotactic polymer. It is in contradiction to my expectation that Me-substituted version, W(=N-2,6-Me_2-Ph)Cl_4·Et_2O (**2**), was also verified to be a useful precatalyst for *cis*-syndioselective ROMP of NB; syndioselectivity of 2 is 92% and almost identical to that of **1**. Even W imido catalyst having relatively bulky isopropyl substituent, W(=N-2,6-i-Pr_2−Ph)Cl_4·Et_2O (**3**), yielded *cis*-syndio-biased polymer. In the case of DCP polymerization, syndioselectivity largely decreased with increasing the size of imido substitute.[4] Whereas stereoselectivity of NB polymerization by **1**−**3** seems to be less affected by steric demands of the substituent on the imido group. Molybdenum oxo

phenolate complex, MoO(2,6-Me_2-phenolate)$_4$ (**4**), afforded *trans*-rich and entirely atactic polymer (Figure II-1a). This result suggested that the 2,6-Me_2-phenolate ligand is not effective for the stereocontrol of the ROMP process of NB.

I have found that the syndiotactic and the atactic H-poly(NB)s were soluble in $CDCl_3$ at 60 °C to be relatively easily determined their meso/racemo ratios. In contrast, the H-poly(NB)s obtained from **5**−**7** were entirely insoluble at the same condition. In the early stage of this study, the tacticities of isotactic polymers could not be clearly observed by changing deuterated solvent, measuring temperature or polymer concentration. Finally, I have found that the methylene carbon C7 and the methine carbons C1,4 were resolved into triplet and doublet, respectively, in CD_2Cl_4 at 125 °C when cryoprobe was employed and measurement conditions were carefully optimized for gaining high resolution (Figure II-1b). Unfortunately, C5,6 carbons were resolved not into doublet but multiplet at the optimized condition. Therefore, at present I did not choose C5,6 carbons to determine tacticity. As seen in Figure II-1b, H-poly(NB)s obtained from **6** were isotactic. It is interesting to note that MoO(*rac*-Biphenolate)$_2$ (**6**) exhibited remarkable ability to regulate the polymerization process into *cis*-isospecific: the obtained poly(NB) had almost all-*cis* geometry, while isotacticity of the hydrogenated product was also almost 100%. ^{13}C NMR spectrum of the poly(NB) from **6** also suggests its highly regulated structure: all-*cis* geometry was verified and only four carbon peaks were observed. In contrast, ^{13}C NMR spectra of another poly(NB)s were complicated and not fully assignable. It is clarified that MoO(Me_4-biphenolate)$_2$ (**5**) promoted *cis*-isoselective ROMP of NB, however, the isotacticity of the obtained H-poly(NB) was moderate and around 80%. W(=NPh)((*R*)-(+)-Biphenolate)$_2$ (**7**) was verified to be the excellent catalyst

for *cis*-isoselective ROMP of NB. Its isoselectivity appeared to be around 90%. Therefore, biphenolate ligands were thought to be effective ligands for the isoselective ROMPs of NB.

II-3-3. Comparison of Stereospecific ROMPs of NB, DCP, and TCD

Scheme II-4 compares the stereocontrol of ROMPs of NB, dicyclopentadiene (DCP), and tetracyclododecene (TCD) by the present catalyst systems. It can be emphasized that the stereoselectivity of the present polymerization systems was highly dependent on the catalyst design and the monomer structure.

Scheme II-4. Summary of the stereocontrol of ROMPs of NB, DCP and TCD by the tungsten- and the molybdenum-based catalysts.

cat.	 cis/trans	m/r	 cis/trans	m/r	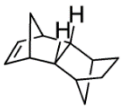 cis/trans	m/r
1	85/15	10/90	90/10	11/89	90/10	14/86
2	89/11	8/92	80/20	29/71	72/28	28/72
3	67/33	30/70	58/42	47/53	36/64	60/40
4	30/70	50/50	10/90	56/44	42/58	70/30
5	80/20	78/22	82/18	71/29	81/19	–
6	100/0	100/0	78/22	95/5	99/1	–
7	90/10	89/11	95/5	95/5	90/10	–

The catalysts derived from tungsten chloride with "small" imido ligand could regulate the enchainment reaction of NB, DCP and TCD into syndioselective. However, its ability for stereocontrol is likely to be limiting. Less steric NB yielded *cis*-syndiotactic poly(NB)s from **1** and **2**, while more steric tricyclic DCP also yielded *cis*-syndiotactic polymer only from **1**. In the case of sterically bulky TCD monomer, **1**-based catalyst introduced syndioselective ROMP, but its syndioselectivity was not very high. Syndioselectivity of NB polymerization with W-imidos seems to be less affected by steric demands of the imido group. Stereoselectivity of TCD polymerization with W-imidos appears to be largely influenced by steric bulkiness of the substituent on the imido group. From these results, one can say that syndioselectivity of the ROMPs by W imido-based catalysts decreases with increasing the steric demands of the imido group as well as of the monomer substituents. Since the propagation species generated from W imido complexes **1**−**3** would only have polymer asymmetry and no catalyst asymmetry at the metal or on the ligand, it is speculative that the syndioregularity might be derived mainly from chain end control/penultimate effect.

In contrast, molybdenum oxyphenolates **4**−**6** tend to induce the *cis*-isoselective ROMPs of these three monomers. Concerning *cis*-selectivity, catalyst **6** introduced all-*cis* polymerization of bicyclic NB and tetracyclic TCD, while low *cis*-selectivity for tricyclic DCP polymerization. This result suggests a possibility of the interaction between metal center and unsaturated bond of cyclopentene ring of approaching DCP or that of polymeryl group. Regarding the stereostructure, isoselectivity of the ROMP by **6** is 100% for NB and above 95% for DCP. **5** yielded iso-biased polymers of which isotacticities were rather low. **4**-based catalyst was ineffective for isoselective ROMP. Considering the

excellent study on the isospecific ROMPs of various monomers by Schrock catalysts,[12-20] it is assumable that the phenolate ligands of **4**−**6** such as racemic-5,5′,6,6′-tertamethyl-3,3′-di-tert-butyl-1,1′-biphenolate would remain on the metal after catalyst aging, and in turn, they would influence the polymerization process. The origin of the stereocontrol effect of Mo oxyphenolates can be explained by the idea that the effects from the phenolate ligands such as ligand asymmetry of bulky biphenolate might overwhelm the effect from the polymer asymmetry. As a consequence, the isoselectivity of the ROMPs by molybdenum oxyphenolate catalysts might come from catalyst control.

Catalyst precursor **7** is also a preferable instance to compare the effects of the ligand for the stereoregulation. Effects of terminal oxo and substituted imido for cis-selectivity and stereoselectivity are vague at this moment; terminal oxo type **6** is effective to attain all-*cis* polymerization of NB and TCD, while imido type **7** is evident to useful for highly *cis*-selective ROMP of DCP. With respect to stereoregularity, terminal oxo type **6** induced isospecific ROMP of NB (and TCD), while imido type **7** yielded less tactic polymers. However, both catalyst precursors proved to have almost identical ability for stereocontrol of ROMP of DCP. To compare the results by **1** and **7**, it can be said that the influences of the biphenolate ligand on the polymerization process could be compared favorably with that of the phenylimido ligand.

II-4. Conclusions

The isospecific and the syndioselective ROMPs of NB were precisely investigated using various W- and Mo-based catalysts. While W(=NPh)Cl_4·Et_2O (**1**) was a useful catalyst precursor for the syndioselective ROMP, MoO(*rac*-Biphenolate)$_2$ (**6**)-based catalysts were effective for the isospecific ROMP. By NMR measurements with well-optimized condition, the high stereoregularities in these polymers were confirmed; as high as 90% for syndiotactic and 100% for isotactic. Although the mechanisms of the stereoselective polymerizations of NB with the W- and Mo-based catalysts had not been completely clarified at the moment, I have considered that the steric structures of both catalysts and monomers would strongly affect the stereoregularity of the polymer chain. The polymerization process of less steric NB appears to be easily controlled by suitably designed catalyst, whereas larger effect from the catalyst may be necessary to govern the stereoselectivity of ROMP of more steric monomers such as DCP.

References

1. Rules, J. D.; Moore, J. S. ROMP Reactivity of *endo*- and *exo*-Dicyclopentadiene. *Macromolecules* **2002**, *35*, 7878-7882.
2. Hayano, S.; Kurakata, H.; Uchida, D.; Sakamoto, M.; Kishi, N.; Matsumoto, H.; Tsunogae, Y.; Igarashi, I. Stereospecific Ring-Opening Metathesis Polymerization of endo-Dicyclopentadiene by Schrock–Hoveyda Catalyst and Novel Mo- and W-based Complexes. Development of Crystalline Hydrogenated Poly(endo-dicyclopentadiene). *Chem. Lett.* **2003**, *32*, 670-671.
3. Hayano, S.; Kurakata, H.; Tsunogae, Y.; Nakayama, Y.; Sato, Y.; Yasuda, H. Stereospecific Ring-Opening Metathesis Polymerization of Cycloolefins Using Novel Molybdenum and Tungsten Complexes Having Biphenolate Ligands. Development of Crystalline Hydrogenated Poly(endo-dicyclopentadiene) and Poly(norbornene). *Macromolecules* **2003,** *36* (20), 7422-7431.
4. Hayano, S.; Tsunogae, Y. Syndiospecific Ring-opening Metathesis Polymerization of endo-Dicyclopentadiene by Tungsten(VI) Phenylimido Catalyst. *Chem. Lett.* **2005**, *34*, 1520.
5. Hayano, S.; Tsunogae, Y. Syndioselective Ring-Opening Metathesis Polymerization of endo-Dicyclopentadiene with Tungsten Complexes Having Imido Ligands: Development of Crystalline Syndiotactic Hydrogenated Poly(endo-dicyclopentadiene). *Macromolecules* **2006,** *39* (1), 30-38.
6. Hayano, S.; Sugawara, T.; Tsunogae, Y. Synthesis, characterization, and properties of crystalline poly(*endo*-dicyclopentadiene) resin made via cis- and isoselective bulk ring-opening metathesis polymerization. *J. Polym. Sci., Part A: Polym. Chem.* **2006**, *44*, 3153.
7. Hayano, S.; Takeyama, Y.; Tsunogae, Y.; Igarashi, I. Hydrogenated Ring-Opened Poly(endo-dicyclopentadiene)s Made via Stereoselective ROMP Catalyzed by Tungsten Complexes: Crystalline Tactic Polymers and Amorphous Atactic Polymer. *Macromolecules* **2006,** *39* (14), 4663-4670.
8. Hayano, S.; Tsunogae, Y. Stereoselective Ring-Opening Metathesis Polymerization by New Mo, W-based Catalysts-Development of Crystalline Hydrogenated Poly (endo-dicyclopentadiene). *Kobunshi Ronbunshu* **2011**, *68*, 199-209.

9. Hayano, S.; Tsunogae, Y. Japanese Laid-Open Patent Publication No. 137935, 2007.
10. Hayano, S.; Nakama, Y. Iso- and Syndio-Selective ROMP of Norbornene and Tetracyclododecene: Effects of Tacticity Control on the Hydrogenated Ring-Opened Poly(cycloolefin)s. *Macromolecules* **2014**, *47*, 7797-7811.
11. Al-Samak, B.; Ebrahimi, V. A.; Carvill, A. G.; Hamilton, J. G.; Rooney, J. J. Determination of the tacticity of ring-opened metathesis polymers of norbornene and norbornadiene by ^{13}C NMR spectroscopy of their hydrogenated derivatives. *Polym. Int.* **1996**, *41*, 85-92.
12. Schrock, R. R. Handbook of Metathesis; Grubbs, R. H., Ed.; Wiley-VCH: Weinheim, Germany, 2003; Vol. 1, pp 8−32 and references therein.
13. Schrock, R. R.; Hoveyda, A. H. Molybdenum and Tungsten Imido Alkylidene Complexes as Efficient Olefin-Metathesis Catalysts. *Angew. Chem., Int. Ed.* **2003**, *42*, 4592-4633.
14. Schrock, R. R. High Oxidation State Multiple Metal−Carbon Bonds. *Chem. Rev.* **2002**, *102*, 145-180.
15. Hoveyda, A. H.; Schrock, R. R. Catalytic Asymmetric Olefin Metathesis. *Chem. Eur. J.* **2001**, *7*, 945-950.
16. Buchmeiser, M. R. Homogeneous Metathesis Polymerization by Well-Defined Group VI and Group VIII Transition-Metal Alkylidenes: Fundamentals and Applications in the Preparation of Advanced Materials. *Chem. Rev.* **2000**, *100*, 1565-1604.
17. Totland, K. M.; Boyd, J. T.; Lavoie, G. G.; Davis, W. M.; Schrock, R. R. Ring Opening Metathesis Polymerization with Binaphtholate or Biphenolate Complexes of Molybdenum. *Macromolecules* **1996**, *29*, 6114-6125.
18. Schrock, R. R.; Lee, J.-K.; O'Dell, R.; Oskam, J. H. Exploring Factors That Determine Cis/Trans Structure and Tacticity in Polymers Prepared by Ring-Opening Metathesis Polymerizations with Initiators of the Type *syn*- and *anti*-$Mo(NAr)(CHCMe_2Ph)(OR)_2$. Observation of a Temperature-Dependent Cis/Trans Ratio. *Macromolecules* **1995**, *28*, 5933-5940.
19. O'Dell, R.; McConville, D. H.; Hofmeister, G. E.; Schrock, R. R. Polymerization of Enantiomerically Pure 2,3-Dicarboalkoxynorbornadienes and 5,6-Disubstituted Norbornenes by Well-Characterized Molybdenum Ring-Opening

Metathesis Polymerization Initiators. Direct Determination of Tacticity in Cis, Highly Tactic and Trans, Highly Tactic Polymers. *J. Am. Chem. Soc.* **1994**, *116*, 3414-3423.

20. McConville, D. H.; Wolf, J. R.; Schrock, R. R. Synthesis of Chiral Molybdenum ROMP Initiators and All-Cis Highly Tactic Poly(2,3-$(R)_2$norbornadiene) (R = CF_3 or CO_2Me). *J. Am. Chem. Soc.* **1993**, *115*, 4413-4414.

Chapter III: Crystal Structures of Stereoregular Hydrogenated Ring-Opened Poly(norbornene)s

III-1. Introduction

As reported in the Chapter II, I have succeeded to synthesize the highly isotactic and syndiotactic H-poly(NB)s for the first time. These polymers have been found to be crystalline. It should be a good chance to know the influence of tacticity on the crystal structure of H-Poly(NB)s.

In the present chapter, I have studied the thermal behavior and the crystal structures of isotactic and syndiotactic H-poly(NB)s as well as those of the atactic H-poly(NB) for comparison. These information will tell us the influence of the stereoregularity on the chain conformation and chain packing mode of poly(NB) having the cyclopentylene rings in the polymer skeletons.

III-2. Experimental Section

III-2-1. Samples

Syndiotactic and isotactic H-poly(NB)s were synthesized by the same procedures as those reported in Chapter II. Basic characterization data of H-poly(NB)s with the various stereoregularities are shown in Table III-1. The *meso*/*racemo* ratio of H-

poly(NB) determined by the ^{13}C-NMR analysis were 10/90 for syndiotactic, 100/0 for isotactic and 53/47 for atactic H-poly(NB).

The polymer films of ~0.2 mm thickness were prepared by the hot pressing *in vacuo* at 200 ºC followed by the slow cooling to room temperature. The uniaxially-oriented samples for the X-ray crystal structure analyses were prepared by stretching the hot-pressed films about three times the original length and annealing in oil bath at 135 ºC for two hours with the fixed length.

Table III-1. Hydrogenated ring-opened poly(NB) samples with different tacticity

Tacticity	M_n [a]	M_w/M_n [a]	*meso*/*racemo* [b]	T_m (°C) [c]	ΔH_m (J/g)
Syndiotactic	22k	2.2	10/90	134.1	56.0
Isotactic	34k	5.2	100/0	177.7	48.3
Atactic	134k	1.8	53/47	147.9	56.1

[a] M_n and M_w were determined by the SEC measured before hydrogenation. [b] *meso*/*racemo* ratio was determined on the basis of the ^{13}C NMR spectra of hydrogenated samples. [c] The peak melting temperature T_m and the enthalpy of melting ΔH_m were analyzed using the DSC data measured at the rate of 10°C/min.

III-2-2 Measurements

The differential scanning calorimetry (DSC) measurements were performed with an SII NanoTechnology X-DSC7000 under dry nitrogen gas flow. The samples were heated to the temperature region about 40 °C higher than their individual melting point,

then the DSC data were recorded in the processes of cooling to 25 °C and heating to the melting temperature at the rate of 10 °C/min.

A Rigaku RINT X-ray diffractometer with Cu-Kα X-ray beam (wavelength λ = 1.542 Å) was used for the WAXD measurement of the unoriented films. The temperature dependences of 1D WAXD profiles were measured for the unoriented samples using a Rigaku TTR X-ray diffractometer, by which both the WAXD profile and thermal data were collected simultaneously at the heating and cooling rates of 5 °C /min. The incident X-ray beam was Cu-Kα line of wavelength 1.542 Å.

The 2-dimensional WAXD patterns of the uniaxially-oriented films were measured using a Rigaku R-Axis Rapid II X-ray diffractometer with a graphite-monochromatized Mo-Kα beam (λ = 0.711 Å). A cylindrical imaging plate with the camera radius of 127.4mm was used as the 2-D detector. The sample strip was set on a goniometer head vertically so that the drawing axis aligns in parallel to the cylindrical axis of the camera. The temperature dependences of 2D-WAXD patterns were measured by setting a uniaxially-oriented sample rod into a home-made brass heater placed in the diffractometer.

Density measurement was conducted with a helium gas displacement pycnometer AccuPyc 1340 (Micrometrics) at 25 °C.

III-3. Results and Discussion

III-3-1. Thermal Properties of Tactic H-Poly(NB)s

The DSC thermograms measured for these samples are shown in Figure III-1. All these H-poly(NB)s showed the clear melting and crystallizing behaviors. The melting point T_m was 134.1 °C for syndiotactic species, 177.7 °C for the isotactic species, and 147.9 °C for atactic H-poly(NB). The last one is slightly higher than the previously reported value (143 ºC).[1] It is noticed that the T_m of the syndiotactic species is lower than that of the isotactic and even the atactic species. The similar behavior was reported for the H-poly(DCP) sample, where the T_m of the isotactic species 293°C is higher than that of the syndiotactic one, 270 °C.[2,3] The difference of the melting temperatures between the 3 types of polymers is originated from the difference of the stereoregularity and so the difference in the crystal structure, as will be described in a later section. The heat of fusion was not largely different among these three polymer samples (cf. Table III-1), implying the similar degree of crystallinity among them.

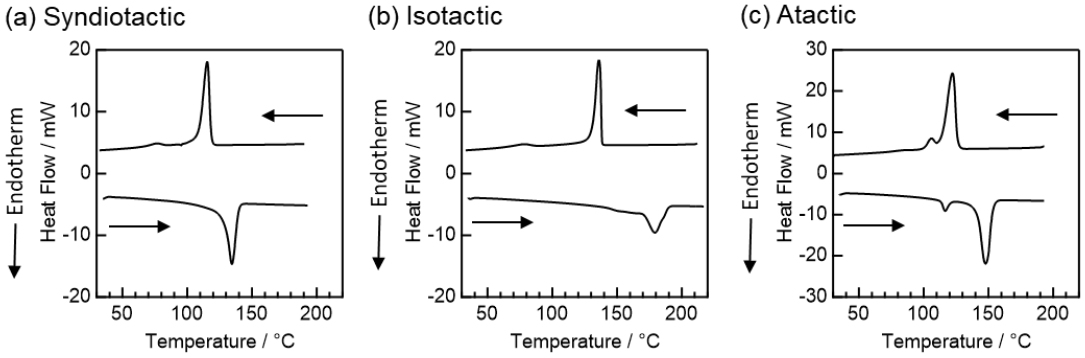

Figure III-1. DSC thermograms measured for the as-pressed film samples of (a) syndiotactic, (b) isotactic and (c) atactic H-poly(NB). The heating and cooling rate were 10°C/min.

In the DSC thermogram of the atactic polymer, a small endothermal peak was detected at 117 °C before the melting in the heating process, which was assigned to the phase transition from the monoclinic crystal of the ordered structure to the pseudohexagonal structure of the rotational disordering of the chains, although the transition temperature is affected more or less by the meso content (101 °C for the *meso* 44% and 120°C for the *meso* 54%).[4,5] In the case of the isotactic sample, also, a broad shoulder is detected at around 150 °C before the melting, which may correspond to the phase transition. The syndiotactic sample does not show this type of endothermic peak, indicating no phase transition. In addition, for the isotactic and syndiotactic samples, I notice a small endothermic peak at around 80 °C in the cooling process from the melt. The origin of this peak cannot be identified at present.

III-3-2. X-ray Diffraction Patterns of Unoriented H-poly(NB)s

Figure III-2 shows the 1D-X-ray diffraction profiles measured for the melt-pressed unoriented H-poly(NB) samples of the three different tactic types at room temperature. The profiles are remarkably different among these samples, reflecting the difference in the crystal structure as will be revealed in a later section. The broad peak overlapping with the main crystalline peaks at around $2\theta = 18^{o}$ is the amorphous halo. The degree of crystallinity estimated from the ratio of the integrated intensity between the crystalline and amorphous peaks was about 48% for syndiotactic species, 42% for the isotactic species and 68% for the atactic sample. In this way, the tacticity of H-poly(NB) is found to give the large influence on the crystal lattice structure.

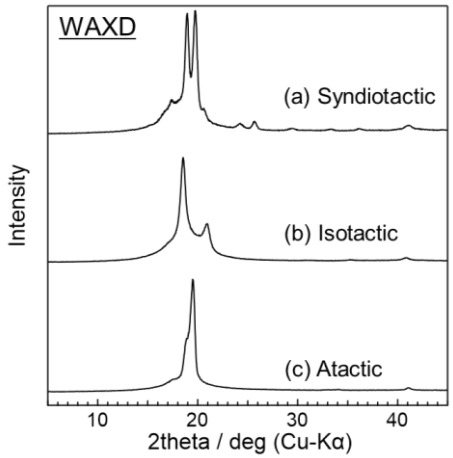

Figure III-2. WAXD profiles of the as-melt-pressed polymer films of (a) syndiotactic, (b) isotactic and (c) atactic H-poly(NB) at room temperature. Cu-Kα X-ray beam (λ = 1.542 Å) was used.

In order to check any possibility of phase transition, the 1D-WAXD profiles were measured for the unoriented samples in the heating and cooling processes. The results are shown in Figure III-3. The plots of the lattice spacings (*d*-spacings) calculated from the WAXD peak positions are shown in Figure III-4. In the case of isotactic H-poly(NB), the two peaks were detected at 2θ = 18.3° and 21.5° at room temperature. As the temperature was increased, these peaks shifted to the lower 2θ side. At around 120 - 130°C, these peaks disappeared, and the new three peaks started to appear at 17.3°, 18.9° and 20.6°. In the molten state these peaks disappeared to give a broad halo peak of the melt. Once the sample was cooled, the two types of peaks were detected with overlapping. At room temperature, the peaks of the original low temperature (LT) phase were stronger, although the high temperature (HT) peak components were still detected. In the case of atactic H-poly(NB), the two peaks observed at room temperature changed into a singlet above 120°C, which appeared again in the cooling process from the melt. The syndiotactic H-

poly(NB) sample did not give any remarkable change of WAXD profile in both the heating and cooling processes. In this way, we can assign the small DSC peaks detected in Figure III-1 to the crystal phase transitions between the LT and HT phases for isotactic and atactic H-poly(NB) samples, respectively. The transition behavior observed for atactic H-poly(NB) is almost same as that reported in references 4 and 5. No phase transition was revealed for syndiotactic H-poly(NB), where the assignment of a small DSC peak in the cooling process from the melt, as shown in Figure III-1 (a) is not known at present, though a possibility of appearance of any other crystal modification might be there.

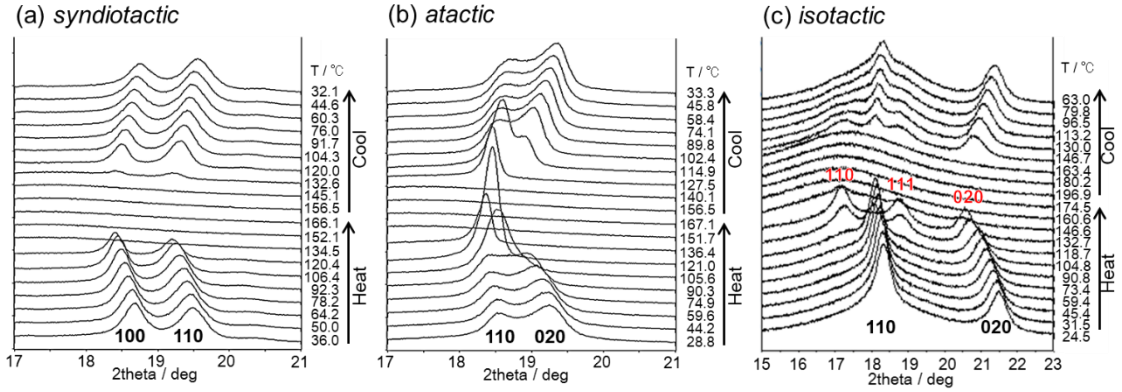

Figure III-3. Temperature dependence of the WAXD profiles measured for the unoriented samples: (a) syndiotactic, (b) atactic and (c) isotactic H-poly(NB)s. The heating and cooling rates were 5°C/min.

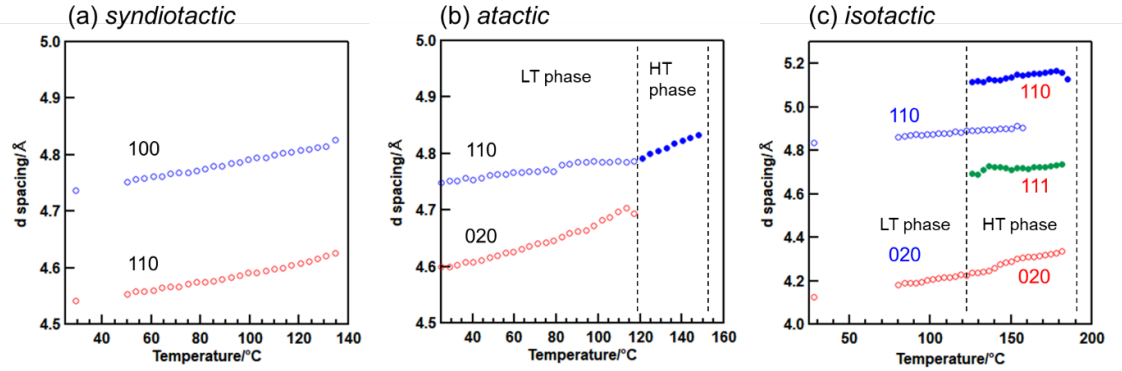

Figure III-4. Plots of *d*-spacings against temperature for (a) syndiotactic, (b) atactic and (c) isotactic H-poly(NB)s (heating process).

III-3-3. Comparison of the 2D X-ray Diffraction patterns of the oriented samples

Figure III-5 shows the 2-dimensional X-ray diffraction patterns of the uniaxially-oriented and annealed samples taken at room temperature. They gave the sharp spots along the many layer lines, indicating the existence of the highly-developed crystallites with the high degree of orientation. The total numbers of the detected diffraction spots were 49, 39 and 14 for the syndiotactic, isotactic and atactic H-poly(NB), respectively. At glance, these diffraction patterns look similar to each other, but the detailed analysis has revealed the remarkable difference in the structural characteristics as described below.

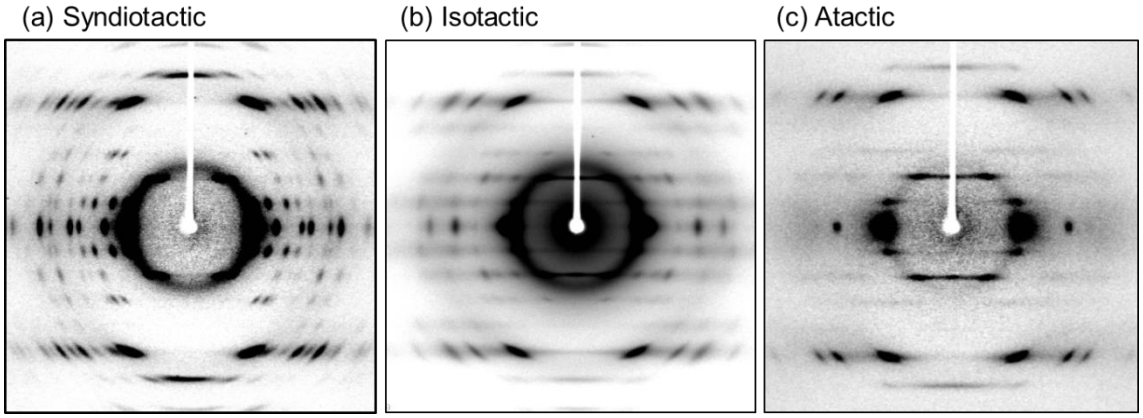

Figure III-5. 2-dimensional WAXD patterns of uniaxially-oriented films of (a) syndiotactic, (b) isotactic and (c) atactic H-poly(NB), which were collected on the cylindrical imaging plate.

Their repeating periods along the chain axis, calculated from the spacings between the layer and equatorial lines using Polanyi's equation,[6] were about 12.5 Å. This value is close to 12.67 Å or five times of the fiber period of planar-zigzag polyethylene crystal (2.534 Å).[7] I can assume that the chains of H-poly(NB) in the crystal cell take almost planar zigzag conformation. A small difference of 0.17 Å between those values

may be attributed to the slight deviation from the complete *trans*-zigzag conformation due to the distorting effect by the cyclopentylene ring structures. In the X-ray diffraction patterns of the isotactic and atactic samples, some streaks are detected along the layer lines. They might come from the disorder in the relative height of the neighboring chains along the *c* axis. On the other hand, the chains of syndiotactic polymer are considered to have a highly-ordered packing structure in the crystal lattice, as judged from the sharp WAXD pattern.

Figure III-6 shows the temperature dependence of 2D-WAXD pattern measured for a uniaxially-oriented isotactic H-poly(NB) sample. The WAXD pattern at room temperature is that of the low-temperature (LT) phase. The clearly-detected strong layer line corresponds to the repeating period 2.5 Å of the *trans*-zigzag chain conformation. In the vicinity of 150°C, the new pattern started to overlap with the original one, and it increased the intensity gradually. The 2D-WAXD pattern at 170 °C is that of the high-temperature (HT) phase. Meridional diffraction peaks appeared strongly. The higher layer lines became weaker, though the heights of the layer lines did not change detectably. It must be noted that the high degree of crystallite orientation was kept even at high temperatures. As seen in Figure III-6, the WAXD pattern obtained by cooling from the HT phase to room temperature was kept unchanged when the sample was tensioned.

Figure III-7 shows the 2D-WAXD patterns of a uniaxially-oriented atactic H-poly(NB) sample at low and high temperatures. The WAXD pattern at room temperature is similar to that of isotactic-H-poly(NB). The layer lines consist of the spot-like Bragg peaks and horizontal streaks. The whole pattern at 127 ^{o}C did not change from that at 27 ^{o}C, but the strong layer line corresponding to the repeating period 2.5 Å became weak

and diffused. However, the characteristic zigzag pattern was still kept, though the streak lines became more remarkable. Opposite to the layer lines, the equatorial line profile became clearer, and the higher-angle peak became sharper and stronger, as shown in Figure III-7 (c). The Bragg peaks on the second layer line became relatively stronger and spot-like.

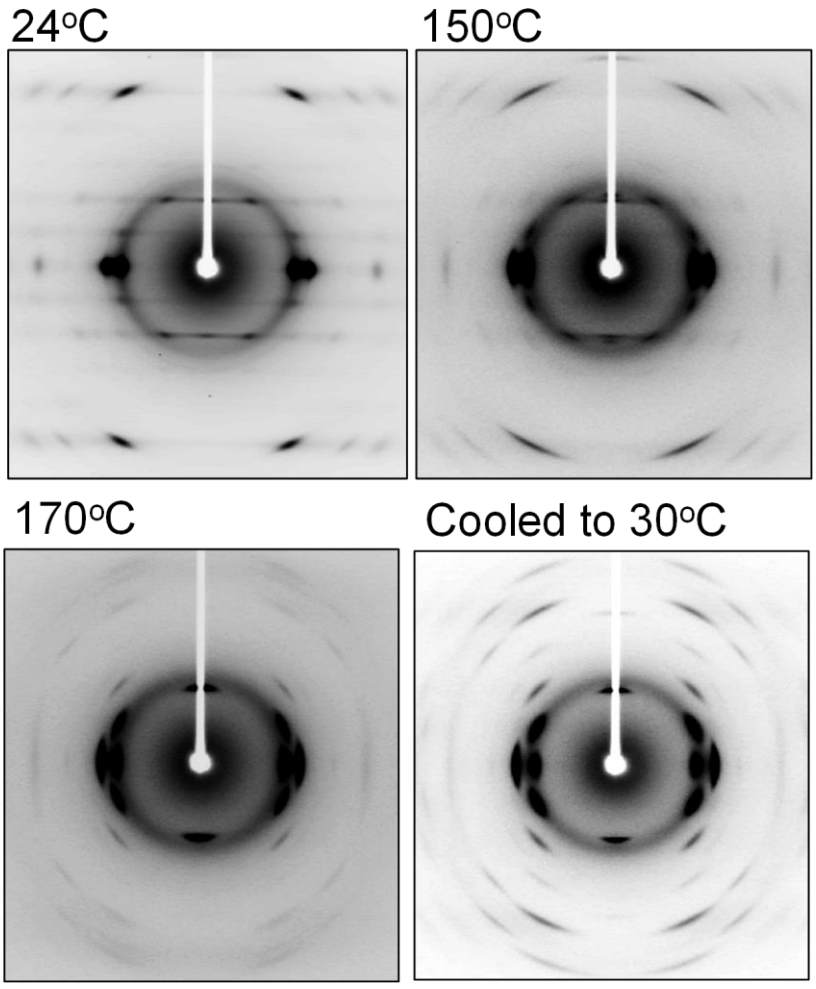

Figure III-6. 2D WAXD patterns measured for uniaxially-oriented isotactic-H-poly(NB) measured in the heating process: 24 °C, 150 °C and 170 °C, and after cooled to 30 °C. The draw axis is vertical.

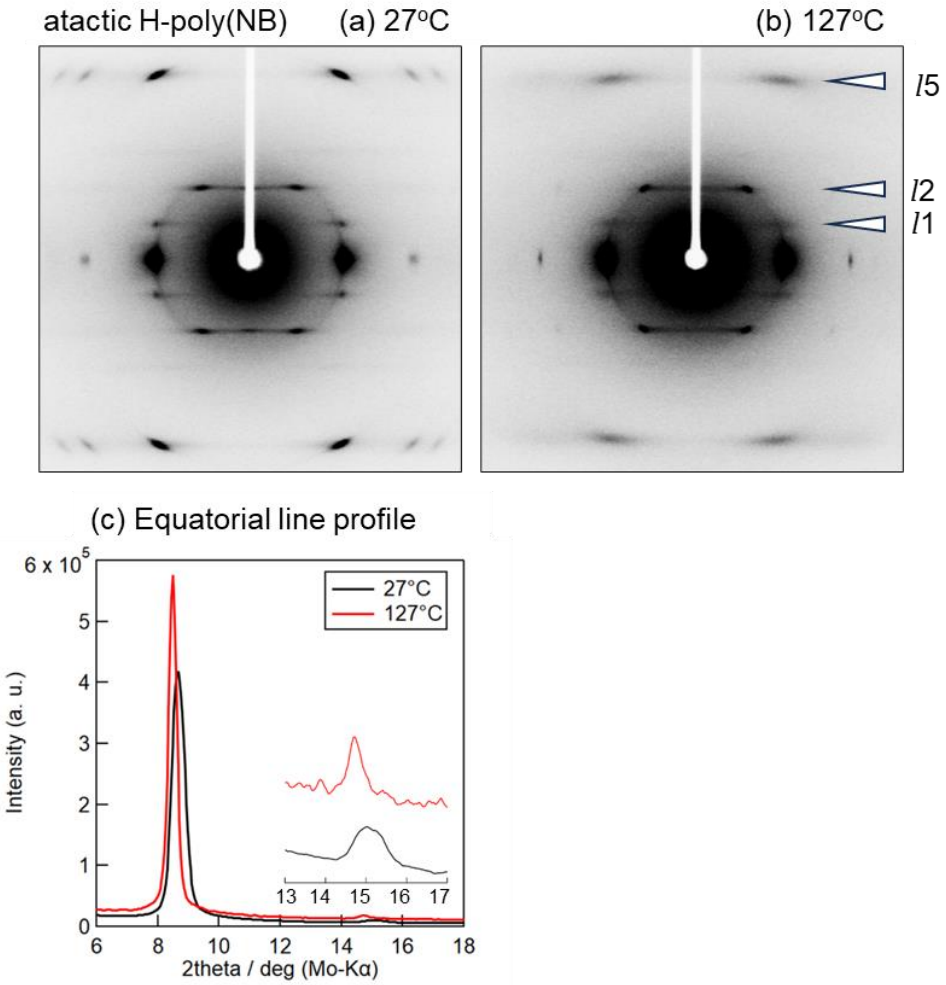

Figure III-7. 2-D WAXD patterns for uniaxially-oriented atactic H-poly(NB) in the heating process. (a) 27°C and (b) 127°C. (c) The equatorial line profiles taken from the 2-D WAXD data.

III-3-4. Crystal Structure Analysis of Syndiotactic H-Poly(NB)

At first, the vertical spacings between the equatorial line and the individual layer lines were measured, from which the repeating period along the chain axis was estimated. The repeating period was 12.58 ± 0.09 Å for the syndiotactic H-poly(NB). As mentioned

above, this value corresponds to the sequence of the 10 CH_2 units contained in the all-*trans* planar-zigzag polyethylene chain.

The other unit cell parameters were determined by following the procedures described in the literature.[6,8] The (x, y) coordinates of the individual diffraction peaks were read out on the 2-D X-ray diffraction pattern, and they were converted to the cylindrical (ξ, ζ) coordinates of the reciprocal lattice. The a^*, b^*, and γ^* were determined using the ξ values of all the observed peaks on all the layer lines with the different ζ values. The α^* and β^* angles were determined from the shifts of the origins of the reciprocal lattice planes with the different ζ values. All of the observed reflections were successfully indexed using the monoclinic unit cell with the following parameters: a^* = 0.137 $Å^{-1}$, b^* = 0.0750 $Å^{-1}$, c^* = 0.0652 $Å^{-1}$, and β^* = 120.0°. The corresponding real unit cell parameters are a = 5.97 Å, b = 9.48 Å, c (chain axis) = 12.58 ± 0.09 Å and β = 60.0 °. Table III-S1 in Appendix III-1 shows the *hkl* indices and the corresponding lattice spacings of the observed diffraction peaks in comparison with the calculated values.

By referring to the observed density (0.99 g/cm^3), the two chains were assumed to be packed in the monoclinic unit cell, where the calculated crystal density was 1.04 g/cm^3. The energetically reasonable chain packing modes were searched by performing the packing energy calculation using a commercial software Cerius^2 (version 4.10, Biovia). The energy optimization was performed starting from the planar zigzag chain model by fixing the repeating period to 12.58 Å, where the molecular mechanics method was used with the potential functions of COMPASS force field.[9] The various space groups were selected by referring to the indices of the observed diffraction peaks (Table III-S1 in Appendix III-1). The chain packing structure models, which were created under

these space group symmetries, were modified in a trial-and-error method so that the observed diffraction profiles were reproduced as well as possible for all the layer lines. Figure III-8 shows the thus-obtained most plausible crystal structure model with the space group $P2_1/c$. Figure III-9 shows the comparison of the observed diffraction profiles with those calculated along the various typical layer lines, where the parameters of the crystallite sizes 100 Å × 100 Å × 100 Å and the crystal strains 0% × 0% × 0% along the *a*, *b* and *c* axes, respectively, and the isotropic temperature factor of C atoms 10 $Å^2$ were assumed in the calculation. The calculated 2-D WAXD pattern is compared with the observed data in Figure III-10. The agreement of the diffraction profile between the observed and calculated ones is fairly good for most of the layer lines, although the relative intensity of the several calculated peaks (for example, 121 diffraction) was to some extent different from the observed ones. To evaluate the degree of agreement between the observed and calculated intensities, the *R* factor was estimated from the integrated intensity of the separated 42 reflection peaks along the equatorial ($l = 0$) to the 6th layer lines. The *R* factor is defined as

$$R = \Sigma|I(\text{obs}) - I(\text{calc})|/\Sigma I(\text{obs}) \text{ x } 100\% \qquad \text{(III-1)}$$

where I(obs) and I(calc) are the observed and calculated diffraction intensities, respectively. The thus-estimated *R* factor was 15.1%. The atomic fractional coordinates are given in Table III-S2 in Appendix III-1. In the present structure analysis, the chain conformation was fixed to the energetically minimized form. The better agreement between the observed and calculated diffraction profiles might be realized by modifying the above structure model furthermore.

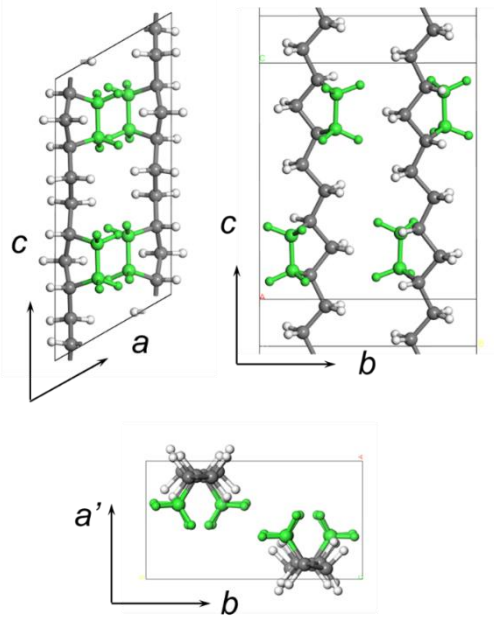

Figure III-8. Crystal structure of syndiotactic H-poly(NB). The lattice parameters are *a* = 5.97 Å, *b* = 9.48 Å, *c* (repeating period) = 12.58 Å and β = 60.0 °. *a*' = *a* sin(β) = 5.17 Å. The side chains are shown in green color.

As seen in Figure III-8, the skeletal chain takes the zigzag form similar to the polyethylene chain. The two cyclopentylene rings are formed along the chain axis as indicated by green color. The cyclopentylene ring takes a so-called puckering form, in which one CH_2 unit is deviated from the coplane formed by the other four C atoms. In other words, the two CH_2 units are out of the zigzag plane formed by the planar-zigzag skeletal chain, as indicated by the green color. As seen in the *a'b*-plane structure viewed along the chain axis, these green-colored CH_2 units of the cyclopentylene rings are excluded from the skeletal plane *to the same side* because of the existence of the *ac*-glide plane cutting the skeletal zigzag plane into two. The two zigzag chains are related by the 2_1 screw axis along the *b* axis as well as by the point of symmetry located at the center of the unit cell. The green-colored side groups of the rings form a kind of the layer along the

b axis, and these layers are repeated along the *a* axis. The relative height of cyclopentylene rings between the neighboring chains is almost the same along the *c* axis.

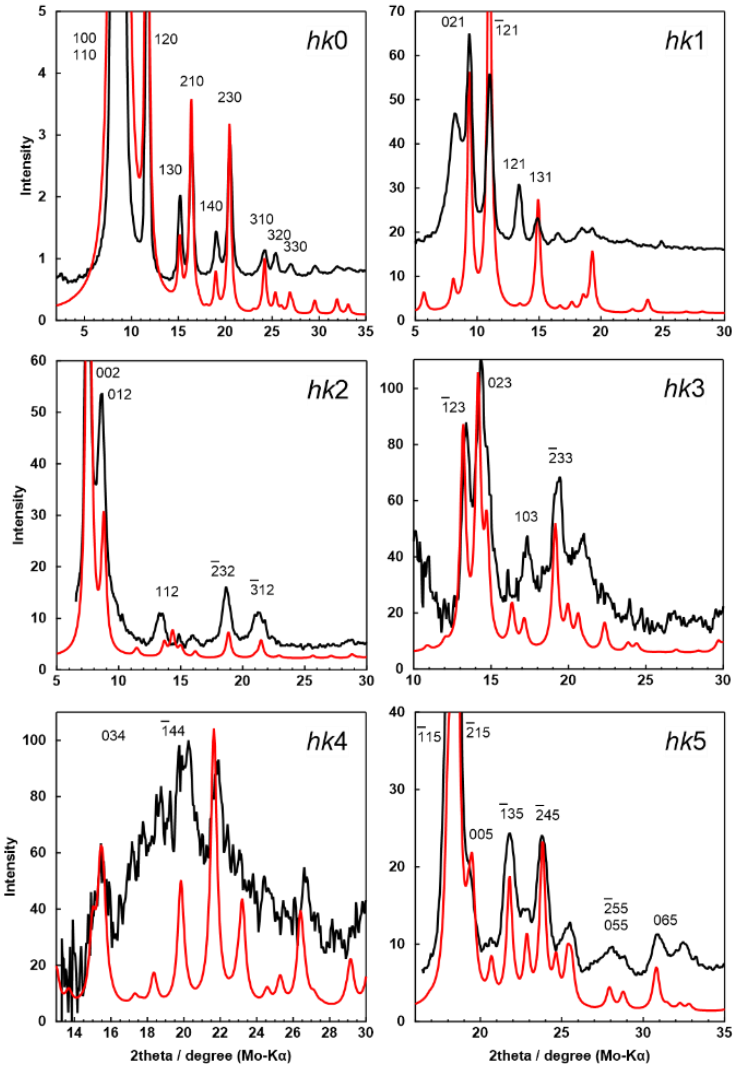

Figure III-9. The X-ray diffraction profiles of syndiotactic H-poly(NB) observed (black) along the layer lines (*hk*0 to *hk*5) in comparison with those calculated (red) for the proposed crystal structure.

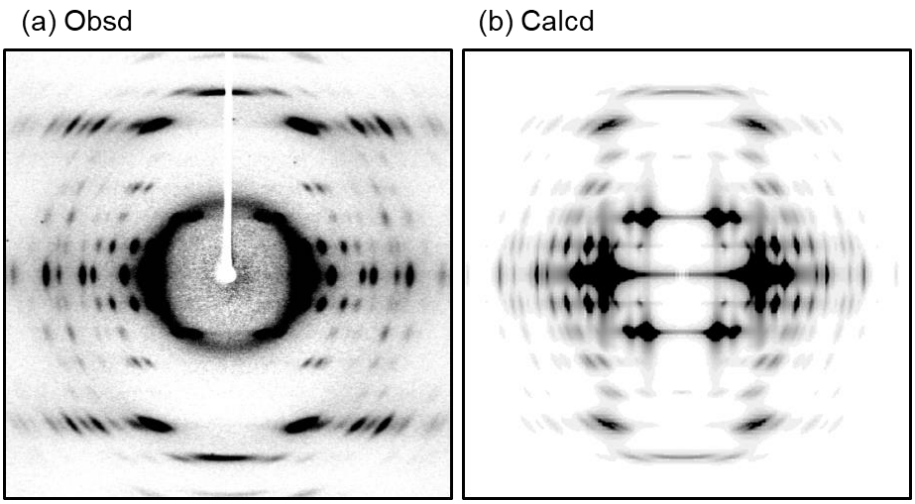

Figure III-10. (a) The observed and (b) calculated 2-D WAXD patterns of the uniaxially-oriented syndiotactic H-poly(NB). The incident X-ray beam is Mo-Kα.

III-3-5. Crystal Structure Analysis of Isotactic H-Poly(NB)

(a) LT (Low Temperature) Phase

By analyzing the 2D X-ray diffraction pattern of the uniaxially-oriented sample of isotactic H-poly(NB) at room temperature, shown in Figure III-2 (b), the unit cell was determined to be of the orthorhombic system with a = 5.95 Å, b = 8.25 Å, c (repeating period) = 12.65 ± 0.19 Å. After many trial-and-error processes, the most plausible space group is $P2_12_12_1$. The two chains are contained in the unit cell, which are related by the 2_1 screw symmetry. The density calculated for this unit cell is 1.02 g/cm^3 in comparison with the observed bulk density 0.99 g/cm^3.

Table III-S3 in Appendix III-1 shows the indices and the lattice spacing of the observed diffraction peaks. The most plausible packing structure, derived after the trial-and-error calculations of the diffraction profiles, is shown in Figure III-11. The atomic

fractional coordinates are given in Table III-S4 in Appendix III-1. Figure III-12 compares the observed diffraction profiles along the layer lines with the calculated ones. The comparison between the observed and calculated 2-D X-ray diffraction patterns is shown in Figure III-13, where the following parameters were assumed for the crystallite size 60 Å × 60 Å × 60 Å, the crystal strain 0.5% × 0.5% × 0.5%, the isotropic temperature factor for C atoms 15 $Å^2$, and the degree of chain orientation 3.0°. The observed diffraction data are reproduced well as a whole. The *R* factor calculated from the integrated intensity of the separated 21 reflection peaks on *hk*0, *hk*1, *hk*2 and *hk*5 layer lines was 23.6%.

As seen in Figure III-11, the conformation of the skeletal chain is essentially the same as that of syndiotactic chain. The two cyclopentylene rings (side group) are attached alternately on the right and left sides of the skeletal plane and related by the 2_1 helical axis passing through the center of the chain. The zigzag skeletal planes of the adjacent chains are aligned approximately in a herringbone mode, just like the chain packing of the orthorhombic polyethylene.[7] There may be some disorder in the relative height along the *c* axis, causing the weak streaks as seen in the 2-D X-ray diffraction pattern (Figure III-13 (b)).

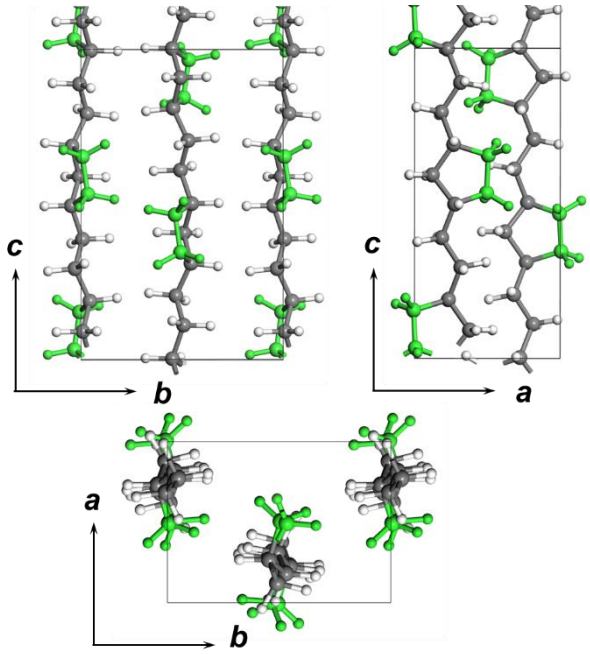

Figure III-11. Crystal structure of isotactic H-poly(NB) in the LT phase. The lattice parameters are a = 5.95 Å, b = 8.25 Å, c (repeating period) = 12.65 Å. The space group is $P2_12_12_1$. The side chains are shown in green color.

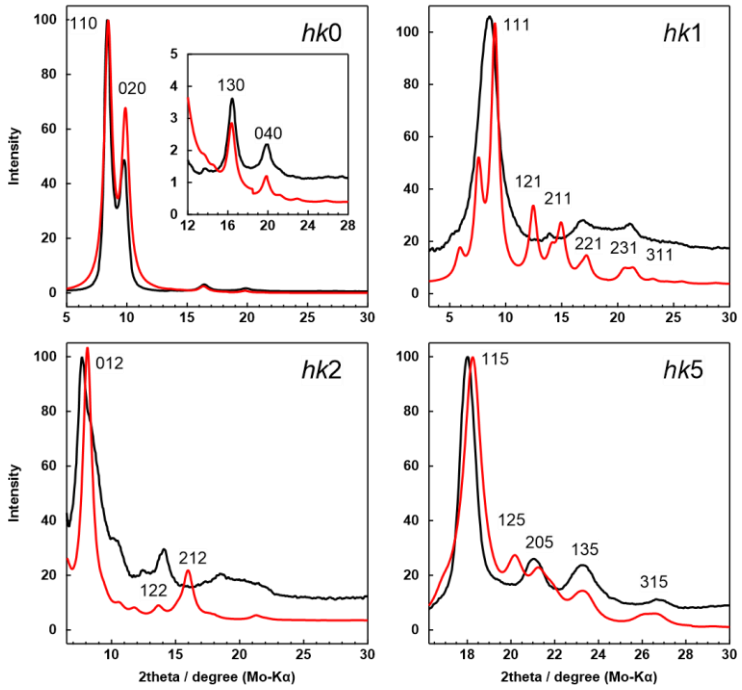

Figure III-12. The X-ray diffraction profiles along the layer lines *hk*0, *hk*1, *hk*2 and *hk*5 observed (black) for isotactic H-poly(NB) in the LT phase, compared with those calculated (red) for the proposed crystal structure.

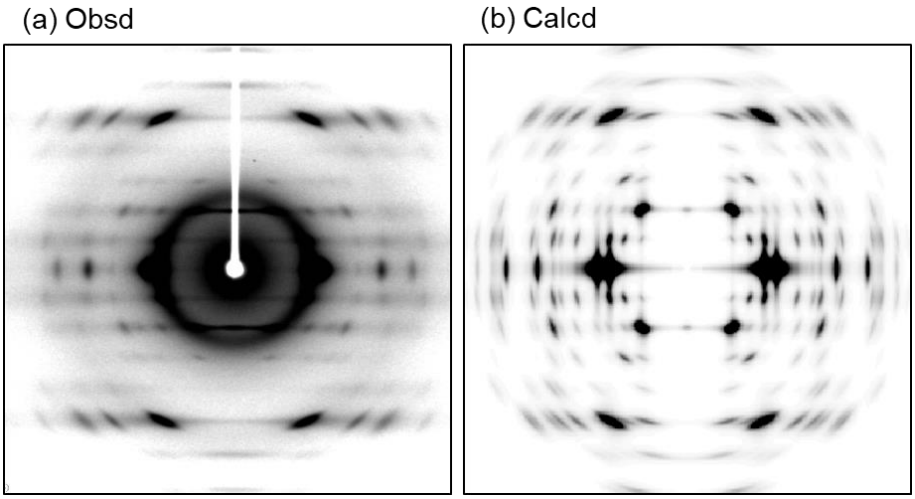

Figure III-13. (a) The observed and (b) calculated 2-D WAXD patterns of the uniaxially-oriented isotactic H-poly(NB) in the LT phase. The incident X-ray beam is Mo-Kα.

(b) HT (High Temperature) Phase

As mentioned above, the HT phase of isotactic-H-poly(NB) was reserved even after cooled to room temperature if the oriented sample was constrained by applying a tensile force along the draw direction. Since the layer lines are clearer compared with those detected at high temperature, and the diffraction pattern itself was not essentially changed at all, the crystal structure analysis of the HT phase was performed using the data of the HT phase after cooled to room temperature. The repeating period along the chain axis was 11.20 Å as estimated from the interlayer spacings. The repeating period is contracted by 11 % from the fully-extended zigzag form, 12.65 Å. The Ring-CH_2-CH_2-Ring segmental parts can change their conformations by the torsional angle changes. But the possible models to explain the above-mentioned shorter repeating period are limited. The two most plausible models were built by introducing the *gauche* bonds as shown in Figure III-14. This idea is consistent with the model proposed by the NMR data analysis.[11] In fact, the above-mentioned repeating period can be reproduced using the *gauche*-containing model. However, the thus-built-up chain conformation was found to be remarkably different depending on the configuration of isotactic-poly(NB) chain. In the present case, the carbon atoms of (*S*) and (*R*) configurations are repeated along the molecular chain. The introduction of $G\bar{T}G$ sequence to C*(*S*)-CH_2-CH_2-C*(*R*) segment causes the appreciably bent chain form as shown in Figure III-14 (2). On the other hand, the $\bar{G}TG$ sequence gives the flat shape of large-zigzag-form as shown in Figure III-14 (1). [It must be noticed that the molecular chain having the opposite sequence of C*(*R*)-CH_2-CH_2-C*(*S*) must take the torsional angles of $G\bar{T}G$.]

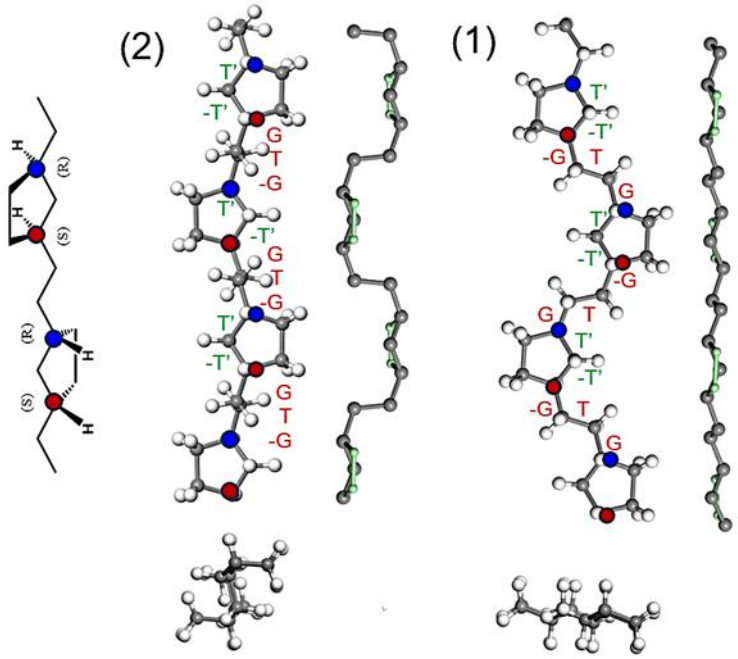

Figure III-14. Two conformation models of isotactic H-poly(NB) HT phase built by introducing $\bar{G}TG$ (model 1) and $GT\bar{G}$ (model 2) sequences for C*(*S*)-CH_2-CH_2-C*(*R*) segment. The small red and blue circles indicate the (*S*) and (*R*) carbon atoms, respectively.

These chain models were packed in the unit cell. The X-ray data analysis revealed the unit cell parameters of a = 6.50 Å, b = 8.62 Å, and c (chain axis) = 11.60 Å at 170 °C, and a = 6.65 Å, b = 8.24 Å, and c (chain axis) = 11.20 Å at 30 °C. The latter values were used in the present analysis, as mentioned above. After many trial-and-error calculations, model-2 could not reproduce the observed X-ray data at all for any possible space groups. On the other hand, the packing structure of model-1 chains with the space group $P2_12_12_1$ was found to be the most plausible candidate for the good reproduction of observed X-ray data. This space group is the same as that of the low-temperature phase. The packing structure is shown in Figure III-15. The calculated WAXD profiles along the several layer lines are compared with the observed data, as shown in Figure III-16. The

2D-WAXD pattern is compared between observed and calculated ones in Figure III-17, where the parameters used were as follows: the crystallite size, a = 100 Å, b = 100 Å, and c = 100 Å; the crystal lattice strain a = 0 %, b = 0 %, and c = 1 %; the isotropic temperature factor = 10 Å^2, and the degree of chain orientation 4°. The R factor was estimated to be 12% for all the observed 24 peaks. The atomic fractional coordinates are listed in Table III-S5 in Appendix III-1.

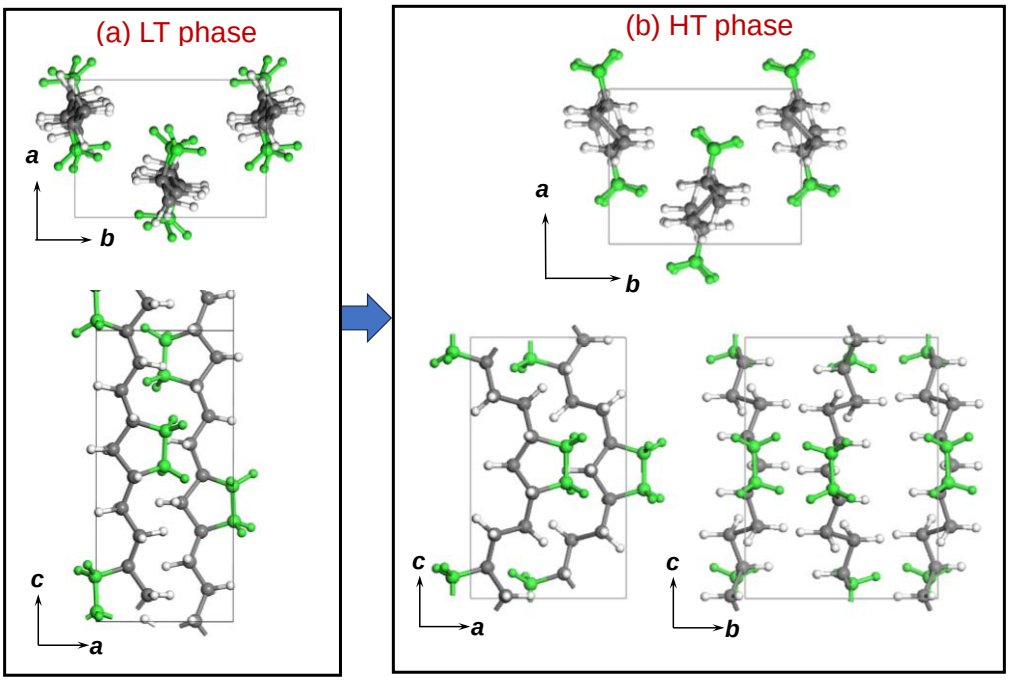

Figure III-15. Crystal structures of isotactic-H-poly(NB): (a) the LT phase and (b) the HT phase (30 °C).

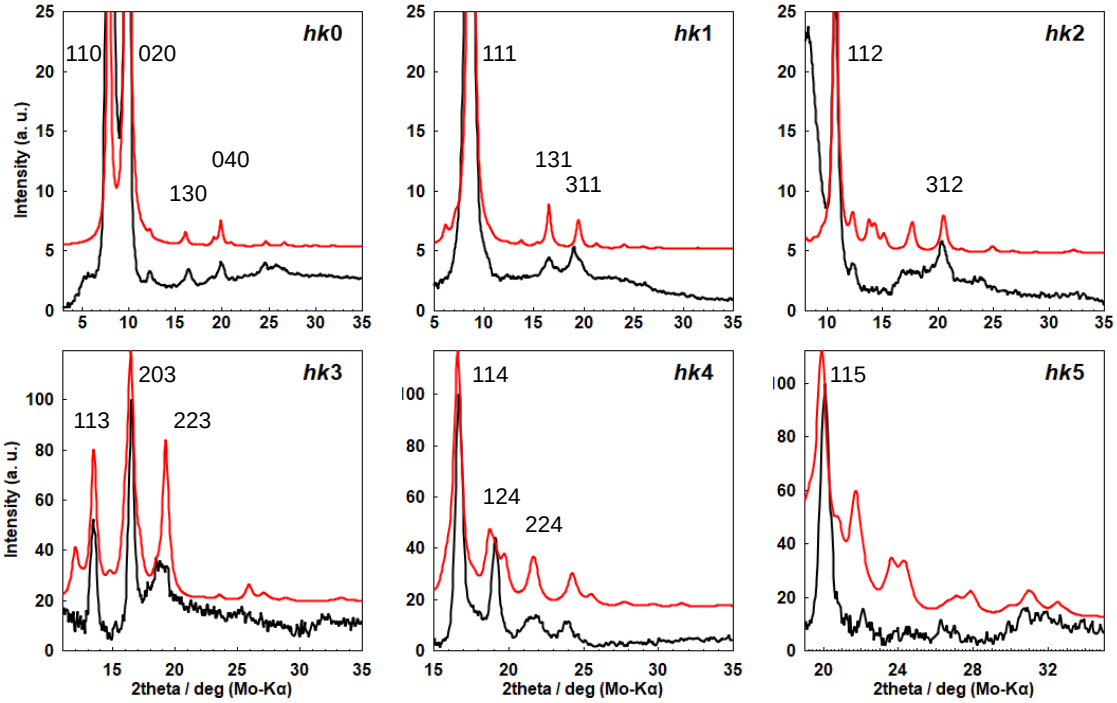

Figure III-16. The observed X-ray diffraction profiles (black color) along the various layer lines of the HT phase of *it*-H-poly(NB) in comparison with those calculated (red) for the crystal structure shown in Figure III-8 (b).

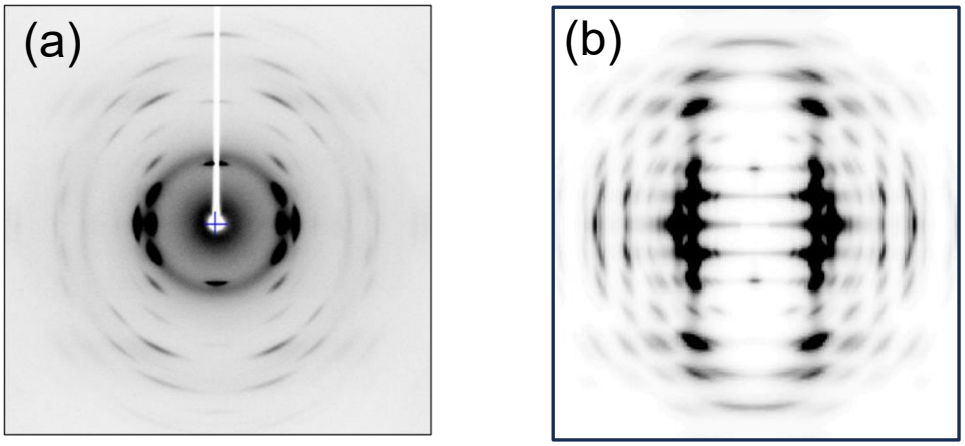

Figure III-17. 2-D WAXD patterns of uniaxially oriented isotactic H-poly(NB) in the HT phase. (a) observed (30 °C) and (b) calculated patterns.

When the crystal structure of isotactic H-poly(NB) in the HT phase is compared with that in the LT phase, we may pick up the several large differences between them.

(i) The *a*-axial length of the HT phase is longer (6.65 Å of HT phase and 5.95 Å of LT phase), while the *b* axial length is almost equal to each other (8.24 Å of HT phase and 8.25 Å of LT phase). The approximately flat chain in the *ac* plane becomes longer along the *a* axis, corresponding to the increase of unit cell size.

(ii) The *c*-axial length is remarkably contracted from the LT phase (12.65 Å) to the HT phase (11.20 Å). The above-mentioned conformational change occurs through the torsional-angle change in the segments of Ring(C(*S*))-CH_2CH_2-Ring(C(*R*)). One speculative conformational transformation model is illustrated in Figure III-10. The Ring-CH_2-CH_2-Ring sequence changes the shape relatively smoothly by the cooperative torsional-angle changes from TTT to $\bar{S}$TS and to $\bar{G}$TG. The direction of the rings is almost fixed (maybe because of the intermolecular constraint due to its bulkiness), and the CH_2CH_2 parts change the relative orientation by about 90^o around the chain axis, as seen in Figure III-18.

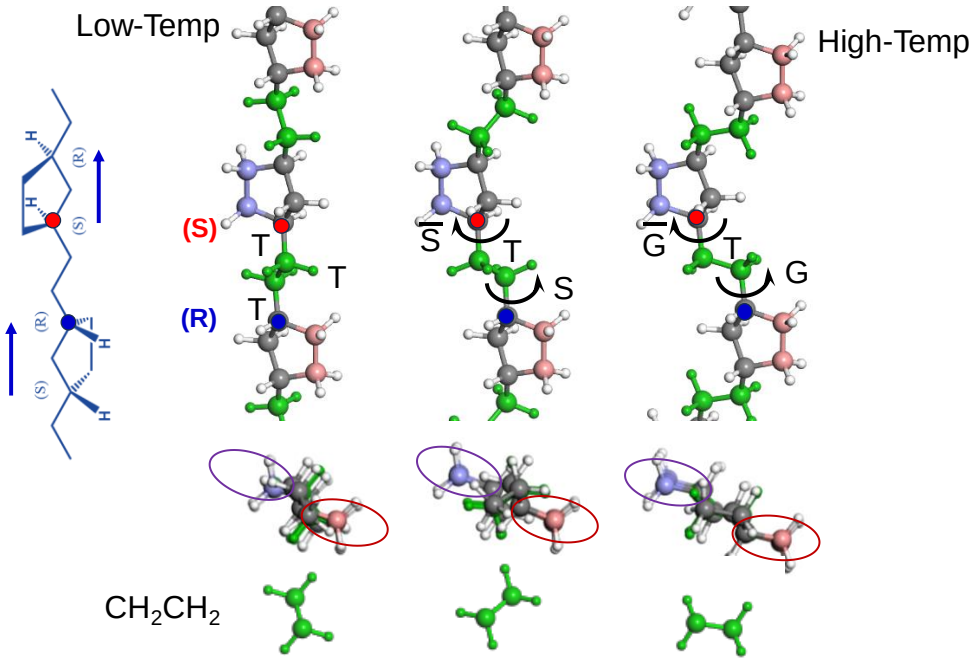

Figure III-18. One transition model from the all-*trans* conformation of LT phase to the $\bar{G}TG$ conformation of HT phase of isotactic H-poly(NB). The conformational change was assumed to occur from T to G *via* S (skew) bonds. The orientation of rings (circled) is kept unchanged, while that of ethylene segment changes by about 90° around the chain axis.

(iii) In the LT phase of the space group $P2_12_12_1$, a molecular chain located at a corner of the unit cell (corner chain) is related to the chain located at the center (center chain) by the 2_1 screw symmetry along the *b* (or *a*) axis. As a result, these two chains are in the relation of upward and downward orientation along the chain axis. Here, the upward and downward chains can be defined using the (*S*)→(*R*) and (*R*)→(*S*) sequences of carbon atom configurations, respectively. Since the space group is kept unchanged, this upward- and downward relation is reserved even in the HT phase.

III-3-6. Crystal Structure Analysis of Atactic H-Poly(NB)

(a) LT Phase

The crystal structure of atactic H-poly(NB) in the LT phase was already proposed by Register et al.[4,5] The meso content of their samples was 44 - 54%. The crystal structure was of the monoclinic type with the unit cell parameters of a = 6.936 Å, b = 9.596 Å, c (repeating period) = 12.420 Å, and β = 130.7° and the space group $C2/c$.[4,5] The atactic sample used in the present study contained the 53% meso sequences, which is in the same range of the meso content as theirs. In such a sense the X-ray diffraction pattern shown in Figure III-5 (c) should be indexed by using their unit cell parameters. Unfortunately, however, it was difficult to apply these parameters directly. The observed lattice spacings are also appreciably different. These situations may come from the not-very-good X-ray diffraction data reported in references 4 and 5 because of the low degree of chain orientation as seen in those reports, compared with our data shown in Figure III-5.

Then, I investigated the crystal structure of our atactic polymer species by analyzing the 2D X-ray diffraction pattern taken for the highly-oriented sample as shown in Figure III-5 (c). By reading out the coordinates of all the observed diffraction peaks in the LT phase, the unit cell parameters were obtained as follows: a = 5.43 Å, b = 9.45 Å, c (chain axis) = 12.41 ± 0.07 Å and $\alpha = \beta = \gamma = 90^{o}$. The comparison of the lattice spacings between the observed and calculated values is listed in Table III-S6 in Appendix III-1. The almost planar-zigzag chains can be assumed from the c axial length, which is the same as that proposed in the literature.[4] The unit cell is rectangular, but the observed X-ray diffraction intensities can be reproduced by using the monoclinic crystal system. After the many trial-and-error procedures, the best space group was $P112_1/n$, in which the two zigzag chains were packed. The density calculated for this unit cell is 1.00 g/cm^3 in comparison with the observed bulk density 0.99 g/cm^3.

By taking the atactic configuration into account, the side rings were assumed to attach on the right and left sides of the planar-zigzag skeletal chain with the 50% probability. The finally derived crystal structure model of atactic H-poly(NB) in the LT phase is shown in Figure III-19. The comparison of the observed diffraction profiles along the several layer lines with those calculated for this model is shown in Figure III-20. The comparison between the observed and calculated 2-D X-ray diffraction patterns is shown in Figure III-21, where the following parameters were assumed for the crystallite size 100 Å × 100 Å × 100 Å, the crystal strain 0.5% × 0.5% × 0.5%, the isotropic temperature factor for C atoms 5 Å^2, and the degree of chain orientation 3.0°. The observed diffraction data are reproduced well as a whole, although the observed horizontal diffuse lines are spotlike in the calculated pattern since the relative-height disorder between the neighboring chains is not taken into account. The R factor estimated from the integrated

intensity of the separated 9 reflection peaks on *hk*0, *hk*1, *hk*2 and *hk*5 layer lines was 5.0 %. The atomic fractional coordinates are shown in Table III-S7 in Appendix III-1. As seen in the model of atactic H-poly(NB) crystal (the LT phase) in Figure III-19, the packing of the molecular chains is good. The highly crystalline character of the atactic H-poly(NB) sample is originated from the good packing of the relatively compact chains. The situation is similar to such crystalline polymers having atactic configuration as atactic poly(acrylonitrile),[10] atactic poly(vinyl alcohol),[11-15] and so on. Judging from the van der Waals radius of the H atom (1.2 Å), the closest intermolecular H…H distances are about 2.4 Å. The anomalously short distance of the H…H pairs found here are about 1.7 – 2.2 Å. Such too short H…H distances were the consequences of the assumption of the virtual coexistence of the ring side groups attached on both side of the skeletal chain.

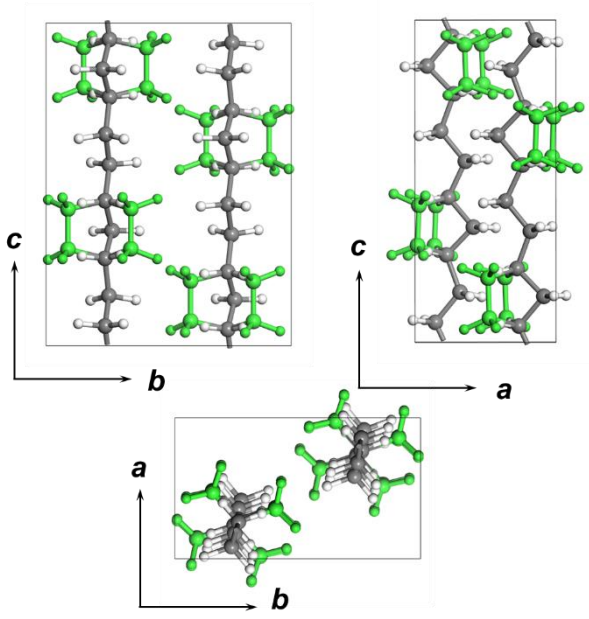

Figure III-19. (a) Crystal structure of atactic H-poly(NB) in the LT phase. The lattice parameters are a = 5.43 Å, b = 9.45 Å, c (chain axis) = 12.41 Å and $\alpha = \beta = \gamma = 90^{o}$. The space group is $P112_1/n$. The side chains are shown in green color. The coexistence of

the different two types of the side ring configurations within the chain is assumed with the 50% probability.

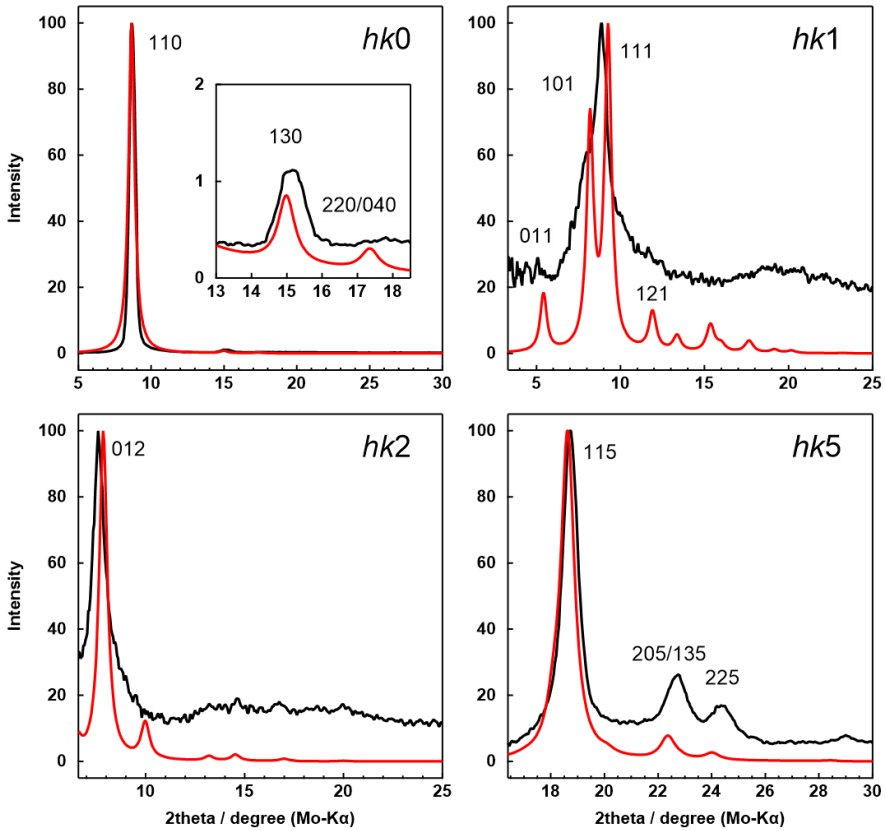

Figure III-20. The X-ray diffraction profiles along the layer lines *hk*0, *hk*1, *hk*2 and *hk*5 observed (black) for atactic H-poly(NB) in the LT phase, compared with those calculated (red) for the proposed crystal structure.

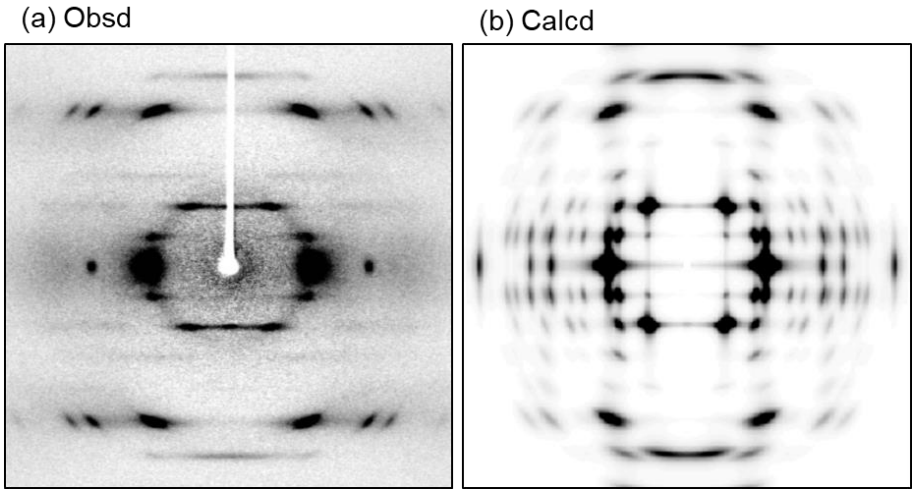

Figure III-21. (a) The observed and (b) calculated 2-D WAXD patterns of the uniaxially-oriented atactic H-poly(NB) in the LT phase. The incident X-ray beam is Mo-Kα. In the calculation, the disorder of the relative height between the neighboring chains in the lattice was not introduced, which should give the streak line as seen in the observed pattern.

(b) HT Phase

As known from the change of two equatorial-line peaks to the singlet at a high temperature, the crystal structure of atactic H-poly(NB) is considered to change to the pseudo-hexagonal type. The unit cell parameters are a = 5.55 Å, b = 9.60 Å, c = 12.40 Å, and β = 90° at 127 °C (cf. a = 5.43 Å, b = 9.45 Å, c = 12.41 Å, β = 90° at 30 °C). The HT phase of atactic H-poly(NB) shows the relatively strong streaks along the layer lines, suggesting the translational disorder of the neighboring chains along the chain axis. The X-ray interlayer spacings indicate the reservation of *trans*-zigzag conformation even in a high temperature region. Then we may speculate that the molecular chains of zigzag shape experience not only the rotational motion around the chain axis but also the

translational motion along the chain axis to give the disorder of relative heights of the neighboring zigzag chains. However, the second layer line is still spot-like, different from the other layer lines. This indicates the translational shift of chains does not occur randomly with an arbitrary magnitude of shift, but the *c*/2 shift occurs although the direction of shift is random, being often called the registered translational disordering.[16] But, the amplitude of *c*/2 shift seems too large to occur for the whole chains. As mentioned above, the rings are statistically positioned right and left in the atactic H-poly(NB) chain. In the high temperature phase, the rings reorient right and left more frequently, which may be caused by the rigid-rotation or the flip-flop motion of the chains. As a result, the averaged orientation of all the rings is almost equivalent to each other and cannot be distinguished anymore. In the case of the low-temperature phase, as illustrated in Figure III-22 (a), the repeat period between the neighboring rings along the chain axis is irregular to give the streaks along the horizontal lines, while the repeat period becomes more regular, (*c*/2), in the high-temperature region (Figure III-22 (b)). As a result, the intensity of original odd layer lines is weaker, and the even layer lines increase the relative intensity as observed in Figure III-7.

As seen in Figure III-7, the sharpening of the equatorial-line peaks may come from the growth of domain structures in the high temperature region. The broad diffraction width at room temperature was found to become sharper above the phase transition temperature. Actually, the full width at the half height was estimated for 110 and 020 peaks (with the slit-width correction using a Si standard peak), from which the crystallite sizes were estimated on the basis of Scherrer's equation.[8] As plotted in Figure III-23 (1), the X-ray coherent crystallite sizes increased remarkably above the transition point. The crystallites of the LT phase are considered to be composed of the aggregations

of small X-ray coherent domains. In the HT phase, the thermal motion occurs actively, and the molecular chains are speculated to rotate around the chain axis. As a result, the distinguishment of the domains disappears, and the originally-small domains are fused into a larger domain to give the sharp diffraction peak as a result.[17] The schematic illustration is given in Figure III-23 (2).

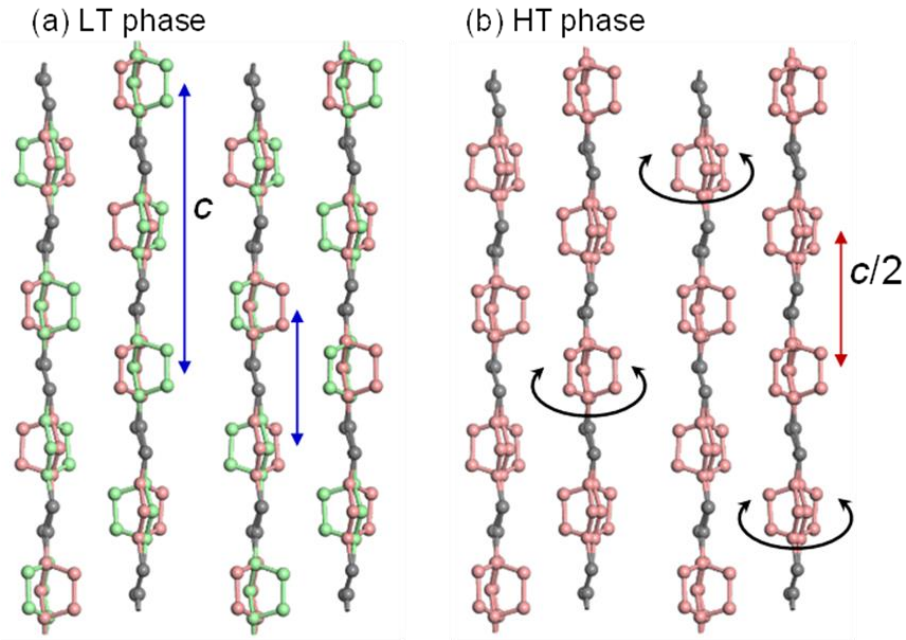

Figure III-22. The disordering of relative height between the neighboring chains of atactic H-poly(NB): (a) in the low-temperature phase, and (b) in the high-temperature phase. In the LT phase, the rightward- and leftward-oriented rings are arrayed randomly but without any exchange, as indicated by green and pink colors. The occupancy of the rings is 0.5 for both the green and pink rings. In the HT phase, the activated thermal motions erase the difference of rightward- and leftward-orientations of rings around the chain axis, as indicated by pink color only. The repeating period becomes approximately *c*/2.

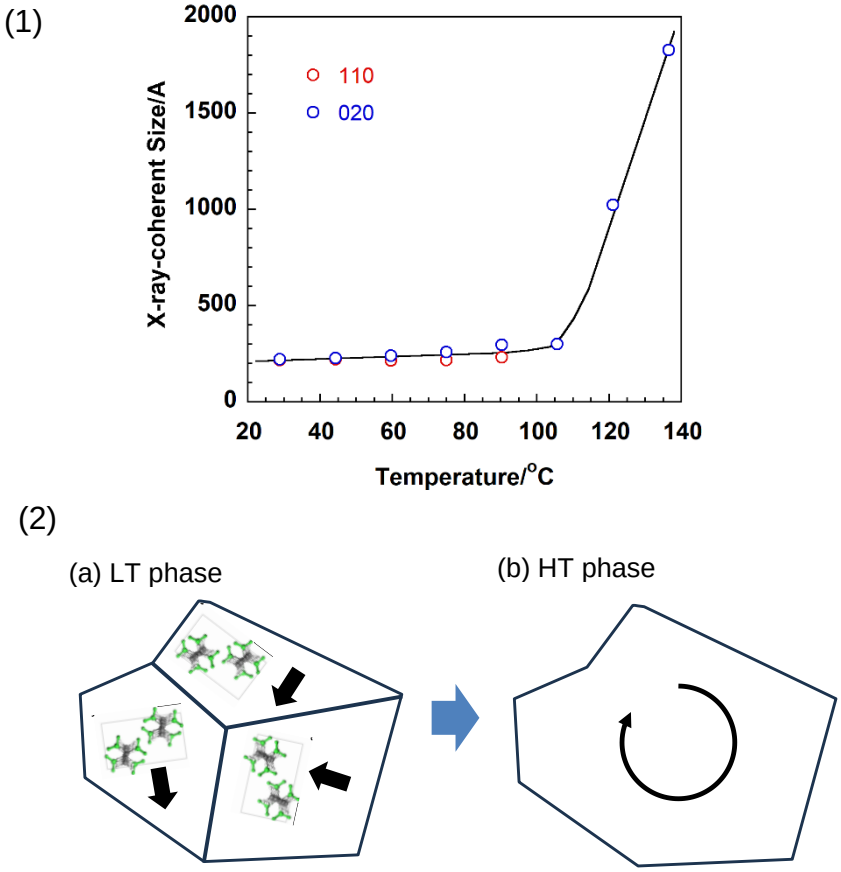

Figure III-23. (1) Temperature dependence of full-width at half peak intensity estimated for 110 and 020 peaks of atactic H-poly(NB) (refer to Figure III-6). (2) (a) the aggregation of small domains in the low-temperature phase, and (b) the large domain in the high-temperature phase due to the radical rotational motions of chains.

III-3-7. Comparison of the Crystal Structures of H-Poly(NB)s with Different Tacticities

The definition of isotactic, syndiotactic and atactic sequences of H-poly(cycloolefin) was described in Chapter I. The explanation was made on the basis of the zigzag conformation of the skeletal chain. The present structure analysis has

confirmed these definitions quite clearly since the skeletal chains were found to take just the planar-zigzag conformations existing in the LT crystal phase. In this way, the NMR analyses have been verified definitely by the present X-ray structure analysis. Besides the chain packing mode is sensitively affected by the degree of tacticity.

As shown in Figure III-24, it is easy to know the relation between the chain conformation and its symmetry. The syndiotactic polymer chain possesses one glide plane, a set of 2-fold rotation axes and a set of mirror planes perpendicular to the chain axis. The 1-dimensional space group or the corresponding factor group is isomorphous to the point group C_{2v}. The isotactic chain possesses the 2_1 screw symmetry along the chain axis, a set of mirror planes perpendicular to the chain axis and a set of points of symmetry, the factor group of which is isomorphous to the point group C_{2h}. The atactic chain does not have any symmetry, the factor group is isomorphous to C_1. These symmetry differences should reflect on the vibrational spectra and also the physical property.

Figure III-25 compares the packing modes of these three polymer species. The syndiotactic and atactic polymers show quite similar positioning of the zigzag chains. The isotactic chains show appreciably different chain packing structure. The difference of the chain packing mode can reflect on the lattice energy and the thermal behavior.

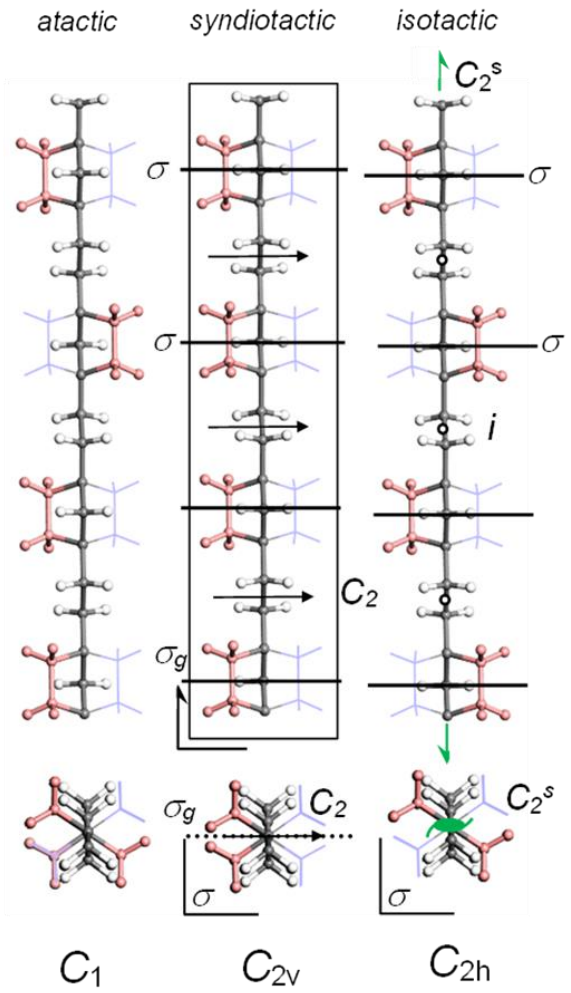

Figure III-24. Comparison of the chain conformation and symmetry among atactic, syndiotactic and isotactic H-poly(NB). C_2, C_2^s, s and s_g are the 2-fold rotation axis, the 2-fold screw axis, the mirror plane and the glide plane, respectively.

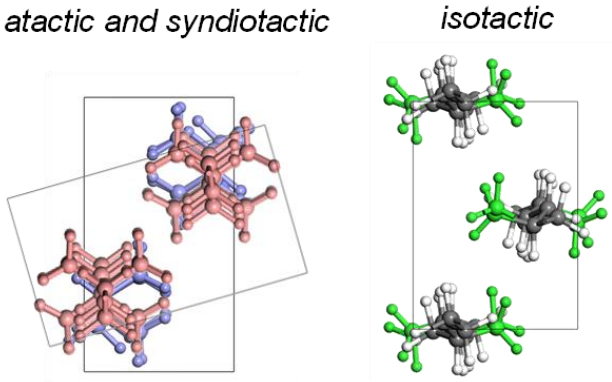

Figure III-25. The overlapped picture of the packing structures of the atactic and syndiotactic chains. The atactic chains are shown with red color.

III-4. Conclusions

The information of the crystal structures of the newly synthesized syndiotactic and isotactic H-poly(NB)s were investigated. The quantitative analysis of the X-ray diffraction data gave the concrete images of the chain conformation and chain packing mode of these polymers in comparison with those of the atactic species. The skeletal chains take essentially the similar planar zigzag conformation in all the species. The cyclopentylene rings are included as the parts of the skeletal chains. However, the CH_2CH_2 side groups of the rings protrude out of the skeletal chain in the different modes depending on the tacticity, which gives the significant difference of the whole shape of the chains and then the difference of the chain packing structure.

The thermal behavior was also found to be different depending on the tacticity. To reveal the relation between the thermal behavior and the crystal structure, the details about the structural changes and the energetical stability in the phase transition phenomena were investigated. I have measured the 2D X-ray diffraction patterns of H-poly(NB) samples of different configurations in the heating process, and confirmed the existence of phase transition between the LT and HT phases for isotactic- and atactic species. The structural analysis revealed the T-G conformational change in the HT phase of isotactic-H-poly(NB). The cooperative T-G conformational exchange of low energy barrier is speculated to play an important role in the generation of the HT phase of isotactic-species. In the case of atactic H-poly(NB), the *trans* conformation was kept even above the transition point. Rather, the *c*/2 translational motion along the chain axis coupled with the rotational motions or the fluctuation of ring side groups is imagined to occur with the appreciably disordered packing. The syndiotactic-H-poly(NB) did not

show a detectable structural change in the whole temperature region below the melting point. The different structural changes in the crystal phase for isotactic, atactic and syndiotactic H-poly(NB)s at high temperatures were found to be closely correlated to the melting behavior.

Appendix III-1. Tables of the crystallographic data of H-poly(NB)s

The indexing data and the atomic fractional coordinates in the crystal lattice for syndiotactic, LT and HT phase of isotactic, and LT phase of atactic H-poly(NB)s are tabulated in **Table III-S1** to **Table III-S7** shown below.

Table III-S1. The *hkl* indices and the observed and calculated lattice spacings estimated for the syndiotactic H-poly(NB) crystal.

h	*k*	*l*	d_o/Å	d_c/Å	*h*	*k*	*l*	d_o/Å	d_c/Å
1	0	0	5.17	5.17	-1	1	5	2.28	2.41
1	1	0	4.60	4.54	-2	1	5	2.23	2.26
1	2	0	3.49	3.49	0	0	5	2.13	2.17
1	3	0	2.70	2.70	-2	3	5	1.99	1.88
2	1	0	2.49	2.49	-1	3	5	1.88	1.96
1	4	0	2.15	2.15	0	3	5	1.80	1.79
2	3	0	2.00	2.00	-2	4	5	1.72	1.66
3	1	0	1.70	1.70	-3	0	5	1.67	1.88
3	2	0	1.62	1.62	1	1	5	1.61	1.69
3	3	0	1.53	1.51	-2	5	5	1.47	1.47
1	0	1	5.01	3.96	0	5	5	1.43	1.43
0	2	1	4.36	4.34	0	6	5	1.34	1.28
-1	2	1	3.71	3.71	0	6	5	1.28	1.28
1	2	1	3.04	3.04	-2	0	6	2.06	2.03
1	3	1	2.74	2.47	-2	1	6	1.99	1.99
0	0	2	5.40	5.42	-2	2	6	1.87	1.87
0	1	2	4.67	4.71	-2	1	7	1.75	1.75
1	1	2	3.03	2.91	-3	0	7	1.65	1.62
-2	3	2	2.17	2.17	-3	0	8	1.52	1.49
-3	1	2	1.91	1.91	-3	1	8	1.46	1.47
-1	2	3	3.10	3.09	-2	2	9	1.33	1.33
0	2	3	2.89	2.87	-4	1	10	1.20	1.16
1	0	3	2.76	2.44	-3	3	10	1.16	1.15
-2	3	3	2.14	2.14					

0	3	4	2.03	2.06
-1	4	4	1.89	1.89

Table III-S2. The atomic fractional coordinates of one crystallographically-asymmetric unit of the syndiotactic H-poly(NB) crystal structure [a, b]

Atom No.	*x*	*y*	*z*	Atom No.	*x*	*y*	*z*
C1	0.138	0.198	1.026	H8	-0.028	0.126	1.075
C2	0.123	0.268	0.920	H9	0.313	0.132	0.990
C3	0.088	0.168	0.834	H10	-0.046	0.340	0.960
C4	0.125	0.267	0.730	H11	0.240	0.086	0.799
C5	0.134	0.196	0.619	H12	-0.100	0.113	0.879
C6	0.363	0.354	0.830	H13	-0.039	0.341	0.770
C7	0.370	0.349	0.705	H14	0.304	0.125	0.574
				H15	-0.038	0.128	0.651
				H16	0.539	0.305	0.821
				H17	0.359	0.463	0.863
				H18	0.543	0.291	0.638
				H19	0.382	0.454	0.666

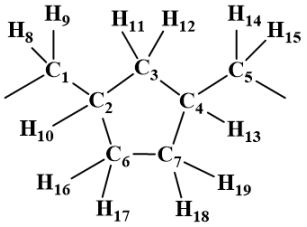

[a] The unit cell parameters are a = 5.97 Å, b = 9.48 Å, c (repeating period) = 12.58 Å and β = 60.0°. Only the coordinates of one asymmetric unit are listed. The positions of the other monomeric units are generated using the $P2_1/c$ symmetry. [b] The atomic numbers are shown for one crystallographically asymmetric unit.

Table III-S3. The *hkl* indices and the observed and calculated lattice spacings estimated for the LT phase of isotactic H-poly(NB) crystal

h	*k*	*l*	d_o/Å	d_c/Å	*h*	*k*	*l*	d_o/Å	d_c/Å
1	1	0	4.83	4.85	1	1	5	2.24	2.23
0	2	0	4.13	4.17	2	0	5	1.93	1.92

2	0	0	2.98	2.95
1	3	0	2.50	2.49
0	4	0	2.06	2.06
1	5	0	1.59	1.58
4	0	0	1.49	1.49
1	1	1	4.51	4.68
2	0	1	2.90	2.90
2	2	1	2.37	2.41
3	1	1	1.91	1.93
0	1	2	5.02	5.31
1	1	2	3.84	3.90
0	2	2	3.46	3.28
1	2	2	2.99	2.92
2	2	2	2.25	2.23
0	1	3	3.75	3.88
1	1	3	3.18	3.20
0	2	3	2.95	2.85
1	2	3	2.64	2.62
2	0	4	2.17	2.09
1	3	4	1.96	1.94
1	3	5	1.78	1.75
3	1	5	1.53	1.54
3	3	5	1.36	1.37
0	1	6	2.04	2.05
1	1	6	1.93	1.92
3	1	6	1.42	1.42
0	1	7	1.77	1.75
1	1	7	1.69	1.69
0	1	8	1.55	1.53
1	1	8	1.50	1.50
1	1	9	1.35	1.33
1	2	9	1.30	1.29
0	2	10	1.21	1.21
2	0	10	1.16	1.15
1	3	10	1.13	1.12

Table III-S4. Atomic fractional coordinates for LT phase of the isotactic H-poly(NB) crystal [a, b]

Atom No.	*x*	*y*	*z*
C1	0.182	1.030	0.794
C2	0.267	0.956	0.690
C3	0.122	0.991	0.591
C4	0.276	0.952	0.497
C5	0.186	1.008	0.389
C6	0.506	1.008	0.655
C7	0.494	1.034	0.533
H8	0.012	0.984	0.810
H9	0.166	1.163	0.785
H10	0.268	0.823	0.699
H11	0.077	1.121	0.589
H12	-0.036	0.922	0.591
H13	0.301	0.819	0.496
H14	0.158	1.140	0.392
H15	0.019	0.952	0.376

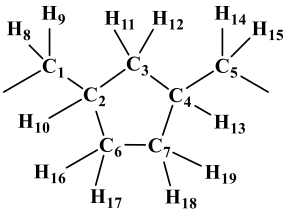

H16	0.629	0.913	0.676
H17	0.562	1.119	0.695
H18	0.645	0.991	0.491
H19	0.480	1.165	0.517

[a] The unit cell parameters are a = 5.95 Å, b = 8.25 Å, c (repeating period) = 12.65 Å. The space group is $P2_12_12_1$. [b] The atomic numbers are shown for one crystallographically-asymmetric unit.

Table III-S5. Atomic fractional coordinates of HT phase of isotactic-H-poly(NB) [a]

atoms	x	y	z
C1	0.649	0.064	0.276
C2	0.601	0.008	0.404
C3	0.726	0.074	0.510
C4	0.606	0.013	0.619
C5	0.655	0.079	0.745
C6	0.386	0.053	0.444
C7	0.385	0.044	0.582

[a] The unit cell parameters (30 °C); a = 6.65 Å, b = 8.24 Å, and c (chain axis) = 11.20 Å, the space group $P2_12_12_1$.

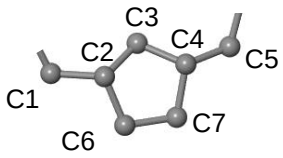

Table III-S6. The *hkl* indices and the observed and calculated lattice spacings estimated for the atactic H-poly(NB) crystal in the LT phase

h	k	l	d_o/Å	d_c/Å	h	k	l	d_o/Å	d_c/Å
1	1	0	4.70	4.71	1	3	5	1.85	1.83
1	3	0	2.70	2.72	2	2	5	1.73	1.71
2	2	0	2.29	2.35	0	0	6	2.08	2.07
1	1	1	4.46	4.40	1	1	6	1.90	1.89

0	0	2	6.21	6.21	1	0	7	1.69	1.69
0	1	2	5.17	5.19	1	1	9	1.33	1.32
1	1	5	2.20	2.20	1	3	10	1.14	1.13

Table III-S7. The atomic fractional coordinates for the atactic H-poly(NB) crystal in the LT phase [a, b]

Atom No.	*x*	*y*	*z*	Occu-pancy	Atom No.	*x*	*y*	*z*	Occu-pancy
C1	0.144	0.762	-0.061	1	H8	-0.021	0.694	-0.068	1
C2	0.262	0.741	0.051	1	H9	0.082	0.874	-0.068	1
C3	0.089	0.775	0.143	1	H10(1)	0.403	0.800	0.056	0.5
C4	0.276	0.740	0.229	1	H10(2)	0.311	0.645	0.058	0.5
C5	0.182	0.759	0.345	1	H11	-0.076	0.705	0.145	1
C6(1)	0.336	0.587	0.077	0.5	H12	0.030	0.888	0.144	1
C7(1)	0.346	0.586	0.201	0.5	H13(1)	0.416	0.798	0.219	0.5
C6(2)	0.482	0.839	0.075	0.5	H13(2)	0.325	0.644	0.222	0.5
C7(2)	0.492	0.838	0.199	0.5	H14	0.021	0.689	0.360	1
					H15	0.125	0.870	0.359	1
					H16(1)	0.194	0.511	0.048	0.5
					H16(2)	0.657	0.799	0.040	0.5
					H17(1)	0.518	0.558	0.041	0.5
					H17(2)	0.447	0.948	0.045	0.5
					H18(1)	0.209	0.510	0.233	0.5
					H18(2)	0.671	0.798	0.230	0.5
					H19(1)	0.532	0.558	0.231	0.5
					H19(2)	0.461	0.947	0.231	0.5

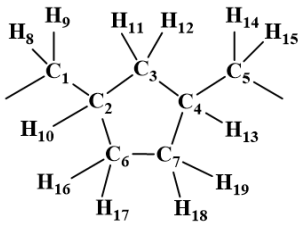

[a] The unit cell parameters are a = 5.43 Å, b = 9.45 Å, c (repeating period) = 12.41 Å. The space group is $P112_1/n$. [b] The atomic numbers are shown below for one crystallographically-asymmetric unit. The occupancy values are 0.5 For C6, C7, H10, H13, H16, H17, H18 and H19.

References

1. Hayano, S.; Nakama, Y. Iso- and Syndio-Selective ROMP of Norbornene and Tetracyclododecene: Effects of Tacticity Control on the Hydrogenated Ring-Opened Poly(cycloolefin)s. *Macromolecules* **2014**, *47*, 7797-7811.
2. Hayano, S.; Kurakata, H.; Tsunogae, Y.; Nakayama, Y.; Sato, Y.; Yasuda, H. Stereospecific Ring-Opening Metathesis Polymerization of Cycloolefins Using Novel Molybdenum and Tungsten Complexes Having Biphenolate Ligands. Development of Crystalline Hydrogenated Poly(endo-dicyclopentadiene) and Poly(norbornene). *Macromolecules* **2003**, *36*, 7422-7431.
3. Hayano, S.; Tsunogae, Y. Syndioselective Ring-Opening Metathesis Polymerization of endo-Dicyclopentadiene with Tungsten Complexes Having Imido Ligands: Development of Crystalline Syndiotactic Hydrogenated Poly(endo-dicyclopentadiene). *Macromolecules* **2006**, *39*, 30-38.
4. Lee, L.-B. W.; Register, R. A. Hydrogenated Ring-Opened Polynorbornene: A Highly Crystalline Atactic Polymer. *Macromolecules* **2005**, *38*, 1216– 1222.
5. Bishop, J. P.; Register, R. A. The Crystal-Crystal Transition in Hydrogenated Ring-Opened Polynorbornenes: Tacticity, Crystal Thickening, and Alignment. *J. Polym. Sci., Part B: Polym. Phys.* **2011**, *49*, 68-79.
6 Tadokoro, H. *Structure of Crystalline Polymers*; John Wiley & Sons: New York, 1979
7 Bunn, C. W. The crystal structure of long-chain normal paraffin hydrocarbons. The “shape” of the CH_2 group. *Trans. Faraday Soc.* **1939**, *35*, 482-490
8. Tashiro, K. *Structural Science of Crystalline Polymers*; Springer Nature Singapore Pte Ltd., 2022
9. Sun, H. COMPASS: An ab Initio Force-Field Optimized for Condensed-Phase Applications Overview with Details on Alkane and Benzene Compounds. *J. Phys. Chem. B*, **1998**, *102*, 38, 7338-7364.
10. Minagawa, M.; Taira, T.; Yabuta, Y.; Nozaki, K.; Yoshii, F. An Anomalous Tacticity-Crystallinity Relationship: A WAXD Study of Stereoregular Isotactic (83-25%) Poly(Acrylonitrile) Powder Prepared by Urea Clathrate Polymerization. *Macromolecules* **2001**, *34*, 3679-3683.
11. Bunn, C. W. Crystal Structure of Polyvinyl Alcohol. *Nature*, **1948**, *161*, 929–930.

12. Nitta, I.; Taguchi, I.; Chatani, Y. Crystal structure of PVA. Ann. Rep. Inst. Fiber Sci. 1957, 10, 1 . This report cannot be gotten anymore. Refer to the textbook shown in ref 28.
13. Taguchi, I. Application to Polymer Substances (in Japanese), “X-ray Crystallography”; Nitta, I., Ed.; Maruzen, 1959; pp 507－604.
14. Cho, J. D.; Lyoo, W. S.; Chvalun,S. N.; Blackwell, J. X-ray Analysis and Molecular Modeling of Poly(vinyl alcohol)s with Different Stereoregularities. *Macromolecules*, **1999**, *32*, 6236-6241.
15. Tashiro, K.; Kusaka, K.; Yamamoto, H.; Hanesaka, M. Introduction of Disorder in the Crystal Structures of Atactic Poly(vinyl Alcohol) and Its Iodine Complex to Solve a Dilemma between X-ray and Neutron Diffraction Data Analyses. *Macromolecules*, **2020**, *53*, 6656-6671
16. Wasanasuk, K.; Tashiro, K. Crystal Structure and Disorder in Poly(L-lactic Acid) δ Form (α’ form) and the Phase Transition Mechanism to the Ordered αForm. *Polymer*, **2001**, *52*, 6097-6109.
17. Tashiro, K.; Tanaka, R.; Ushitora, K.; Kobayashi, M. Annealing Effect on Ferroelectric Phase Transitional Behavior of Vinylidene Fluoride-Trifluoroethylene Copolymers: An Interpretation Based on the Concept of Domain and trans-gauche Conformational Disorder, *Ferroelectrics*, **1995**, *171*, 145 - 162.

Chapter IV : Conformations of Stereoregular Hydrogenated Ring-Opened Poly(norbornene)s in Dilute Solution

IV-1. Introduction

The single chain conformation of linear polymers in dilute solution is characterized in terms of the characteristic ratio C_∞, which is defined by[1]

$$C_\infty = \lim_{n\to\infty} \frac{\langle R^2 \rangle_0}{nb^2} \qquad \text{(IV-1)}$$

where $\langle R^2 \rangle_0$ is the mean square end-to-end distance of the polymer chain in the unperturbed state, n is the number of main-chain bonds, and b is the (average) bond length. As mentioned in Chapter I, Fetters and his coworkers[2-6] demonstrated that C_∞ is closely related to melt viscoelastic properties for various polyolefins. Thus, C_∞ is the basically important parameter to control rheological properties.

In this study, I characterized the single chain conformations of syndiotactic, isotactic, and atactic H-poly(NB)s, in dilute solution by using size-exclusion chromatography with an on-line multi-angle light scattering detector (SEC-MALS), molecular dynamics simulation (MD), and the rotational isomeric state (RIS) model. The characteristic ratios C_∞ of the three H-poly(NB)s were compared with those of polyethylene (PE) and poly(propylene) (PP).[1,4-7]

IV-2. Experiment and Simulation

IV-2-1. Samples

Syndiotactic and isotactic H-poly(NB)s were synthesized as described in Chapter II. Stereospecific ROMP was carried out using $WNPhCl_4Et_2O$ and MoO(*rac*-Biphenolate)$_2$ (catalyst **1** and **6** in the Chapter II) for syndiospecific and isospecific polymerization, respectively. For non-stereospecific polymerization, the Grubbs 2nd generation catalyst, $(H_2IMes)(PCy_3)Cl_2Ru{=}C(H)Ph$ (H_2IMes = 1,3-dimesityl-4,5-dihydroimidazolylidene), was used. The chemical transfer hydrogenation of the obtained poly(NB)s gave the fine powders of crystalline H-poly(NB)s. Basic characterization data of H-poly(NB)s with the various stereoregularities are shown in Table IV-1. The *meso*/*racemo* ratios of H-poly(NB)s determined by the ^{13}C-NMR analysis were 10/90 for syndiotactic, 100/0 for isotactic and 53/47 for atactic H-poly(NB). The molecular weight of the polymer needed to be large enough for SEC-MALS measurement described below. The weight average molecular weights M_w of the polymers ranged from 23×10^4 to 32×10^4. The molecular weight distributions M_w/M_n of samples ranged from 1.2 to 2.7.

Table IV-1. Samples used in this study; H-poly(NB)s with different tacticity

polymer	*meso*/*racemo* [a]	$M_w/10^3$ [b]	$N_0/10^3$ [c]	M_w/M_n [b]
syndiotactic H-poly(NB)	10/90	240	2.50	2.0
isotactic H-poly(NB)	100/0	324	3.38	2.7
atactic H-poly(NB)	53/47	228	2.38	1.2

[a] *meso*/*racemo* ratio was determined from the ^{13}C NMR spectrum recorded in $C_2D_2Cl_4$ at 125 °C. [b] M_w and M_n were determined by the SEC-MALS measurement in 1,2,4-trichlorobenzene at 140 °C. [c] Degree of polymerization.

IV-2-2. Measurements

SEC-MALS measurements were conducted to evaluate the molecular weight M and the root-mean-square radii of gyration $\langle S^2 \rangle^{1/2}$ of H-poly(NB)s in 1,2,4-trichlorobenzene (TCB) at 140 ºC. SEC-MALS consists of an HLC-8321GPC/HT SEC system (Tosoh, Japan) equipped with three TSKgel GMH-HR-H(20)HT gel columns (Tosoh, Japan), a built-in refractive index (RI) detector (Tosoh, Japan), and a DAWN HELEOS II MALS detector (Wyatt Technology, USA). The wavelength of the MALS incident light λ was 644 nm, the flow rate was 1.0 mL/min, and the concentrations of solutions injected were 1 mg/mL. Test polymer solutions were prepared by mixing a vacuum-dried polymer sample with TCB, and shaking at 140 °C for 1 h. The solution was filtered with a 0.5 μm sintered metal filter at the temperature before the SEC-MALS measurement.

The RI detector was calibrated by the signal obtained by injecting a TCB solution containing a known quantity of a standard linear polyethylene at 140 °C. The refractive index increment $\partial n/\partial c$ for standard polyethylene (SRM1475) is -0.106cm^3/g.[8,9] The $\partial n/\partial c$ values for H-poly(NB)s in 140 °C TCB were determined from the concentration of the injected solution and the RI peak area to be -0.030 cm^3/g, -0.039 cm^3/g, and -0.034 cm^3/g for atactic, syndiotactic, and isotactic H-poly(NB)s, respectively, of which absolute values were considerably smaller than that for polyethylene. The MALS detector was calibrated by measuring the 90° scattering intensity of the solvent at 140 °C to estimate the excess Rayleigh ratio R_θ at the scattering angle θ of the test solution.

The resulting SEC-MALS data obtained were analyzed to determine M and $\langle S^2 \rangle^{1/2}$ by using the Zimm plot

$$\frac{Kc}{R_\theta} = \frac{1}{MP(\theta)} \tag{IV-2}$$

where c is the polymer mass concentration, K is the optical constant defined by

$$K \equiv \frac{4\pi^2 {n_0}^2}{\lambda^4 N_A}\left(\frac{\partial n}{\partial c}\right)^2 \tag{IV-3}$$

with the solvent refractive index n_0, the Avogadro constant N_A, and the intramolecular interference factor $P(\theta)$. As recommended by Sun et al.,[10,11] the following Debye function was utilized for $P(\theta)$:[12]

$$P(\theta) = \frac{2\left(e^{-x} + x - 1\right)}{x^2}, \quad x \equiv \langle S^2 \rangle k^2, \quad k \equiv \frac{4\pi n_0}{\lambda}\sin\left(\frac{\theta}{2}\right) \tag{IV-4}$$

Two adjustable parameters M and $\langle S^2 \rangle^{1/2}$ were determined by fitting Eq. IV-2 with Eq. IV-4 to experimental Kc/R_θ at each elution time. Because the polymer concentration of the eluted solution is dilute enough, the intermolecular interference effect was ignored when using Eq. IV-2.

Figures IV-S1 - IV-S3 in Appendix IV-1 show elution curves for isotactic, syndiotactic, and atactic H-poly(NB), and Figure IV-1 shows Zimm plots for e.g. syndiotactic H-poly(NB) in TCB at 140 °C in different elution times. Slightly scattered data points at high k may have come from experimental errors in the scattering intensities due to the small $|\partial n/\partial c|$. As indicated by red curves in the figure, Eqs. IV-2 and IV-4 give straight lines over the whole k^2 range investigated when they fit the plots at longer elution times (lower M), but the equations provide slightly upturned curves when they were used to fit the data at shorter elution times (higher M). Thus, if the Zimm plots at shorter elution

times were fitted with straight lines over the whole k^2 range investigated, both M and $\langle S^2 \rangle^{1/2}$ might be overestimated in the high M region.

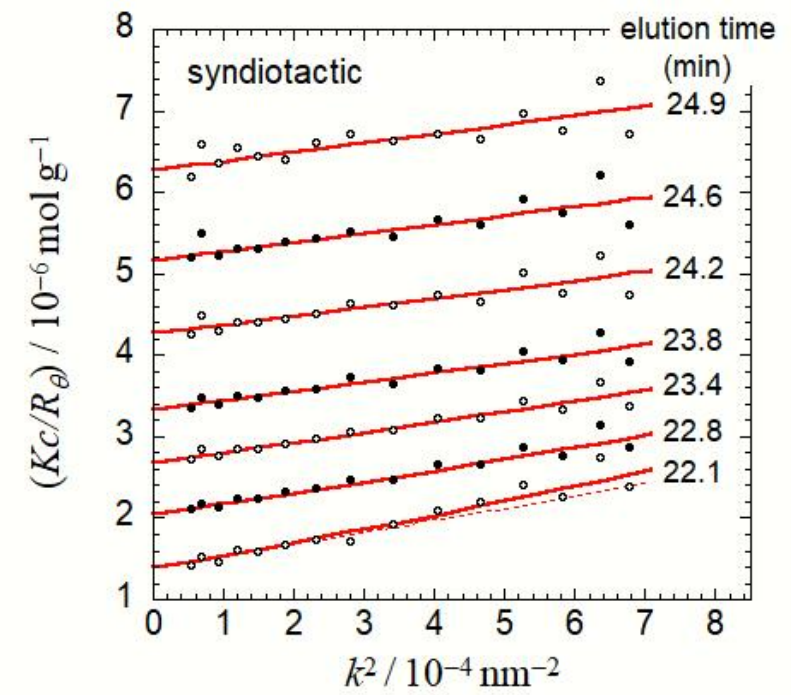

Figure IV-1. Zimm plots for syndiotactic H-poly(NB) in TCB at 140 ºC in different elution times. The red solid curves show the fitting results with Eqs. IV-2 and IV-4; the red dotted line indicates the initial slope of the Zimm plot at the elution time = 22.1 min.

IV-2-3. MD simulation

Using all-atom molecular dynamics (MD) simulations, a single 30-mer chain of syndiotactic, isotactic, or atactic H-poly(NB) was generated in a simulation box containing 3182 TCB molecules. The *meso*/*racemo* ratios of the generated polymer chains were 0/100, 100/0 and 50/50 for syndiotactic, isotactic and atactic, respectively. Winmostar (Winmostar Version 11, X-Ability Co., Ltd., Tokyo, Japan, 2022) was used to run these simulations. An energy minimization on the initial configuration was

performed to eliminate the unphysical overlaps. Subsequent equilibrium simulations were performed for 9 ns at 900 K and 30 ns at 415 K. Following the equilibration, a production run was carried out for 270 ns at 415 K (142 °C).

All polymer simulations were performed with NVT ensembles by using velocity rescaling with a stochastic term (coupling time 1 ps).[13] The density of the systems was 1226 kg/m^3, as estimated from a simulation of the TCB solution under NPT ensemble at 415 K and 1 atm by using the velocity rescaling with a stochastic term (coupling time 1 ps) and barostat with a stochastic term (coupling time 1 ps). The nonbonded interaction cutoff was set at 0.9 nm, the particle mesh Ewald (PME) approach was used to calculate long-range Coulombic interactions, and the linear constraint solver (LINCS) algorithm[14] was used to fix the bond lengths of hydrogen atoms. All simulations were performed with the OPLS-AA force field[15] using GROMACS software[16] with a time step of 2 fs. The side length of the simulation box was about 9.2 nm, which was larger than twice the radius of gyration of the polymer chains, thus providing a dilute polymer solution condition. The mean square radius of gyration $\langle S^2 \rangle$ and the distribution functions of 5 internal rotational angles of a single polymer chain were evaluated by averaging the trajectory of polymer chain every 5000 steps during a production run for 270 ns.

IV-3. Results and Discussion

IV-3-1. Radius of Gyration

Figure IV-2 shows the double logarithmic plot of the radius of gyration $\langle S^2 \rangle^{1/2}$ vs. the number of the main-chain bonds n for syndiotactic, isotactic, and atactic H-poly(NB)s;

the data were determined in TCB at 140 °C with SEC-MALS. Here, n values were calculated from the molecular weight M on the assumption that H-poly(NB) chains had five main-chain bonds per repeat unit ($n = M/19.2$). The solid line in the figure is to guide the eye with isotactic H-poly(NB) (blue circles). The data points for syndiotactic H-poly(NB) (red circles) and atactic H-poly(NB) (green circles) almost fit the same line but deviated slightly upward and downward, respectively. The slope of the solid line was 0.6, which indicates that all the H-poly(NB)s were flexible polymers affected by the excluded volume effect in TCB at 140 °C. Plus symbols in the figure indicate the same plot for the linear polyethylene (PE) in 135 °C TCB, and the data were obtained by Sun *et al.*[10] with SEC-MALS. The data points for PE deviated downward from the solid line.

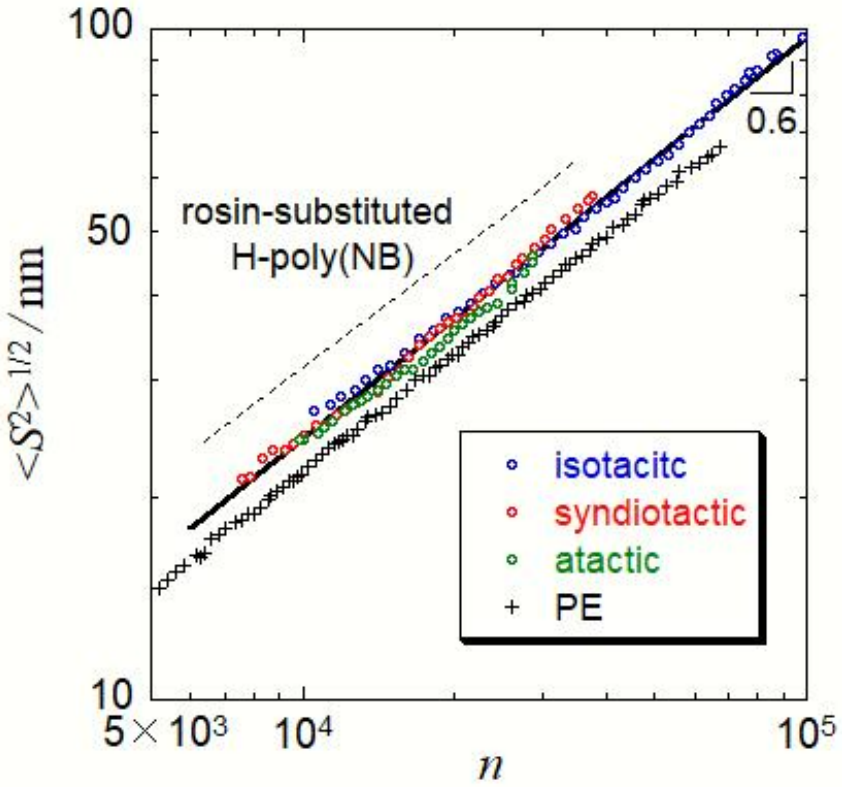

Figure IV-2. Plots of the radius of gyration $\langle S^2 \rangle^{1/2}$ against the number n of carbon atoms in the main chain of syndiotactic (red), isotactic (blue), and atactic (green) H-poly(NB)s in TCB at 140 °C for data obtained with SEC-MALS. The data for polyethylene (PE) and rosin-substituted H-poly(NB) were taken from references 10 and 17.

Recently, Hamidi and Ganewatta[17] investigated the properties of a rosin-substituted H-poly(NB) in dilute tetrahydrofuran (THF) solutions at 35 °C by using SEC with an on-line static and dynamic light scattering detector, as well as viscometer and refractometer. Their results for the molecular weight dependence of $\langle S^2 \rangle^{1/2}$ are shown by the thin dotted line in Figure IV-2, which deviated slightly upward from the solid line for isotactic H-poly(NB), although the slope was close to 0.6.

Table IV-2 lists MD simulation results of $\langle S^2 \rangle^{1/2}$ for syndiotactic, isotactic, and atactic H-poly(NB)s with the degree of polymerization of 30 (n = 150). The $\langle S^2 \rangle^{1/2}$ values increased in the order of syndiotactic, atactic, and isotactic H-poly(NB)s, which was different from the order of $\langle S^2 \rangle^{1/2}$ obtained by SEC-MALS in the high n region, as shown in Figure IV-2.

Table IV-2. MD simulation results of $\langle S^2 \rangle^{1/2}$ for syndiotactic, isotactic, and atactic H-poly(NB)s with the degree of polymerization of 30 (n = 150)

polymer	$\langle S^2 \rangle^{1/2}$/nm	statistical error/nm
syndiotactic H-poly(NB)	2.42	±0.11
isotactic H-poly(NB)	2.62	±0.08
atactic H-poly(NB)	2.49	±0.05

IV-3-2. Analysis by the Wormlike Chain Model

The wormlike chain is a continuous elastic wire model,[18] in which the straight rod is the energetically most stable conformation, and it corresponds to all *trans* conformation of polyolefin chains. For polyolefin chains in which the main chain consists of n

carbon–carbon single bonds, the contour length L of the wormlike chain model is given by

$$L = nh, \quad h = b\sin\left(\theta'/2\right) \tag{IV-5}$$

where b, θ', and h are the bond length and bond angle of the main-chain and the contour length per main-chain bond, respectively. For repeat periods along the chain axis for H-poly(NB)s in the crystalline state described in Chapter III, h was estimated as 0.125 nm. Since the stiffness of the wormlike chain was expressed in terms of the persistence length q, the square radius of gyration $\langle S^2\rangle_0$ of the (unperturbed) wormlike chain is calculated with[19]

$$\langle S^2\rangle_0 = \frac{1}{3}Lq - q^2 + \frac{2q^3}{L}\left[1 - \frac{q}{L}\left(1 - \mathrm{e}^{-L/q}\right)\right] \tag{IV-6}$$

When the wormlike chain was perturbed by the excluded-volume effect, the square radius of gyration $\langle S^2\rangle$ is expanded by[18]

$$\begin{gathered}\langle S^2\rangle = {\alpha_\mathrm{S}}^2(z')\langle S^2\rangle_0 \\ {\alpha_\mathrm{S}}^2(z') \equiv \left[1 + 10z' + \left(\tfrac{70}{9}\pi + \tfrac{10}{3}\right)z'^2 + 8\left(\sqrt{\pi}z'\right)^3\right]^{2/15} \\ \times\left(0.933 + 0.067\,\mathrm{e}^{-0.85z' - 1.39z'^2}\right)\end{gathered} \tag{IV-7}$$

with the (intermolecular) scaled excluded-volume parameter z' defined by

$$z' \equiv \left(\frac{3}{2\pi}\right)^{3/2} \cdot \frac{3}{4}K(L/2q)\frac{B}{2q}\left(\frac{L}{2q}\right)^{1/2} \tag{IV-8}$$

Here, B is the excluded-volume strength, and $K(L/2q)$ is the function of $L/2q$ (the Kuhn statistical segment number) given by the following interpolation formula for $L/2q > 6$:

$$K(x) = \frac{4}{3} - \frac{2.711}{\sqrt{x}} + \frac{7}{6x} \tag{IV-9}$$

In general, $\langle S^2 \rangle$ for the wormlike chain can be calculated by Eqs. IV-5– IV-9 as a function of n when two fitting parameters q and B are given. However, as pointed out by Norisuye and his coworkers,[20,21] the excluded-volume effect becomes experimentally visible only when $L/2q$ is larger than 20 – 50 except for polyelectrolyte in aqueous sodium chloride. Thus, I may determine q for H-poly(NB) by using Eq. IV-6 to fit the MD simulation results at n = 150 without considering the excluded-volume effect. On the other hand, the SEC-MALS results of $\langle S^2 \rangle^{1/2}$ at higher n are affected by the excluded-volume effect, and the parameter B was estimated by fitting the SEC-MALS results with Eq. IV-7.

Figure IV-3 shows the fitting results for syndiotactic, isotactic, and atactic H-poly(NB)s in TCB at 140 ^{o}C, and the solid and dashed curves indicate theoretical values for the perturbed and unperturbed wormlike chain calculated with Eqs. IV-7 and IV-6, respectively. Although gaps between the MD and SEC-MALS results are large, the theoretical curves smoothly connect both results, demonstrating that both results were consistent each other. The values of q and B determined by the fits are listed in Table IV-3. The isotactic H-poly(NB) chain was slightly stiffer than syndiotactic H-poly(NB), but the excluded-volume effect of the isotactic polymer is slightly weaker than syndiotactic polymer in TCB at 140 ^{o}C, so $\langle S^2 \rangle^{1/2}$ of the isotactic H-poly(NB) was smaller than that of the syndiotactic polymer at higher n (cf. Figure IV-2).

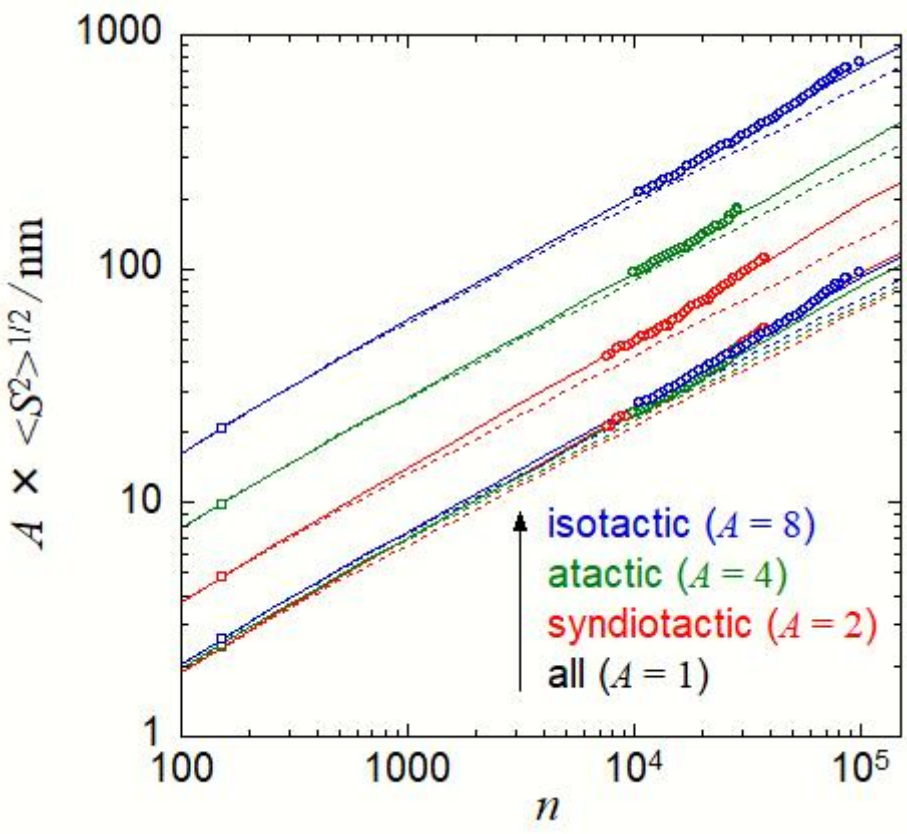

Figure IV-3. Fitting results of the radii of gyration $\langle S^2 \rangle^{1/2}$ for syndiotactic, isotactic and atactic H-poly(NB)s in TCB at 140 °C, obtained from SEC-MALS and MD simulations by the wormlike chain model; the solid and dashed curves show theoretical values for the perturbed and unperturbed wormlike chain calculated by Eqs. IV-7 and IV-6, respectively.

The persistence length q for isotactic H-poly(NB) was larger than that for syndiotactic H-poly(NB), and the value for atactic H-poly(NB) was between those for the two stereoregular H-poly(NB)s. On the other hand, the excluded volume effect for syndiotactic H-poly(NB) in TCB at 140 °C was stronger than those for isotactic and atactic H-poly(NB)s. Since B was related to the binary cluster integral of the repeat unit and the to the Flory-Huggins interaction parameter χ,[22,23] the higher strength B for syndiotactic H-poly(NB) implied a higher affinity between the polymer and solvent

and/or a lower cohesive energy density of the polymer component. The melting temperature of syndiotactic H-poly(NB) was considerably lower than that of isotactic and atactic H-poly(NB)s as described in Chapter III, indicating a lower cohesive energy density of syndiotactic H-poly(NB).

Table IV-3. Values of the persistence length *q*, the excluded-volume strength *B*, and the characteristic ratio C_∞ determined by the wormlike chain model analyses for syndiotactic, isotactic, and atactic H-poly(NB)s in TCB at 140 °C, along with literature values of C_∞ for polyethylene and syndiotactic, isotactic and atactic polypropylenes

polymer	*q*/nm	*B*/nm	C_∞
syndiotactic H-poly(NB)	1.1	0.15	11[a]
isotactic H-poly(NB)	1.3	0.08	14 [a]
atactic H-poly(NB)	1.2	0.06	12 [a]
polyethylene			6.8–8.5[1,4-6]
syndiotactic polypropylene			7.3–9.2[1,5-7]
isotactic polypropylene			5.7–6.2[1,5-7]
atactic polypropylene			4.9–6.6[1,4-7]

[a] Calculated by Eq. IV-10 from *q* listed in the second column along with h = 0.125 nm and b = 0.154 nm.

The polymer chain conformation is often characterized by the characteristic ratio C_∞, which is related to *q* and *h* of the wormlike chain model by[24]

$$C_\infty = \frac{2h}{b^2} q \qquad \text{(IV-10)}$$

Table IV-3 lists C_∞ values for syndiotactic, isotactic, and atactic H-poly(NB)s, which were calculated from *q*, and compares them with the C_∞ values reported in the literature for polyethylene as well as syndiotactic, isotactic, and atactic polypropylenes.[1,4-

[7] The characteristic ratios for H-poly(NB)s were definitely larger than those for polyethylene and polypropylenes. This may be due to the cyclopentane ring in the main chain of H-poly(NB)s (see below).

For polypropylene, C_∞ of syndiotactic polymer was larger than that of isotactic one, and the opposite was true for the H-poly(NB)s. However, the sequence of main-chain carbon atoms bearing side groups were very different for H-poly(NB) and polypropylene. As shown in Scheme IV-1 for the H-poly(NB) chain, two main-chain carbon atoms within the cyclopentane ring among the five main-chain carbon atoms in each repeat unit had the methylene groups, while every other main-chain carbon atom had the methyl groups for polypropylene. Thus, stereoregularity may have affected H-poly(NB) and polypropylene chains in a very different way.

Scheme IV-1. Chemical structures of isotactic and syndiotactic H-poly(NB)s, in which the main-chain bonds are numbered from 1 to 5.

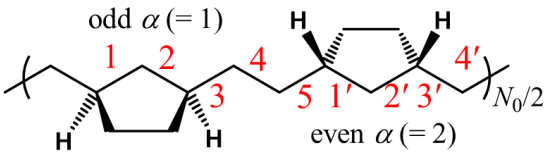

isotactic H-poly(NB)

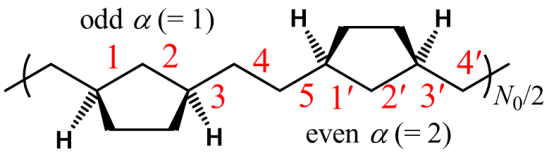

syndiotactic H-poly(NB)

Recently, Hamidi and Ganewatta[17] analyzed the molecular weight dependence of the intrinsic viscosity for a rosin-substituted H-poly(NB) in THF at 35 °C to estimate C_∞. However, their data are limited to $n > 2000$, where q (or C_∞) and B are difficult to determine separately; the theory of the intrinsic viscosity for the wormlike touched bead

model contains an additional unknown parameter, the bead diameter. Here, I can only say that their results of the radius of gyration (cf. Figure IV-2), the intrinsic viscosity and the hydrodynamic radius were not inconsistent with our results of C_∞ for H-poly(NB)s because all their results were fitted using the wormlike chain parameters that were consistent with our C_∞.

Yun et al.[25] reported the wormlike chain parameters for 1,4-addition rich poly(1,3-cyclohexadiene) in THF at 40 °C (near the theta point). Inserting their results (h = 0.1 nm, q = 0.65 nm) into Eq. IV-10, C_∞ = 5.5 was obtained for this polymer, which was considerably smaller than those for H-poly(NB)s. Three main-chain bonds are included in the six-member ring of poly(1,3-cyclohexadiene) with the microstructure of 1,4-addition. The ring structure forces the two main-chain bonds to adopt the *trans* conformation, but the remaining main-chain bonds adopt the *cis* conformation. The *cis* conformation may reduce C_∞ of this cycloolefin polymer.

IV-3-3. Analysis by the RIS Model

The RIS model[1,7] is a more realistic discrete (atomistic) chain model than the wormlike chain model, and the polymer chain conformation can be discussed in terms of the atomistic structure and the internal rotational state of the polymer main chain. The internal rotational state is, however, approximated by finite discrete states.

The repeat units indexed by α of isotactic and syndiotactic H-poly(NB)s consist of five main-chain bonds, numbered as 1 to 5, as illustrated in Scheme IV-1. The MD simulation, as described in the section **IV-2-3**, used the bond lengths b_i of bond i (= 1 – 5) and the bond angles $\theta_i' \equiv \pi - \theta_i$ between the bond vectors $\mathbf{b}_i$ and $\mathbf{b}_{i+1}$ listed in Table

IV-4. Moreover, the same MD simulation provides distribution functions of the internal rotational angles ϕ_i of the bond i ($\phi_i = 0$ at the *trans* conformation), as shown in Figure IV-4. The internal rotational angles ϕ_1 and ϕ_2 were restricted within narrow ranges near the *trans* conformation because the bonds 1 and 2 are in the cyclopentylene ring. On the other hand, the distributions of ϕ_3, ϕ_4, and ϕ_5 are trimodal, ant the peak positions are listed in the fourth to sixth column of Table IV-4. The three preferential angles ϕ_3, ϕ_4, and ϕ_5 correspond to the *trans*, *gauche*$^+$, and *gauche*$^-$ conformations, although they deviated slightly from $\phi = 0$ or ±120°. Because of the opposite stereo-symmetry for the repeat units of syndiotactic H-poly(NB) with odd and even α in Scheme IV-1, the angular distributions of the odd and even repeat units for syndiotactic H-poly(NB) were anti-symmetric around $\phi_i = 0$.

Table IV-4. Bond lengths, bond angles, and the internal rotational angles of H-poly(NB) obtained with the MD Simulations; $\phi_i^{(\alpha)}$ ($\alpha = 1, 2$) is ϕ_i for the repeat unit α

i	b_i	$\pi - \theta_i$	isotactic	syndiotactic	
			$\phi_i^{(1)} = \phi_i^{(2)}$	$\phi_i^{(1)}$	$\phi_i^{(2)}$
1	1.54 Å	105 °	–21 °	–21 °	21 °
2	1.54 Å	114 °	21 °	21 °	–21 °
3	1.55 Å	114 °	4 °, 116 °, –120 °	4 °, 116 °, –120 °	4 °, 120 °, –116 °
4	1.55 Å	114 °	4 °, 116 °, –116 °	4 °, 116 °, –116 °	4 °, 116 °, –116 °
5	1.55Å	114 °	4 °, 116 °, –120 °	4 °, 116 °, –120 °	4 °, 120 °, –116 °

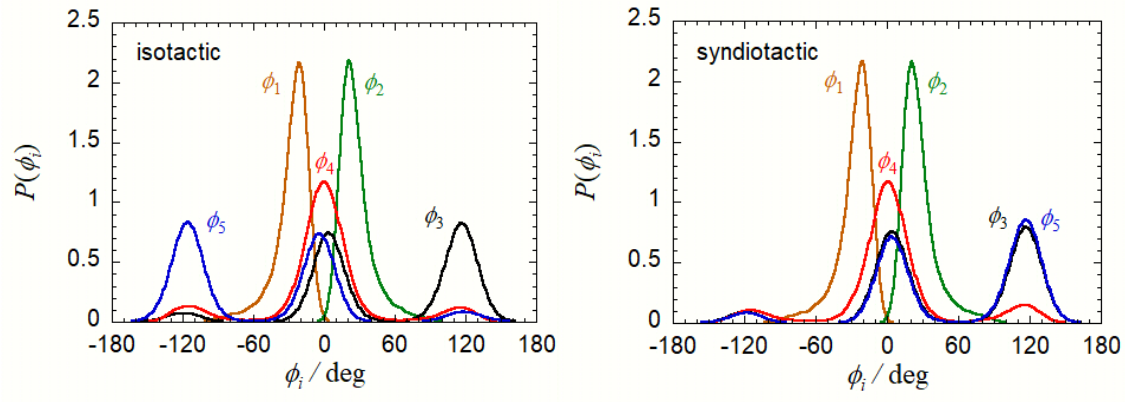

Figure IV-4. Distribution functions of the internal rotational angles ϕ_i of the bond i (= 1 – 5) for isotactic and syndiotactic H-poly(NB) obtained by the MD simulation.

Based on the RIS model, I approximate that bonds 1 and 2 can take only a single internal rotational state (called as the "*trans*" conformation) and bonds 3, 4, and 5 can take three discrete internal rotational states (called as the "*trans*," "*gauche*$^+$," and "*gauche*$^-$" conformations). This RIS model simplifies the statistical average with respect to the polymer main-chain conformation.

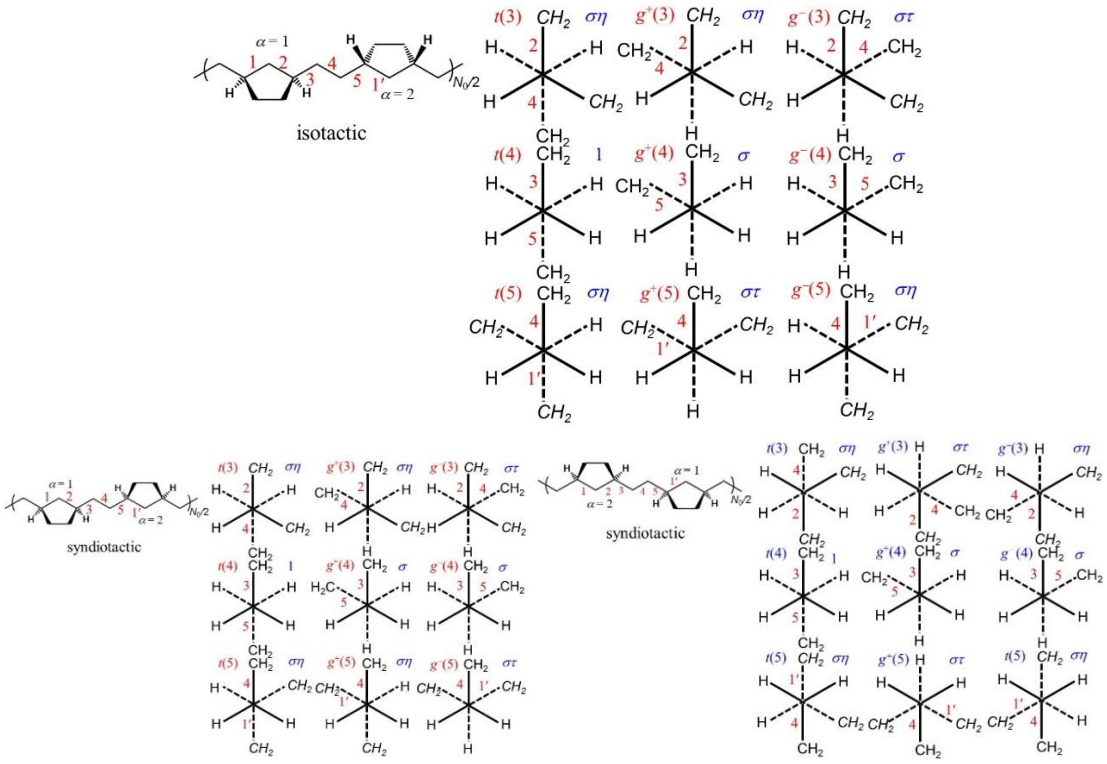

Figure IV-5. Schematic illustrations of non-bonded interactions depending on the single rotational angles ϕ_3, ϕ_4, and ϕ_5 of isotactic (top) and syndiotactic (bottom) H-poly(NB)s.

Figure IV-5 schematically illustrates non-bonded interactions depending on the single rotational angles ϕ_3, ϕ_4, and ϕ_5 of isotactic and syndiotactic H-poly(NB)s. From the illustrations, the statistical weight matrices $\mathbf{U}_3^{(\alpha)}$, $\mathbf{U}_4$, and $\mathbf{U}_5^{(\alpha)}$ of the bonds 3, 4, and 5 may be given by

$$\mathbf{U}_3^{(1)} = \mathbf{U}_3^{(2)} = \begin{pmatrix} 1 & 1 & 1 \\ 1 & 1 & \omega \\ 1 & \omega & 1 \end{pmatrix} \begin{pmatrix} \sigma\eta & 0 & 0 \\ 0 & \sigma\eta & 0 \\ 0 & 0 & \sigma\tau \end{pmatrix} = \begin{pmatrix} \sigma\eta & \sigma\eta & \sigma\tau \\ \sigma\eta & \sigma\eta & \sigma\tau\omega \\ \sigma\eta & \sigma\eta\omega & \sigma\tau \end{pmatrix} \qquad \text{(IV-11)}$$

$$\mathbf{U}_4 = \begin{pmatrix} 1 & 1 & 1 \\ 1 & 1 & \omega \\ 1 & \omega & 1 \end{pmatrix} \begin{pmatrix} 1 & 0 & 0 \\ 0 & \sigma & 0 \\ 0 & 0 & \sigma \end{pmatrix} = \begin{pmatrix} 1 & \sigma & \sigma \\ 1 & \sigma & \sigma\omega \\ 1 & \sigma\omega & \sigma \end{pmatrix} \qquad \text{(IV-12)}$$

$$\mathbf{U}_5^{(1)} = \mathbf{U}_5^{(2)} = \begin{pmatrix} 1 & 1 & 1 \\ 1 & 1 & \omega \\ 1 & \omega & 1 \end{pmatrix} \begin{pmatrix} \sigma\eta & 0 & 0 \\ 0 & \sigma\tau & 0 \\ 0 & 0 & \sigma\eta \end{pmatrix} = \begin{pmatrix} \sigma\eta & \sigma\tau & \sigma\eta \\ \sigma\eta & \sigma\tau & \sigma\eta\omega \\ \sigma\eta & \sigma\tau\omega & \sigma\eta \end{pmatrix} \quad \text{(IV-13)}$$

for isotactic H-poly(NB), and

$$\mathbf{U}_3^{(1)} = \mathbf{U}_5^{(1)} = \begin{pmatrix} 1 & 1 & 1 \\ 1 & 1 & \omega \\ 1 & \omega & 1 \end{pmatrix} \begin{pmatrix} \sigma\eta & 0 & 0 \\ 0 & \sigma\eta & 0 \\ 0 & 0 & \sigma\tau \end{pmatrix} = \begin{pmatrix} \sigma\eta & \sigma\eta & \sigma\tau \\ \sigma\eta & \sigma\eta & \sigma\tau\omega \\ \sigma\eta & \sigma\eta\omega & \sigma\tau \end{pmatrix} \quad \text{(IV-14)}$$

$$\mathbf{U}_4 = \begin{pmatrix} 1 & 1 & 1 \\ 1 & 1 & \omega \\ 1 & \omega & 1 \end{pmatrix} \begin{pmatrix} 1 & 0 & 0 \\ 0 & \sigma & 0 \\ 0 & 0 & \sigma \end{pmatrix} = \begin{pmatrix} 1 & \sigma & \sigma \\ 1 & \sigma & \sigma\omega \\ 1 & \sigma\omega & \sigma \end{pmatrix} \quad \text{(IV-15)}$$

$$\mathbf{U}_3^{(2)} = \mathbf{U}_5^{(2)} = \begin{pmatrix} 1 & 1 & 1 \\ 1 & 1 & \omega \\ 1 & \omega & 1 \end{pmatrix} \begin{pmatrix} \sigma\eta & 0 & 0 \\ 0 & \sigma\tau & 0 \\ 0 & 0 & \sigma\eta \end{pmatrix} = \begin{pmatrix} \sigma\eta & \sigma\tau & \sigma\eta \\ \sigma\eta & \sigma\tau & \sigma\eta\omega \\ \sigma\eta & \sigma\tau\omega & \sigma\eta \end{pmatrix} \quad \text{(IV-16)}$$

for syndiotactic H-poly(NB). Here, rows and columns of the matrices are indexed in the order the *trans*, *gauche*$^+$, *gauche*$^-$. In the matrices, σ, η, and τ are the statistical weights of the rotational states shown in Figure IV-5, and ω is the statistical weight of the pentane effect when the bonds 3 and 4 take *gauche*$^+$ and *gauche*$^-$ (or *gauche*$^-$ and *gauche*$^+$) conformations, respectively.[1,7] (In Figure IV-5, the italicized *CH*$_2$ indicates the methylene group in the cyclopentylene ring, for which the non-bonded interaction may be different from that for the polypropylene chain in the same rotational state.) The partition function $Z^{(\alpha)}$ for the sequence of the bonds 2 to 5 in the H-poly(NB) chain is given by

$$Z^{(\alpha)} = \begin{pmatrix} 1 & 0 & 0 \end{pmatrix} \mathbf{U}_3^{(\alpha)} \mathbf{U}_4 \mathbf{U}_5^{(\alpha)} \quad \text{(IV-17)}$$

where the bond 2 is fixed to the *trans* conformation. The total partition function Z_{N_0} for an H-poly(NB) chain with a degree of polymerization of N_0 is given by

$$Z_{N_0} = \left(Z^{(1)} Z^{(2)} \right)^{N_0/2} \tag{IV-18}$$

It is noted that the internal rotation of bond 1 is independent of internal rotations of the preceding repeat units, so that Z_{N_0} is the simple product of the partition functions for all repeat units.

Nonbonding interactions depending on ϕ_3, ϕ_4, and ϕ_5 for H-poly(NB) may approximate those for polypropylene, polymethylene, and polypropylene, respectively. Flory and his coworkers[1] tried to estimate the nonbonding interaction energies E_σ, E_η, E_τ, and E_ω, which were defined as

$$\sigma \equiv \exp\left(-\frac{E_\sigma}{RT} \right), \quad \eta \equiv \exp\left(-\frac{E_\eta}{RT} \right), \quad \tau \equiv \exp\left(-\frac{E_\tau}{RT} \right), \quad \omega \equiv \exp\left(-\frac{E_\omega}{RT} \right) \tag{IV-19}$$

for polymethylene and polypropylene. Based on their results, I utilize the following energies to calculate the characteristic ratios for isotactic and syndiotactic H-poly(NB)s.

$$\begin{gathered} E_\sigma = 2.1 \text{ kJ/mol} \left(= 0.50 \text{ kcal/mol} \right), \quad E_\eta = 0 \text{ kJ/mol}, \\ E_\omega = 8.4 \text{ kJ/mol} \left(= 2.0 \text{ kcal/mol} \right) \end{gathered} \tag{IV-20}$$

Flory[1] indicated that permissible values of E_τ were between 2.3 kJ/mol (= 0.5 kcal/mol) and 11 kJ/mol (= 2.6 kcal/mol) for polypropylene, from thermodynamic and spectroscopic data for 2-methylbutane.

The characteristic ratio C_∞ or the unperturbed mean square end-to-end distance $\langle R^2 \rangle_0$ of the H-poly(NB) chain with the degree of polymerization N_0 is calculated by[1]

$$\left(\sum_{i=1}^{5} b_i^2 \right) C_\infty \equiv \lim_{N_0 \to \infty} \frac{\langle R^2 \rangle_0}{N_0} = \lim_{N_0 \to \infty} \frac{1}{N_0} \sum_{\alpha,\beta=1}^{N_0} \sum_{i,j=1}^{5} \langle \mathbf{b}_i^{(\alpha)} \cdot \mathbf{b}_j^{(\beta)} \rangle \tag{IV-21}$$

where $\mathbf{b}_i^{(\alpha)}$ ($\mathbf{b}_j^{(\beta)}$) is the bond vector for the ith (jth) bond (i, j = 1 – 5) in the αth (βth) repeat unit (α, β = 1 – N_0) and $\langle \cdots \rangle$ indicates the statistical average over all possible

conformations; b_i is the bond length for the ith bond. Details of the actual calculation with Eq. IV-21 are explained in the Appendix IV-2 (cf. Eqs. IV-S12 and IV-S13). The statistical averages appearing in Eqs. S12 and S13 are determined by using the statistical weights appearing in the partition function given by Eq. IV-17.

Table IV-5 lists the characteristic ratios C_∞ for isotactic, syndiotactic and atactic H-poly(NB)s calculated with the RIS model by Eq. IV-21 with two values of E_τ. The theoretical C_∞ for syndiotactic H-poly(NB) was consistent with the experimental result at E_τ = 5.6 kJ/mol, and that for isotactic H-poly(NB) was consistent with the experimental result at E_τ = 9.4 kJ/mol. These values of E_τ are within the permissible ranges Flory proposed.[1] The theoretical C_∞ for atactic H-poly(NB) was slightly less than the experimental result, although the atactic sample used in this study was not perfectly atactic (*meso*/*racemo* = 53/47; cf. Table IV-1).

Table IV-5. Characteristic ratios C_∞ for isotactic, syndiotactic and atactic H-poly(NB)s at 140 °C calculated with RIS model.[a]

E_τ/kJ mol^{-1}	τ	C_∞		
		isotactic H-poly(NB)	syndiotactic H-poly(NB)	atactic H-poly(NB)
5.6	0.195	12.6	11.0	10.8
9.4	0.064	14.0	11.6	11.3

a Statistical weights σ, η, and ω were calculated by Eqs. IV-19 and IV-20.

As mentioned above, the correlation of the internal rotation states for H-poly(NB) was limited within each repeat unit (cf. Eq. IV-18). On the other hand, the correlation of

the internal rotation states for polyethylene and polypropylene ranged over the whole polymer chain due to the sequential pentane effect.[7,8] As the result, stereoregular polypropylenes exhibit helical nature, which affects the characteristic ratio. It is known that the RIS model for the three RIS (*trans*, *gauche*$^+$, and *gauche*$^-$) cannot precisely predict the experimental C_∞ values for stereoregular polypropylenes.[7,8] In some ways, the RIS analyses of cycloolefin polymers are easier than those of polyolefins.

IV-4. Conclusions

I investigated single chain conformations of syndiotactic, isotactic, and atactic hydrogenated ring-opened polynorbornenes (H-poly(NB)s) in 1,2,4-trichlorobenzene (TCB) at 140 °C by size exclusion chromatography equipped with a multi-angle light-scattering online detector (SEC-MALS) and molecular dynamics (MD) simulation. By combining the results of SEC-MALS and MD simulation, I determined the characteristic ratios C_∞ of the H-poly(NB)s (cf. Table IV-3). The experimental results of C_∞ were compared favorably with those of RIS model.

The C_∞ values of the H-poly(NB)s were definitely larger than those of polyethylene and polypropylenes. The main chain of H-poly(NB) contains five bonds per repeating unit. The RIS analysis demonstrates that the internal rotations of three main-chain bonds out of the cyclopentane ring were essentially same as those of main-chain bonds of polyethylene and polypropylenes. On the other hand, the two remaining main-chain

bonds included in the cyclopentane ring were restricted near the *trans* conformation, and this restriction enlarged C_∞ values of the H-poly(NB)s relative to those for the polyolefins.

Appendix IV-1. SEC-MALS data

Figures IV-S1 to IV-S3 show elution curves for the syndiotactic, isotactic, and atactic H-poly(NB) samples in 140 ºC TCB obtained by the light scattering detector (LS, $\theta = 90$ °) and refractometer (RI). Red and blue circles in the figure indicate the results of M and $\langle S^2 \rangle^{1/2}$ determined by fitting with the Debye function.

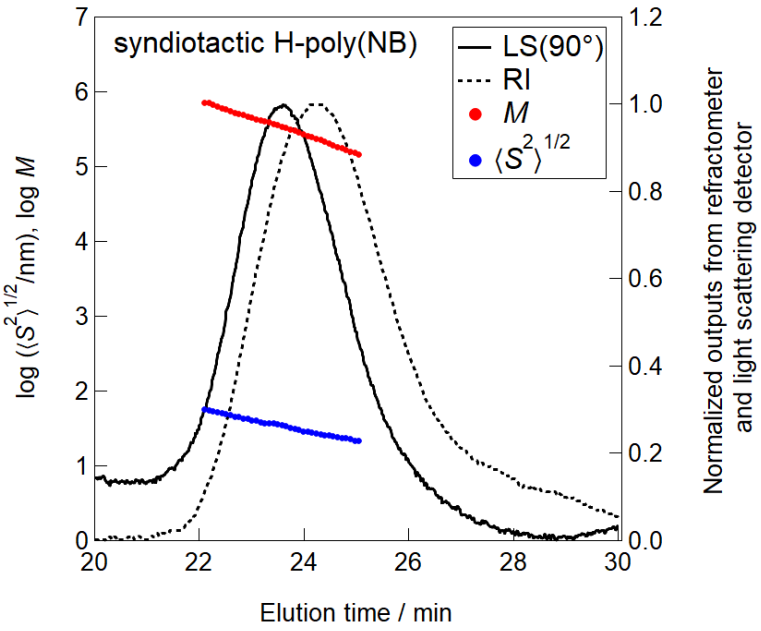

Figure IV-S1. Elution curves obtained from the light scattering detector and refractometer with the plots of M and $\langle S^2 \rangle^{1/2}$ determined by fitting with the Debye function for the syndiotactic H-poly(NB) samples.

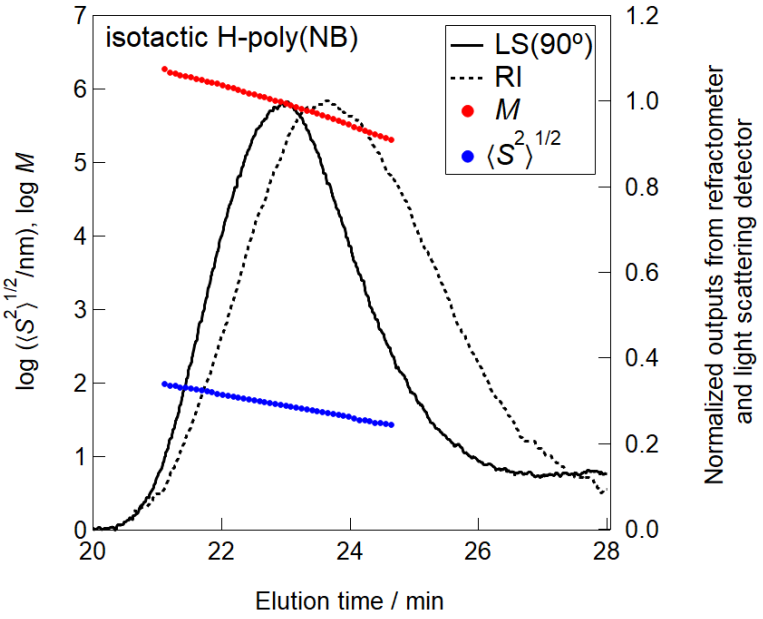

Figure IV-S2. Elution curves obtained from the light scattering detector and refractometer with the plots of M and $\langle S^2 \rangle^{1/2}$ determined by fitting with the Debye function for the isotactic H-poly(NB) samples.

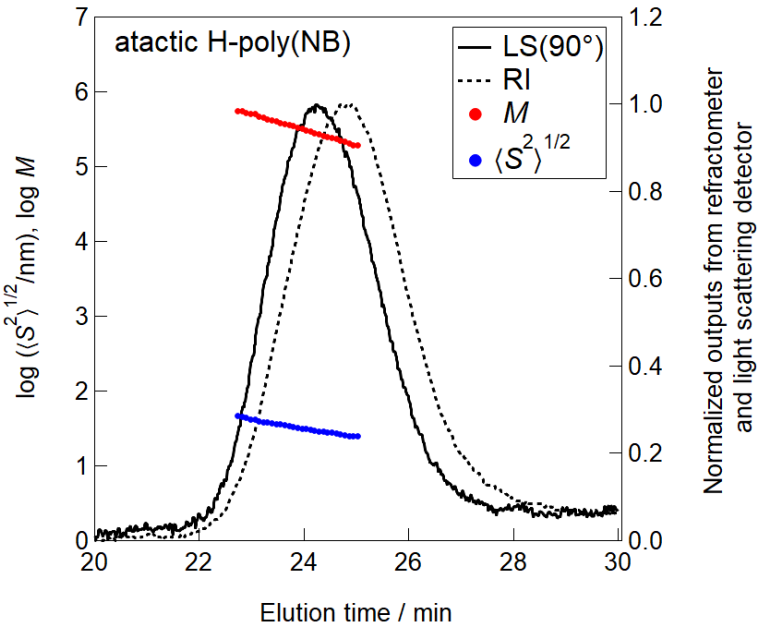

Figure IV-S3. Elution curves obtained from the light scattering detector and refractometer with the plots of M and $\langle S^2 \rangle^{1/2}$ determined by fitting with the Debye function for the atactic H-poly(NB) samples.

Appendix IV-2. Calculation of the Characteristic Ratio by the RIS model

Method of calculating the characteristic ratio by the RIS model is given below.

The unperturbed mean square end-to-end distance $\langle R^2\rangle_0$ of the H-poly(NB) chain with the degree of polymerization N_0 is calculated by (cf. Scheme 2 in the text)

$$\langle R^2\rangle_0 = \sum_{\alpha,\beta=1}^{N_0}\sum_{i,j=1}^{5}\langle \mathbf{b}_i^{(\alpha)}\cdot\mathbf{b}_j^{(\beta)}\rangle = \sum_{\alpha=1}^{N_0}\left(\sum_{i=1}^{5} {b_i}^2 + 2\beta^{(\alpha)}\right) + 2\sum_{i,j=1}^{5}\Omega_{ij} \qquad \text{(IV-S1)}$$

with

$$\beta^{(\alpha)} \equiv \sum_{i=1}^{4}\sum_{j=i+1}^{5}\langle \mathbf{b}_i^{(\alpha)}\cdot\mathbf{b}_j^{(\alpha)}\rangle, \quad \Omega_{ij} \equiv \sum_{\alpha=1}^{N_0-1}\sum_{\beta=\alpha+1}^{N_0}\langle \mathbf{b}_i^{(\alpha)}\cdot\mathbf{b}_j^{(\beta)}\rangle \qquad \text{(IV-S2)}$$

where $\mathbf{b}_i^{(\alpha)}$ indicates the $\mathbf{b}_i$ bond in the αth repeating unit and $\langle\cdots\rangle$ indicates the statistical average over all possible conformations.

I choose the direction of all $\mathbf{b}_i^{(\alpha)}$ bonds (i = 1 – 5, α = 1 – N_0) to be parallel to the x-axis of the $\mathbf{b}_i^{(\alpha)}$ bond coordinate system. Then, $\mathbf{b}_i^{(\alpha)}$ is written as

$$\mathbf{b}_i^{(\alpha)} = \begin{pmatrix} b_i & 0 & 0 \end{pmatrix} \qquad \text{(IV-S3)}$$

in the $\mathbf{b}_i^{(\alpha)}$ bond coordinate system, and each term in $\beta^{(\alpha)}$ and Ω_{ij} of Eq. IV-S2 is written as

$$\langle \mathbf{b}_i^{(\alpha)}\cdot\mathbf{b}_j^{(\alpha)}\rangle = \mathbf{b}_i^{(\alpha)}\langle \mathbf{T}_i^{(\alpha)}\cdots\mathbf{T}_{j-1}^{(\alpha)}\rangle\mathbf{b}_j^{(\alpha)\mathrm{T}} \qquad \text{(IV-S4)}$$

$$\langle \mathbf{b}_i^{(\alpha)}\cdot\mathbf{b}_j^{(\beta)}\rangle = \mathbf{b}_i^{(\alpha)}\langle \mathbf{T}_i^{(\alpha)}\cdots\mathbf{T}_5^{(\alpha)}\mathbf{T}_1^{(\alpha+1)}\cdots\mathbf{T}_{j-1}^{(\beta)}\rangle\mathbf{b}_j^{(\beta)\mathrm{T}} \qquad \text{(IV-S5)}$$

Here, $\mathbf{T}_i^{(\alpha)}$ is the transformation matrix which converts the $\mathbf{b}_{i+1}^{(\alpha)}$ bond coordinate system to the $\mathbf{b}_i^{(\alpha)}$ bond coordinate system (or the $\mathbf{b}_1^{(\alpha+1)}$ bond coordinate system to the $\mathbf{b}_5^{(\alpha)}$ bond coordinate system), and the superscript T indicates the transpose of the row vector to the column vector. Using the bond angle $\pi - \theta_i^{(\alpha)}$ between $\mathbf{b}_i^{(\alpha)}$ and $\mathbf{b}_{i+1}^{(\alpha)}$ (or between $\mathbf{b}_5^{(\alpha)}$

and $\mathbf{b}_1^{(\alpha+1)}$) and the internal rotational angles $\phi_i^{(\alpha)}$ of the bond $\mathbf{b}_i^{(\alpha)}$, $\mathbf{T}_i^{(\alpha)}$ is written as

$$\mathbf{T}_i^{(\alpha)} = \begin{pmatrix} \cos\theta_i^{(\alpha)} & \sin\theta_i^{(\alpha)} & 0 \\ \sin\theta_i^{(\alpha)}\cos\phi_i^{(\alpha)} & -\cos\theta_i^{(\alpha)}\cos\phi_i^{(\alpha)} & \sin\phi_i^{(\alpha)} \\ \sin\theta_i^{(\alpha)}\sin\phi_i^{(\alpha)} & -\cos\theta_i^{(\alpha)}\sin\phi_i^{(\alpha)} & -\cos\phi_i^{(\alpha)} \end{pmatrix} \tag{IV-S6}$$

Under the RIS approximation, $\beta^{(\alpha)}$ and the summation of Ω_{ij} at sufficiently large N_0 in Eq. IV-S2 are explicitly written as

$$\begin{aligned} \beta^{(\alpha)} = {} & \mathbf{b}_1\mathbf{T}_1^{(\alpha)}\mathbf{b}_2{}^{\mathrm{T}} + \mathbf{b}_1\mathbf{T}_1^{(\alpha)}\mathbf{T}_2^{(\alpha)}\mathbf{b}_3{}^{\mathrm{T}} + \mathbf{b}_1\mathbf{T}_1^{(\alpha)}\mathbf{T}_2^{(\alpha)}\langle\mathbf{T}_3^{(\alpha)}\rangle\mathbf{b}_4{}^{\mathrm{T}} \\ & + \mathbf{b}_1\mathbf{T}_1^{(\alpha)}\mathbf{T}_2^{(\alpha)}\langle\mathbf{T}_3^{(\alpha)}\mathbf{T}_4^{(\alpha)}\rangle\mathbf{b}_5{}^{\mathrm{T}} + \mathbf{b}_2\mathbf{T}_2^{(\alpha)}\mathbf{b}_3{}^{\mathrm{T}} + \mathbf{b}_2\mathbf{T}_2^{(\alpha)}\langle\mathbf{T}_3^{(\alpha)}\rangle\mathbf{b}_4{}^{\mathrm{T}} \\ & + \mathbf{b}_2\mathbf{T}_2^{(\alpha)}\langle\mathbf{T}_3^{(\alpha)}\mathbf{T}_4^{(\alpha)}\rangle\mathbf{b}_5{}^{\mathrm{T}} + \mathbf{b}_3\langle\mathbf{T}_3^{(\alpha)}\rangle\mathbf{b}_4{}^{\mathrm{T}} + \mathbf{b}_3\langle\mathbf{T}_3^{(\alpha)}\mathbf{T}_4^{(\alpha)}\rangle\mathbf{b}_5{}^{\mathrm{T}} + \mathbf{b}_4\langle\mathbf{T}_4^{(\alpha)}\rangle\mathbf{b}_5{}^{\mathrm{T}} \end{aligned} \tag{IV-S7}$$

and

$$\begin{aligned} \frac{2}{N_0}\sum_{i,j=1}^{5}\Omega_{ij} = {} & \mathbf{B}^{(1)}\left(\mathbf{E} - \langle\mathbf{T}^{(2)}\rangle\langle\mathbf{T}^{(1)}\rangle\right)^{-1}\left(\langle\mathbf{T}^{(2)}\rangle\mathbf{B}'^{(1)\mathrm{T}} + \mathbf{B}'^{(2)\mathrm{T}}\right) \\ & + \mathbf{B}^{(2)}\left(\mathbf{E} - \langle\mathbf{T}^{(1)}\rangle\langle\mathbf{T}^{(2)}\rangle\right)^{-1}\left(\langle\mathbf{T}^{(1)}\rangle\mathbf{B}'^{(2)\mathrm{T}} + \mathbf{B}'^{(1)\mathrm{T}}\right) \end{aligned} \tag{IV-S8}$$

where

$$\langle\mathbf{T}^{(\alpha)}\rangle \equiv \mathbf{T}_1^{(\alpha)}\mathbf{T}_2^{(\alpha)}\langle\mathbf{T}_3^{(\alpha)}\mathbf{T}_4^{(\alpha)}\mathbf{T}_5^{(\alpha)}\rangle \tag{IV-S9}$$

$$\mathbf{B}^{(\alpha)} \equiv \mathbf{b}_1\langle\mathbf{T}^{(\alpha)}\rangle + \mathbf{b}_2\mathbf{T}_2^{(\alpha)}\langle\mathbf{T}_3^{(\alpha)}\mathbf{T}_4^{(\alpha)}\mathbf{T}_5^{(\alpha)}\rangle + \mathbf{b}_3\langle\mathbf{T}_3^{(\alpha)}\mathbf{T}_4^{(\alpha)}\mathbf{T}_5^{(\alpha)}\rangle + \mathbf{b}_4\langle\mathbf{T}_4^{(\alpha)}\mathbf{T}_5^{(\alpha)}\rangle + \mathbf{b}_5\langle\mathbf{T}_5^{(\alpha)}\rangle \tag{IV-S10}$$

$$\mathbf{B}'^{(\alpha)} \equiv \mathbf{b}_1 + \mathbf{b}_2\mathbf{T}_1^{(\alpha)\mathrm{T}} + \mathbf{b}_3\mathbf{T}_1^{(\alpha)}\mathbf{T}_2^{(\alpha)\mathrm{T}} + \mathbf{b}_4\mathbf{T}_1^{(\alpha)}\mathbf{T}_2^{(\alpha)}\langle\mathbf{T}_3^{(\alpha)}\rangle^{\mathrm{T}} + \mathbf{b}_5\mathbf{T}_1^{(\alpha)}\mathbf{T}_2^{(\alpha)}\langle\mathbf{T}_3^{(\alpha)}\mathbf{T}_4^{(\alpha)}\rangle^{\mathrm{T}} \tag{IV-S11}$$

As shown in Figure 4, the distributions of ϕ_i for syndiotactic H-poly(NB) of the odd and even repeating units are anti-symmetric, so that $\beta^{(2)}$, $\langle\mathbf{T}^{(2)}\rangle$, $\mathbf{B}^{(2)}$, and $\mathbf{B}'^{(2)}$ for the even repeating unit of syndiotactic H-poly(NB) are not identical with $\beta^{(1)}$, $\langle\mathbf{T}^{(1)}\rangle$, $\mathbf{B}^{(1)}$, and $\mathbf{B}'^{(1)}$

for the odd repeating unit. (For isotactic H-poly(NB), those quantities for the even and odd repeating units are identical.) Inserting Eqs. IV-S7– IV-S11 into Eq. IV-S1, I have the characteristic ratio C_∞ given by

$$\left(\sum_{i=1}^{5} b_i^{\,2}\right) C_\infty \equiv \lim_{N_0\to\infty} \frac{\langle R^2\rangle_0}{N_0} = \sum_{i=1}^{5} b_i^{\,2} + \frac{1}{2}\left(\beta^{(1)} + \beta^{(2)}\right) + \mathbf{B}^{(1)}\left(\mathbf{E} - \langle \mathbf{T}^{(2)}\rangle\langle \mathbf{T}^{(1)}\rangle\right)^{-1}\left(\langle \mathbf{T}^{(2)}\rangle \mathbf{B}'^{(1)\mathrm{T}} + \mathbf{B}'^{(2)\mathrm{T}}\right) + \mathbf{B}^{(2)}\left(\mathbf{E} - \langle \mathbf{T}^{(1)}\rangle\langle \mathbf{T}^{(2)}\rangle\right)^{-1}\left(\langle \mathbf{T}^{(1)}\rangle \mathbf{B}'^{(2)\mathrm{T}} + \mathbf{B}'^{(1)\mathrm{T}}\right) \quad \text{(IV-S12)}$$

To estimate C_∞ from Eq. IV-S12, I have to calculate the statistical averages $\langle \mathbf{T}_3{}^{(\alpha)}\rangle$, $\langle \mathbf{T}_3{}^{(\alpha)}\mathbf{T}_4{}^{(\alpha)}\rangle$, and $\langle \mathbf{T}_3{}^{(\alpha)}\mathbf{T}_4{}^{(\alpha)}\mathbf{T}_5{}^{(\alpha)}\rangle$. The averages can be made by using the statistical weights appearing in the partition function given by Eq. IV-17 in the text.

For the perfectly atactic H-poly(NB) chain, the *d* and *l* configurations appear randomly on each monomer unit, and C_∞ must be averaged over the *d* and *l* configurations for all monomer units. Thus C_∞ for the perfectly atactic H-poly(NB) is calculated by

$$\left(\sum_{i=1}^{5} b_i^{\,2}\right) C_\infty = \sum_{i=1}^{5} b_i^{\,2} + 2\overline{\beta} + 2\overline{\mathbf{B}}\left(\mathbf{E} - \overline{\langle \mathbf{T}\rangle}\right)^{-1}\overline{\mathbf{B}'}^{\mathrm{T}} \quad \text{(IV-S13)}$$

where

$$\overline{\beta} \equiv \tfrac{1}{2}\left(\beta^{(1)} + \beta^{(2)}\right) \quad \text{(IV-S14)}$$

$$\overline{\mathbf{B}} \equiv \tfrac{1}{2}\left(\mathbf{B}^{(1)} + \mathbf{B}^{(2)}\right), \quad \overline{\mathbf{B}'}^{\mathrm{T}} \equiv \tfrac{1}{2}\left(\mathbf{B}'^{(1)} + \mathbf{B}'^{(2)}\right) \quad \text{(IV-S15)}$$

$$\overline{\langle \mathbf{T}\rangle} \equiv \tfrac{1}{2}\left(\langle \mathbf{T}^{(1)}\rangle + \langle \mathbf{T}^{(2)}\rangle\right) \quad \text{(IV-S16)}$$

References

1. Flory, P. J. *Statistical Mechanics of Chain Molecules*; Wiley: New York, 1969.
2. Mays, J.; Hadjichristidis, N.; Fetters, L. J., Characteristic Ratios of Model Polydienes and Polyolefins. *Macromolecules* **1984,** *17*, 2723-2728.
3. Hattam, P.; Gauntlett, S.; Mays, J. W.; Hadjichristidis, N.; Young, R. N.; Fetters, L. J., Conformational Characteristics of Some Model Polydienes and Polyolefins. *Macromolecules* **1991,** *24*, 6199-6209.
4. Fetters, L. J.; Lohse, D. J.; Richter, D.; Witten, T. A.; Zirkel, A. Connection between Polymer Molecular Weight, Density, Chain Dimensions, and Melt Viscoelastic Properties. *Macromolecules* **1994**, *27*, 4639-4647.
5. Fetters, L. J.; Lohse, D. J.; Graessley, W. W. Chain Dimensions and Entanglement Spacings in Dense Macromolecular Systems. *J. Polym. Sci.: Part B: Polym. Phys.* **1999**, *37*, 1023-1033.
6. Fetters, L. J.; Lohse, D. J.; Garcia-Franco, C. A.; Brant, P.; Richter, D. Prediction of Melt State Poly(R-olefin) Rheological Properties: The Unsuspected Role of the Average Molecular Weight per Backbone Bond, *Macromolecules* **2002**, *35*, 10096-10101.
7. Mattice, W. L.; Suter, U. W. *Conformational Theory of Large Molecules*. Wiley-Interscience, New York, 1994
8. MacRury, T. B.; McConnell, M. L., Measurement of the absolute molecular weight and molecular weight distribution of polyolefins using low-angle laser light scattering. *J. Appl. Polym. Sci.* **1979,** *24* (3), 651-662.
9. Grinshpun, V.; O'Driscoll, K. F.; Rudin, A., High-Temperature Size Exclusion Chromatography of Polyethylene. In *Size Exclusion Chromatography*, American Chemical Society: 1984; Vol. 245, pp 273-280.
10. Sun, T.; Brant, P.; Chance, R. R.; Graessley, W. W. Effect of Short Chain Branching on the Coil Dimensions of Polyolefins in Dilute Solution. *Macromolecules* **2000**, *34*, 6812-6820.
11. Brant, P.; Ruff, C. J.; Sun, T. Effect of Tacticity on the Dilute Solution Coil Dimensions of Poly(*a*-olefin)s, *Macromolecules* **2005**, *38*, 7181-7183.
12. Debye, P. Molecular-Weight Determination by Light Scattering. *J. Phys. Colloid Chem.* **1947**, *51*, 18-32
13. Bussi, G.; Donadio, D.; Parrinello, M., Canonical sampling through velocity rescaling. *J. Chem. Phys.* **2007,** *126*, 014101.

14. Hess, B., P-LINCS: A Parallel Linear Constraint Solver for Molecular Simulation. *J. Chem. Theor. Comput.* **2008,** *4*, 116-122.
15. Jorgensen, W. L.; Maxwell, D. S.; Tirado-Rives, J., Development and testing of the OPLS all-atom force field on conformational energetics and properties of organic liquids. *J. Am. Chem. Soc.* **1996**, *118*, 11225−11236.
16. Abraham, M. J.; Murtola, T.; Schulz, R.; Pall, S.; Smith, J. C.; Hess, B.; Lindahl, E., GROMACS: High performance molecular simulations through multi-level parallelism from laptops to supercomputers. *SoftwareX* **2015**, *1*, 19 −25.
17. Hamidi, N.; Ganewatta, M. S. Influence of the rosin pendant groups on the solution properties of a high molecular weight hydrogenated polynorbornene. *Polymer* **2021**, *232*, 124167.
18. Yamakawa, H.; Yoshizaki, T. *Helical Wormlike Chains in Polymer Solutions (2nd Ed.)*. Springer, Heidelberg (2016).
19. Benoit, H.; Doty, P. Light Scattering from Non-Gaussian Chains. *J. Phys. Chem.* **1953**, *57*, 958-963.
20. Norisuye, T.; Fujita, H. Excluded Volume Effects in Dilute Polymer Solutions. XIII. Effects of Chain Stiffness. *Polym. J.* **1982**, *14*, 143-147.
21. Norisuye, T.; Tsuboi, A.; Teramoto, A. Remarks on Excluded-Volume Effects in Semiflexible Polymer Solutions. *Polym. J*. **1996**, *28*, 357-361.
22. Yamakawa, H. *Modern Theory of Polymer Solutions*. Harper & Row, New York (1971).
23. Flory, P. J. *Principles of Polymer Chemistry*. Cornell Univ. Press, Ithaca, New York (1953).
24. Sato, T.; Terao, K.; Teramoto, A.; Fujiki, M. Molecular Properties of Helical Polysilylenes in Solution. *Polymer* **2003**, *44*, 5477-5495.
25. Yun, S. I.; Terao, K.; Hong, K.; Melnichenko, Y. B.; Wignall, G. D.; Britt, P. F.; Mays, J. W. Solution Properties of 1,3-Cyclohexadiene Polymers by Laser Light Scattering and Small-Angle Neutron Scattering. *Macromolecules* **2006**, *39*, 897-899.

Chapter V: Summary and Conclusions

In this thesis work, I investigated syntheses, crystal structures , and single chain conformations of stereoregular hydrogenated ring-opened poly(norbornene)s, H-poly(NB)s, categorized as cycloolefin polymers. Since polyolefins are both academically and industrially important polymers, Chapter I describes the brief history of the studies on polyolefins as well as cycloolefin polymers. In such a historical context, the present thesis contributes to structural characterizations of the newly synthesized stereoregular cycloolefin polymers.

Chapter II is concerned with syntheses of stereoregular H-poly(NB)s. Isospecific and syndioselective ring-opening metathesis polymerizations (ROMP) of norbornene (NB) were thoroughly investigated for the first time. *Cis*-isospecific ROMPs of NB were achieved with Mo-based catalyst, and *cis*-syndioselective ROMPs of NB proceeded in the presence of W-based catalysts. The polymerization results of NB were compared with those of tricyclic dicyclopentadiene (DCP) and tetracyclic tetracyclododecene (TCD) to reveal the factor that would affect the stereocontrol of the ROMP of cycloolefins.

Using thus provided stereoregular H-poly(NB)s, their basic characteristics were investigated in the following chapters. In Chapter III, the crystal structures of syndiotactic and isotactic H-poly(NB)s in comparison with the already reported atactic one were examined by the analyses of the X-ray diffraction data. The skeletal chains in the crystal cell take essentially the similar planar zigzag conformation in all the species. The

cyclopentylene rings are included as the parts of the skeletal chains. However, the CH_2CH_2 side groups of the rings protrude out of the skeletal chain in different modes depending on the tacticity, which gives the significant difference in the whole shape of the chains and then the difference in the chain packing structure. In addition, the existence of phase transition between the low temperature (LT) and high temperature (HT) phases for isotactic and atactic species in the heating process was confirmed. The structural analysis revealed the *trans-gauche* (T-G) conformational change in the HT phase of isotactic H-poly(NB) caused by the thermally-activated cooperative torsional motions. In the case of atactic H-poly(NB) which has disordered packing, the translational motion along the chain axis coupled with the rotational motions or the fluctuation of ring side groups is imagined to occur above the transition point even though the *trans* conformation was kept. The syndiotactic H-poly(NB) did not show such structural change in the whole temperature region below melting point. The presence or absence of phase transitions is thought to have a large influence to the melting behavior of H-poly(NB). The crystal-crystal phase transition to more stable structure observed in isotactic H-poly(NB) were thought to contribute to raise the melting temperature.

Chapter IV deals with the single chain conformations of syndiotactic, isotactic, and atactic H-poly(NB)s in 1,2,4-trichlorobenzene at 140 °C. By combining the data obtained from size-exclusion chromatography with an on-line multi-angle light scattering detector measurements and molecular dynamics simulations, I determined the characteristic ratios C_∞ of the H-poly(NB)s. The results of C_∞ of the H-poly(NB)s are definitely larger than those of polyethylene and polypropylenes. The experimental results of C_∞ were favorably compared by the rotational isomeric state model. The two main-

chain bonds included in the cyclopentane ring are restricted near the trans conformation, and this restriction enlarges C_∞ of the H-poly(NB)s.

The stronger excluded volume effect for syndiotactic H-poly(NB) in TCB at 140 ^oC than those for isotactic and atactic H-poly(NB)s implied a higher affinity between the polymer and solvent and/or a lower cohesive energy density of the polymer component. A lower cohesive energy density of syndiotactic H-poly(NB) may decrease the melting temperature considerably lower than that of isotactic and atactic species.

List of Publications

1. Hayano, S.; Nakama, Y. Iso- and Syndio-Selective ROMP of Norbornene and Tetracyclododecene: Effects of Tacticity Control on the Hydrogenated Ring-Opened Poly(cycloolefin)s. *Macromolecules* **2014**, *47*, 7797-7811. (Chapter II)

2. Nakama, Y.; Hayano, S.; Tashiro, K. Influence of Tacticity on the Crystal Structures of Hydrogenated Ring-Opened Poly (norbornene)s. *Macromolecules* **2021**, *54*, 8122−8134. (Chapter III)

3. Nakama, Y.; Hayano, S.; Tashiro, K., X-ray-Analyzed Structural Changes in the Crystal Phase Transitions of Hydrogenated Ring-Opened Poly(norbornene)s with Different Stereoregularities. *Macromolecules* **2024,** *57* (4), 1677-1687. (Chapter III)

4. Nakama, Y.; Natori, S.; Hayano, S.; Sato, T. Conformations of Hydrogenated Ring-Opened Poly(norbornene)s in Dilute Solution. *Polymer Journal* **2024**, Online ahead of print https://doi.org/10.1038/s41428-023-00852-y. (Chapter IV)

Other related papers

5. Kafle, N.; Makita, Y.; Zheng, Y.; Schwarz, D.; Kurosu, H.; Pan, P.; Eagan, J. M.; Nakama, Y.; Hayano, S.; Miyoshi, T. Roles of Conformational Flexibility in the Crystallization of Stereoirregular Polymers. *Macromolecules* **2021**, *54*, 5705−5718.

6. Zheng, Y.; Kafle, N.; Schwarz, D.; Eagan, J. M.; Hayano, S.; Nakama, Y.; Pan, P.; Miyoshi, T., Asymmetric Molecular Dynamics and Anisotropic Phase Separation in the Cocrystal of the Crystalline/Crystalline Polymer Blend. *ACS Macro Lett* **2022,** *11* (2), 193-198.

List of Patents

1. Hayano, S.; Nakama, Y. Norbornene ring-opening polymer hydride and its production method. Japanese Laid-Open Patent Publication No. 011886, 2019. International Laid-Open Patent Publication No. 188720, 2019. Japanese Granted Patent Publication No. 7207403, 2023.

2. Sawaguchi, T.; Hayano, S.; Nakama, Y.; Kanda, H. Ring-opening polymer hydride, resin composition, and molded product. Japanese Laid-Open Patent Publication No. 158702, 2020. Japanese Granted Patent Publication No. 7247704, 2023.